

Design Framework for Multi-Cell Multi-User Visible Light Communications (VLC) Networks

Pham Van Thanh

A DISSERTATION

SUBMITTED IN PARTIAL FULFILLMENT OF THE REQUIREMENTS
FOR THE DEGREE OF DOCTOR OF PHILOSOPHY
IN COMPUTER SCIENCE AND ENGINEERING

Graduate Department of Computer and Information Systems
The University of Aizu
December 21, 2018



© Copyright by Pham Van Thanh 2018

All Rights Reserved

To my family

Contents

Contents	v
List of Figures	x
List of Notations	xii
List of Abbreviations	xiii
Abstract	xvi
1. Introduction	1
1.1 History of Visible Light Communications Development	2
1.2 Practical Applications of Visible Light Communications	3
1.2.1 Wireless Local Area Networks	3
1.2.2 Indoor Positioning	4
1.2.3 Vehicle Communications	4
1.3 Fundamentals of Visible Light Communications	5
1.3.1 VLC Transmitter	6
1.3.2 VLC Receiver	7
1.3.3 VLC Channel	8
1.4 Motivations and Scope of the Study	10
1.4.1 Single User Configuration	11
1.4.2 Multi-User Configuration	12

1.4.3	Scope of the Study	12
1.5	Original Contributions	14
1.6	Design Framework	15
1.7	Thesis Organization	18
2.	Information Capacity of Amplitude-Constrained Scalar Gaussian Channels [61, 62]	20
2.1	Amplitude-Constrained Scalar Gaussian Channels	20
2.1.1	Lower Bound	21
2.1.2	Upper Bound	22
2.1.3	Numerical Example and Asymptotic Behaviors	23
2.2	Amplitude-Constrained Scalar Gaussian Interference Channels	24
2.2.1	Lower Bound	24
2.2.2	Upper Bound	25
2.2.3	Numerical Example and Asymptotic Behaviors	26
3.	Multi-user MIMO Visible Light Communications and Linear Precoding [61]	28
3.1	Introduction	28
3.2	Linear Precoding for Multi-user MIMO Visible Light Communications	30
3.2.1	Matched Filter Precoding	32
3.2.2	Zero-Forcing Precoding	33
3.2.3	Regularized Zero-Forcing Precoding	34
3.3	Optical Power Constraints	35
4.	Physical Layer Security in Multi-user MIMO Visible Light Communications [76, 77]	37
4.1	Introduction	37
4.1.1	Physical Layer Security	38
4.1.2	Physical Layer Security in Visible Light Communications	39

4.2	Precoding Design	40
4.2.1	Motivations and Objectives	40
4.2.2	System Model	42
4.2.3	Bound on Secrecy Sum-Capacity	43
4.2.4	Known \mathbf{H}_e	44
4.2.5	Unknown \mathbf{H}_e	44
4.2.6	Numerical Results and Discussions	46
4.3	Artificial Noise Design	50
4.3.1	Motivations and Objectives	50
4.3.2	AN-aided Precoding Model	51
4.3.2.1	Unknown Eavesdropper's CSI	52
4.3.2.2	Known Eavesdropper's CSI	53
4.3.3	Optical Power Constraint	55
4.4	General AN-aided Precoding Design	55
4.4.1	Unknown Eavesdropper's CSI	55
4.4.2	Known Eavesdropper's CSI	58
4.5	AN-Aided ZF Precoding	61
4.5.1	Unknown Eavesdropper's CSI	61
4.5.2	Known Eavesdropper's CSI	63
4.6	Numerical Results and Discussions	64
4.7	Conclusions	67
5.	Multi-cell Multi-user Visible Light Communications Networks [62]	69
5.1	Introduction	69
5.1.1	Motivations	69
5.1.2	Objectives	71
5.2	Network Model	72

5.2.1	Precoding Model and Broadcast Transmission	73
5.2.2	ZF Precoding and Optical Power Constraint	75
5.3	Cell Coordination/Cooperation Strategies	77
5.3.1	Per-Cell Coordinated Precoding	77
5.3.2	Coordinated Precoding	79
5.3.3	Partial Cooperative Precoding with Data Sharing	81
5.4	Numerical Results and Discussions	83
5.5	Conclusions	90
6.	Summary and Future Research	92
6.1	Summary	92
6.2	Future Research	94
6.2.1	User Max-main Fairness	94
6.2.2	Physical Layer Security with the Presence of Multiple Eaves-droppers	95
Appendices	96
Appendix A	A Proof of Proposition 1 in Chapter 2	96
Appendix B	A Proof of Theorem 1 in Chapter 4	97
B.1	Differential Entropy of the Sum of Uniform Random Variables	97
B.2	Data Processing Inequality [64, Theorem 2.8.1]	98
B.3	Derivation of Eq. (4.7)	99
Bibliography	100

List of Figures

1.1	A schematic diagram of a point-to-point VLC system.	5
1.2	A geographical propagation model of an indoor VLC system.	8
1.3	Different indoor MIMO VLC configurations.	10
1.4	Design Framework	17
2.1	Exact, lower and upper bounds capacities of amplitude-constrained scalar Gaussian channels.	21
2.2	Lower and upper capacity bounds of amplitude constrained interference channels.	26
3.1	A geographical configuration of an MU-MIMO VLC system.	29
3.2	A schematic diagram of an MU-MIMO VLC system.	30
3.3	Nonlinear LED transfer characteristic.	35
4.1	The wiretap channel [78] with three parties: a sender (Alice), a legitimate user (Bob) and an eavesdropper (Eve).	38
4.2	MU-MISO VLC system with N_T LED arrays for K non-cooperative legitimate pairs of user (Alice and Bob) with mutual confidentiality, and one Eavesdropper (Eve).	42
4.3	A geometrical configuration of the considered MU-MIMO VLC wiretap channel.	45
4.4	Averaged peak SNR of legitimate users: known and unknown \mathbf{H}_e	47

4.5	Averaged maximum secrecy sum-rate: known and unknown \mathbf{H}_e	48
4.6	Maximum secrecy sum-rate for different positions of the eavesdropper: known \mathbf{H}_e	49
4.7	Maximum secrecy sum-rate for different positions of the eavesdropper: unknown \mathbf{H}_e	50
4.8	Schematic diagram of AN-aided precoding scheme: unknown \mathbf{H}_e	52
4.9	Schematic diagram of AN-aided precoding scheme: known \mathbf{H}_e	54
4.10	Max-min fairness of users' SINRs with respect to AN adjusting factor: unknown \mathbf{H}_e	65
4.11	Max-min fairness of users's SINRs with respect to average LED array transmit power: unknown \mathbf{H}_e , $\rho = 0.5$	66
4.12	Max-min fairness of users's SINR with respect to average LED array transmit power: known \mathbf{H}_e	67
5.1	Multi-user multi-cell VLC network and illumination area.	73
5.2	Geometrical configuration of a multi-user multi-cell MU-MIMO VLC systems with 8 LEDs arrays.	85
5.3	Maximum sum-rate distribution for different cooperative schemes.	86
5.4	Average maximum sum-rate versus average LED array transmitted power: 2-by-2.	86
5.5	Average maximum sum-rate versus average LED array transmitted power: 1-by-3.	87
5.6	Average maximum sum-rate versus average LED array transmitted power: 3-by-3.	87
5.7	Average maximum sum-rate versus average LED array transmitted power: 2-by-4.	88
5.8	Convergence behavior of Algorithm 3: 2-by-2.	89
5.9	Convergence behavior of Algorithm 3: 3-by-3.	90

List of Notations

A	Matrix
I _N	the identity matrix of size N
a	Vector
e _n	the all zero vector with the n -th element begin 1
1 _N	the all 1 vector of size N
0 _{M × N}	the all zero matrix of size $M \times N$
A ^T	the transpose of matrix A
[A] _{i,j}	the element at the i -th row and the j -th column of the matrix A
[A] _{i,:}	the i -the row vector of matrix A
·	the absolute value operator
$\ \cdot\ _1$	the L_1 norm
$\ \cdot\ _F$	the Frobenius norm
$\mathbb{E}[\cdot]$	the statistical expectation operator
$\log(\cdot)$	the natural logarithm
\cup	the union operator
$\mathbb{I}(\cdot; \cdot)$	the mutual information in nats
$h(\cdot)$	the differential entropy in nats
\otimes	the Kronecker product
\circ	the Hadamard product
\mathbb{R}	the real number set
\mathbb{R}_+	the positive real number set
rank(A)	rank of matrix A
dim(A)	dimension of matrix A

List of Abbreviations

AC	Alternating Current
AN	Artificial Noise
AP	Access Point
APD	Avalanche Photodiode
AWGN	Additive White Gaussian Noise
BD	Block Diagonalization
CCCP	Convex-Concave Procedure
CoMP	Coordinated Multipoint
CPU	Central Processing Unit
CSI	Channel State Information
CSK	Color Shift Keying
DC	Direct Current
EPI	Entropy Power Inequality
FDM	Frequency Division Multiplexing
FFR	Fractional Frequency Reuse
FOV	Field of View
GPS	Global Positioning System
ICI	Inter-channel Interference
IM/DD	Intensity Modulation/Direct Detection
ITS	Intelligent Transport System
I2V	Infrastructure-to-Vehicle
JT	Joint Transmission
LED	Light Emitting Diode
LoS	Light-of-Sight

MCP	Multi-cell Processing
MF	Matched Filter
MHz	Megahertz
MIMO	Multiple Input Multiple Output
MISO	Multiple Input Single Output
MSE	Mean Square Error
MU	Multi-user
MUI	Multi-user Interference
NLoS	Non Light-of-Sight
OFDM	Orthogonal Frequency Division Multiplexing
OMEGA	hOME Gigabit Access
OOK	On-Off Keying
OWC	Optical Wireless Communications
PAM	Pulse Amplitude Modulation
PD	Photodiode
PDF	Probability Density Function
PPDM	Pulse Position Division Multiplexing
QoS	Quality of Service
RC	Repetition Coding
RF	Radion Frequency
RGB	Red-Green-Blue
RZF	Regularized Zero-Forcing
SCM	Subcarrier Multiplexing
SISO	Single Input Single Output
SM	Spatial Modulation
SMP	Spatial Multiplexing
SNR	Signal-to-Noise Ratio
SINR	Signal-to-Interference-plus-Noise Ratio
SOCP	Second-order Cone Program
SOP	Secrecy Outage Probability
TDM	Time Division Multiplexing
THz	Terahertz
UFR	Unity Frequency Reuse
V2V	Vehicle-to-Vehicle

VoIP	Voice over IP
VLC	Visible Light Communications
VLCA	Visible Light Communications Association
VLCC	Visible Light Communications Consortium
V-PPM	Variable Pulse-Postion Modulation
WPAN	Wireless Personal Area Network
WSMSE	Weighted Sum Mean Square Error
ZF	Zero-Forcing

Abstract

With the explosive growth of mobile devices, it is forecasted that the global data traffic from 2016 to 2021 will increase from 7 exabytes to 49 exabytes per month. To address this tremendous demand given the spectrum scarcity problem in radio-frequency (RF) communications, there has been a great deal of interest in research and development of optical wireless communications (OWC), which can be an alternative or complementary to the existing wireless technologies. In particular for indoor applications, visible light communications (VLC), which is a subset of OWC, has been gaining a lot of attention from both academia and industry over the last decade.

One on hand, due to the broadcast nature of the visible light, VLC can be categorized as broadcast networks, which are capable of serving multiple users. On the other hand, this raises concerns in security and privacy as any users located within the illuminated area can gain accessibility of the transmitted signals making eavesdropping is a possible threat. In addition to security at network and transport layers, security at physical layer (also known as physical layer security) has been emerging as a completely new measure against eavesdropping. In this dissertation, our first objective is to design efficient methods to enhance physical layer security in multi-user VLC systems.

To support even a larger number of users, it is conceivable that the multi-cell configuration is a natural progression in the development of VLC. We introduce in this thesis a concept of multi-cell VLC networks, where each cell composes of multiple light-emitting diode (LED) transmitters to support multiple users by means of precoding techniques. In such multi-cell multi-user networks, the presence of intra-cell and inter-cell interferences, which can severely degrade the system performance,

is inevitable due to the overlapping of multiple signals at each user. Therefore, the second objective of the thesis is to design cell coordination/cooperation strategies and their corresponding coordinated/cooperative precoding to alleviate, or possibly, to cancel out the intra-cell and inter-cell interferences. The performances of the proposed strategies in terms of users' sum-capacity are extensively evaluated and compared.

Chapter 1

Introduction

The last decade has witnessed an explosive growth in the number of mobile devices and bandwidth-demanding applications. According to data from GSM association, there were 5 billion mobile subscribers globally as of Q2 2017 [1]. By 2020, almost three quarters of the world population will be connected by mobile devices. In addition to that, the popularity of data-intensive multimedia applications, such as high-definition video streaming and mobile augmented reality, have led to an exponential increase in the mobile traffic. A recent study by Cisco System Inc. shows that the global mobile traffic will increase 7-fold from 7 exabytes to 49 exabytes per month within the period from 2016 to 2021 [2]. Given the current overcrowded of radio spectrum, this tremendous data traffic demand requires an urgent need to develop new wireless communications technologies.

The advances and massive deployment of light-emitting diodes (LEDs) over the traditional incandescent and fluorescent lamps have paved the way for a new kind of wireless technology called visible light communications (VLC) [3–5]. Using LEDs as the transmitting devices, VLC is able to provide a dual functionality: illumination and at the same time data transmission. However, more importantly, VLC operates over a nearly unlimited and license-free light spectrum (380 nm - 780 nm or 400 THz bandwidth), which is 10,000 times wider than that of the radio spectrum. This effectively addresses the spectrum scarcity problem of radio frequency (RF) commu-

nlications. The immunity of visible light signal to other electromagnetic sources makes VLC easy to be coexisted with existing wireless technologies. Additionally, VLC can also operate in the areas where radio signals are undesirable or prohibited, such as airplanes and hospitals. Due to the widespread utilization of LEDs, it is also conceivable that VLC will play an important role in the future ubiquitous networking [6, 7].

1.1. History of Visible Light Communications Development

The history of VLC dates back to the late nineteenth century with the invention of photophone by Alexander Graham Bell [8]. The photophone was able to transmit speech on modulated sunlight over several hundred meters. Since then until the popularity of LEDs at the start of the twentieth century, there have been no significant developments of VLC. The idea of using LEDs for both illumination and communications began to take shape in 2003 by Nakagawa and Takana in Nakagawa Laboratory at Keio University [9,10]. After these pioneering works, there were numerous research activities focusing on developing high speed VLC systems to support mobile devices and transport vehicles [11–16]. This led to the establishment of Visible Light Communications Consortium (VLCC) in Japan in 2003, which was succeeded by the Visible Light Communications Association (VLCA) in 2014 [17, 18]. During its operation, the VLCC has proposed two standards, namely: Visible Light Communication System Standard and Visible Light ID System Standard in 2007. In addition to VLCC and VLCA, large research projects, such as the hOME Gigabit Access (OMEGA) (Europe, 2008) [19], Smart Lighting Engineering Research Center (USA, 2008) [20], Center on Optical Wireless Applications (USA, 2011) [21] have been launched to further promote the development of VLC.

To open the road for commercialization, VLC has also been standardized for wireless personal area networks (WPANs) in IEEE 802.15.7, which included the physical layer and link layer design specifications [22]. In particular for the phys-

ical layer, the standard specified three different modulation schemes: On-Off Keying (OOK), variable pulse-position modulation (V-PPM) and color-shift keying (CSK) with various data rates ranging from 11 kbps to 96 Mbps. Nevertheless, VLC systems can achieve much higher data rates when more advanced modulation and transmission schemes are applied. Specifically, orthogonal frequency-division multiplexing (OFDM) and multiple-input multiple-output (MIMO) are the two most promising techniques to boost the data rate performance. It has been experimentally reported in [23] that a 1 Gbps VLC transmission can be achieved in laboratory conditions using four-channel MIMO link, each transmitting signals at 250 Mbps using OFDM. Using a single gallium nitride LED which exhibits a 3-dB modulation bandwidth of at least 60 MHz, a 3 Gbps OFDM VLC link was demonstrated in [24].

1.2. Practical Applications of Visible Light Communications

1.2.1. Wireless Local Area Networks

The most expected application of VLC is indoor information-broadcast where each illumination devices (e.g., LED luminaries) act as wireless access points (APs) in much the same way as Wi-Fi APs. For indoor scenarios, typical VLC APs provide a coverage area of $1 - 10 \text{ m}^2$, which is called VLC atto-cell [25, 26]. This relatively small coverage area requires a deployment of multiple VLC atto-cell to meet the lighting requirements and to broaden the service area. Furthermore, it is expected that VLC will be deployed in conjunction with Wi-Fi where VLC provides a high-speed downlink transmission (necessary for data-intensive applications such as video streaming) whereas Wi-Fi is responsible for the uplink connection [27, 28]. Considered as the dominant application of VLC, the focus of this thesis is thus on designs of indoor VLC systems for information broadcasting.

1.2.2. Indoor Positioning

Categorized as a wireless technology, VLC can also be used as a new approach for indoor positioning. Thanks to the advancements in wireless technology, there are several positioning techniques, which have been already available for commercial use, such as Global Positioning System (GPS), Wi-Fi positioning systems. Of which, GPS is the most popular technology with the accuracy of few meters for outdoor applications. For indoor scenario, however, GPS performs very poor due to satellite signal blockage by roofs, walls and floors. In contrast to GPS, Wi-Fi positioning technique is able to provide an accuracy of 1 to 10 meters for indoor environment, depending heavily on the usage environment. Characterizing an accurate propagation model for each Wi-Fi access point in a real indoor environment is extremely complex due to multi-path propagation phenomena and therefore usually resulting in a relatively poor positioning accuracy [29]. Deploying Wi-Fi positioning systems requires an existence of Wi-Fi networks as a part of the communication infrastructure, otherwise it will cause expensive and time-consuming infrastructure deployment. Furthermore, Wi-Fi signal can interfere with other wireless signal like microwave (usually generated by ovens) or Bluetooth signal which consequently degrades the reliability of the systems. Compared to these technologies, VLC-based indoor positioning can take advantages of the existing lighting infrastructure, thus reducing considerably the deployment cost. Furthermore, since light signals do not interfere with other radio signals and their propagation are less subject to multipath effect, VLC-based indoor positioning can provide higher accuracy [30–33].

1.2.3. Vehicle Communications

Although VLC is expected to predominantly used for indoor applications, it also has a great potential for outdoor vehicular communications. As the number of automobiles increases rapidly with increasing traffic accidents, the Intelligent Transport System (ITS) tries to incorporate different technologies to reduce of number of accidents as

well as improve the efficiency of the transportation system. Among them, VLC is a promising candidate for vehicle-to-vehicle (V2V) and infrastructure-to-vehicle (I2V) communications due to the widespread usage of LEDs in vehicle light systems and traffic light. Furthermore, it is foreseeable that the future street lighting will also be LED based. Thus, this particular scenario of VLC-based I2V has a huge potential in providing high data rates communications and stability [34, 35].

1.3. Fundamentals of Visible Light Communications

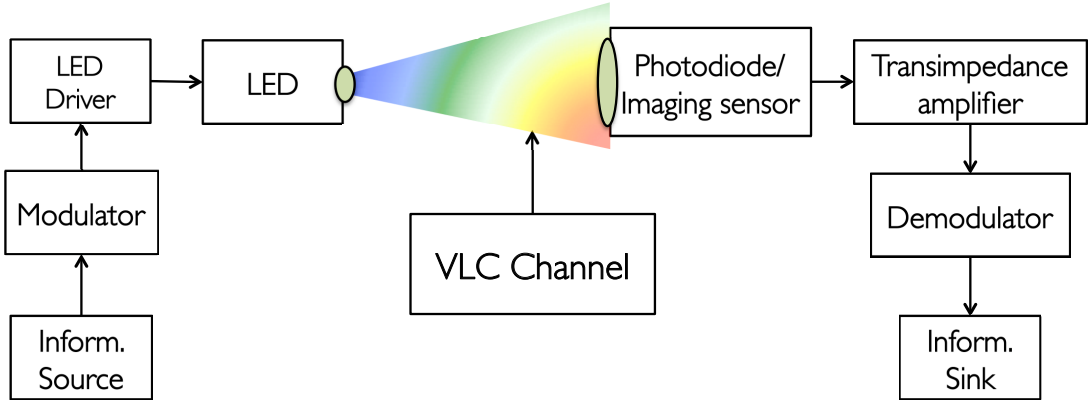


Figure 1.1: A schematic diagram of a point-to-point VLC system.

Figure 1.1 illustrates a schematic diagram of a typical point-to-point VLC system, which consists of three main parts: transmitter, receiver and VLC channel. At the transmitting side, the information source, after being modulated by a specific modulation scheme, is used as the drive current for the input of the LEDs. Due to some requirements for lighting purposes (e.g., dimming, flickering), further signal processing on the drive current might be needed at the LED driver. Different from RF communications, the incoherent light source of VLC makes phase and amplitude modulation techniques impossible to be applied. Instead, VLC systems use the simple Intensity Modulation with Direction Detection (IM/DD). Using IM/DD, the intensity of the emitted light is modulated in accordance to the variations of the drive current. At the receiving side, the received optical signal is converted into an electrical signal by

using a photodiode and an image sensor. A transimpedance amplifier is used to convert the obtained current to a voltage signal, which is then demodulated to recover the original data.

In the following, an overview of transmitter, receiver and VLC channel components are provided.

1.3.1. VLC Transmitter

The transmitter in a VLC system is predominantly an LED luminaire. Though other light sources such as fluorescent and incandescent lamp can also be used as the transmitter, LEDs exhibit a number of advantages in terms of power consumption, life expectancy, light conversion efficiency as illustrated in Table 5.1. An LED lamp

Light source Criterion	Incandescent	Fluorescent	LEDs
Power consumption (watt)	60W	14W	6W
Life expectancy (hours)	1,200	10,000	100,000
Light-conversion efficiency	5%	25%	50%
Mercury free	No	No	Yes

Table 1.1: A comparison among incandescent, fluorescent and LEDs.

usually contain many LED chips to provide sufficient illumination. The lamp also includes a driver circuit, which, in normal operation, is used to adjust the brightness by controlling the current flowing through the lamp. When the lamp is used as a VLC transmitter, the drive circuit is modified to modulate the data by varying the intensity of the emitted light. For example, the simple OOK modulation can be realized by choosing two different levels of the emitted light intensity, which correspondingly represent bit “1” and “0”.

Although VLC can provide both illumination and communication functions simultaneously, for indoor applications, illumination is still the primary purpose. As a result, while LED light is the most commonly used form of the light source. Generally, there are two ways of producing commercial white LED light

1. **Blue LED with phosphor coating.** In this way, a blue LED covered by a

yellow phosphor coating is used to generate white LED light [36]. The blue photons produced by the LED either traverse through the phosphor coating without any changes or they are converted into yellow photons. The combinations of the blue and the yellow photons create white light. By adjusting the thickness of the phosphor coating, the number of yellow photons can be controlled, thus different variations of the white light (color temperature) can be produced. This method has advantages of low cost and ease of implementation. However, the phosphor coating limits the switching speed of the LED to a few MHz, thus reduce the modulation bandwidth.

2. **Red-Green-Blue (RGB) combination.** In this method, white light is produced by properly mixing red, blue and green LED light together. The RGB combination method is more preferable for communication purpose as it offers higher modulation bandwidth and also enables the use of Color Shift Keying (CSK) which modulates the data using three different colors of the LEDs [22]. The drawbacks of this method are high cost and difficulty in balancing each red, blue and blue component to create white light. Therefore, the RGB LEDs are not popular for lighting purposes.

1.3.2. VLC Receiver

The receiver in a VLC system is responsible for converting the received optical signal to an electrical signal. Two types of VLC receivers with different operating mechanisms can be used, namely: photodiode (photodetector) and image sensor.

1. **Photodiode (PD).** A photodiode is a semiconductor device that converts light into an electrical current through the photoelectric effect. The most commonly used PD is the PIN, which comprises a wide, undoped intrinsic semiconductor region between a p-type semiconductor and an n-type semiconductor region. Aside from PIN, the more advance and also more expensive avalanche photodiode (APD), which possesses an internal gain through a phenomenon called the avalanche multiplication process, can also be used.

2. Image sensor. An image sensor (also known as camera sensor) is a sensor which is embedded on most of today's smartphones and tablets to capture videos and images. This potentially turns every single mobile device to a VLC receiver. An image sensor can be seen as a matrix of many photodiodes arranged on an integrated circuit. When the receiver is an image sensor, the “rolling shutter” property can be used to receive data at a faster rate.

1.3.3. VLC Channel

This section briefly describes channel model for the propagation of visible light, specifically for indoor scenarios. Under this conditions, the light signal coming out from an LED transmitter reaches the receiver through multiple propagation paths due to reflections off the surfaces as illustrated in Fig. 1.2 . As a result, the channel response

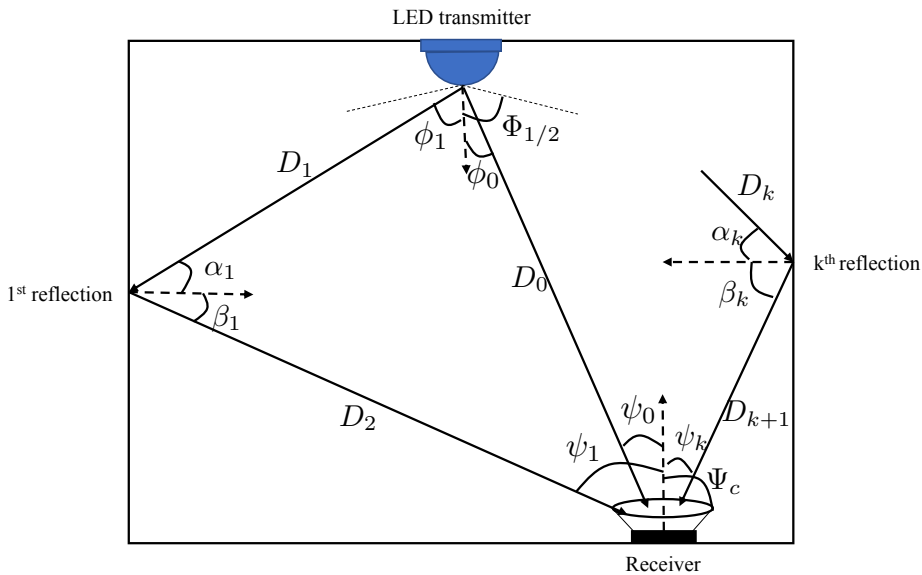


Figure 1.2: A geographical propagation model of an indoor VLC system.

h the sum of a line-of-sight (LoS) component h_{LoS} and multiple non light-of-sight (NLoS) components h_{NLoS}

$$h = h_{\text{LoS}} + \int_{\text{walls}} dh_{\text{NLoS}}^{(k)}, \quad (1.1)$$

where $dh_{\text{NLoS}}^{(k)}$ is the channel response of the NLoS component on the k -th reflection.

In practice, most LED sources have Lambertian beam distribution where the emission intensity is given as

$$L(\phi) = \frac{l+1}{2\pi} \cos^l(\phi), \quad (1.2)$$

with ϕ is the angle of irradiance and l is the order of Lambertian emission determined by the semi-angle for half illuminance of the LED $\Phi_{1/2}$ as $l = \frac{-\log(2)}{\log(\cos \Phi_{1/2})}$. For the LoS link, h_{LoS} is given by [10]

$$h_{\text{LoS}} = \begin{cases} \frac{A_r}{D_0^2} L(\phi_0) T_s(\psi_0) g(\psi_0) \cos(\psi_0) & , 0 \leq \psi_0 \leq \Psi_c, \\ 0 & , \psi_0 > \Psi_c, \end{cases} \quad (1.3)$$

where A_r and D_0 are the active area of the PD and the distance from the LED array to the PD, respectively. ψ_0 is the angle of incidence, $T_s(\psi_0)$ is the gain of the optical filter and Ψ_c denotes the optical field of view (FOV) of the PD. $g(\psi)$ is the gain of the optical concentrator and given by

$$g(\psi_0) = \begin{cases} \frac{\kappa^2}{\sin^2 \Psi_c} & , 0 \leq \psi_0 \leq \Psi_c, \\ 0 & , \psi_0 > \Psi_c, \end{cases} \quad (1.4)$$

where κ is the refractive index of the concentrator.

For the NLoS components, assume that each reflection is on a small region of the wall with area dA_{wall} and the surface reflector coefficient ρ_{ref} , the channel response on the k -th reflection is given by [10]

$$dh_{\text{NLoS}}^{(k)} = \begin{cases} \frac{A_r}{\pi D_k^2 D_{k+1}^2} \rho_{\text{ref}} dA_{\text{wall}} L(\phi_k) \cos(\alpha_k) \cos(\beta_k) T_s(\psi_k) g(\psi_k) \cos(\psi_k) & , 0 \leq \psi_k \leq \Psi_c, \\ 0 & , \psi_k > \Psi_c \end{cases} \quad (1.5)$$

However, in most cases, only LoS link is taken into consideration since it accounts for more than 95% of the total received optical power at the receiver [10]. Quantitatively, even the strongest NLoS component is at least 7 dB lower than the weakest LoS one [37]. For the sake of simplicity, we thus consider the LoS propagation path for performance analyses in this dissertation.

1.4. Motivations and Scope of the Study

For indoor environments, as a matter of fact that illumination is still the primary purpose, multiple LED arrays (LED luminaries) should be deployed to meet the lighting requirements. Since each LED array can act as a transmitting unit, this configuration inherently creates the multiple-input multiple-output (MIMO) transmission scheme. From the communications perspective, the benefit of the MIMO configuration is twofold. Firstly, due to the low modulation bandwidth of the LEDs, achieving high data rate is one of the major concerns. The MIMO transmission can overcome the problem and provide high data rates by means of spatial multiplexing. Secondly, MIMO configurations can facilitate the achieving physical alignment between LED transmitters and mobile users. As a result, recent theoretical research and experiments on VLC have shifted to studying the potential of MIMO-VLC systems [23, 24, 37–46].

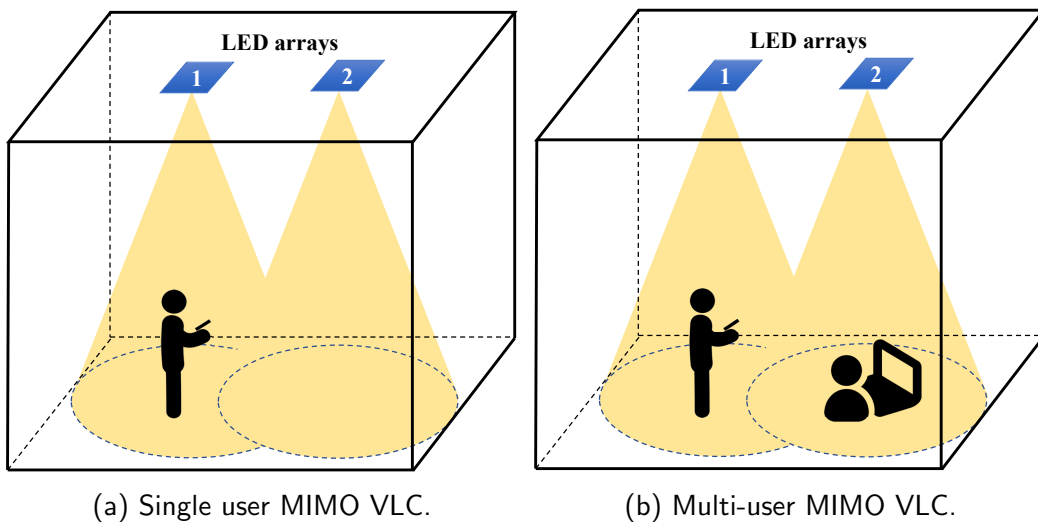


Figure 1.3: Different indoor MIMO VLC configurations.

1.4.1. Single User Configuration

As an emerging technology, the majority of previous works on VLC focused on improving its performance and practicality for the single user configuration (unicast transmission) as illustrated in Fig. 1.3a. In this configuration, generally, there are three transmission techniques proposed in the literature, namely: Repetition Coding (RC), Spatial Multiplexing (SM) and Spatial Modulation (SM).

1. **Repetition Coding (RC)**. This is the simplest technique where all LED transmitters simultaneously transmit the same signal. At the receiver, the received signals are constructively combined to increase the link reliability.
2. **Spatial Multiplexing (SMP)**. In SMP, each LED transmitter transmits an independent data stream to a receiver. By employing multiple receivers, this transmission scheme enables multiple parallel single-input single-output (SISO) links, thus enhances the spectral efficiency. The main challenge in implementing SMP is the strict alignment between transmitters and receivers to avoid inter-channel interference (ICI). Initial theoretical studies on SMP considered employing subcarrier multiplexing (SCM) for each LED transmitter and evaluated the impact of optical beat interference due to the use of the same wavelength at LED transmitters [47, 48].
3. **Spatial Modulation (SM)**. SM exploits the transmitter spatial degrees of freedom to extend the conventional signal constellation diagram to include an additional spatial dimension [49, 50]. Specifically, each LED transmitter is assigned a unique spatial symbol and when the data bits to be transmitted match the spatial symbol, the LED transmitter is activated. Since only one transmitter is active during one symbol duration, ICI is completely avoided. Thus, SM enables a lower decoding complexity compared to other schemes [51, 52].

1.4.2. Multi-User Configuration

Due to the broadcast nature of visible light, VLC can be categorized as broadcast networks, which are capable of serving multiple users. Hence, it can be seen that the next step towards realizing practical VLC systems is the development of multi-user (MU) MIMO configurations as shown in Fig. 1.3b. Different from the single-user configuration, the coexistence of multiple users poses a challenge in sharing transmission resources (e.g., time, bandwidth) in such a way that it needs to meet some key requirements of user fairness, spectral and energy efficiency. Since the modulation bandwidth of commercial LEDs is limited, low spectral efficiency multiplexing techniques such as Time Division Multiplexing (TDM) and Frequency Division Multiplexing (FDM) are attractive options for MU-MIMO VLC. However, spatial degrees of freedom introduced by multiple LED transmitter enables the use of pre-coding techniques, which can exploit the full available bandwidth.

The idea of precoding techniques is to pre-process users' data symbols with respect to a specific criterion based on the availability of users' channel state information (CSI) at the transmitters. Several studies on precoding design for MU-MIMO VLC systems, which mainly focus on linear precoding algorithms with either mean square error (MSE) or zero-forcing (ZF) criterion, have been reported. In particular, for the case of multi-PD receivers [53–55] studied the use of block diagonalization (BD) precoding [56] which can be regarded as a generalization of the ZF precoding. In case of single-PD receivers, or the MU-MISO configuration, precoding matrices based on the MSE criterion were designed to minimize the sum MSE [57] or to minimize the maximum MSE among users, i.e., max-min fairness MSE, [58].

1.4.3. Scope of the Study

Aside from improving performance and practicality, security and privacy are also important aspects in designing practical VLC systems. This is because the broadcast nature of visible light presents a challenge in guaranteeing secure and confidential com-

munications in the presence of unauthorized users. Any users within the illuminated area can gain accessibility of the transmitted signals, thus making eavesdropping a possible threat. Traditionally, the security of data transmission is performed at network and transport layers by means of key-based cryptographic techniques. However, possible flaws in the mathematical foundation and recently discovered weaknesses of these techniques have motived researchers to look at another security measures. In addition to security at upper layers, security at the physical layer (also known as physical layer security) has been emerging as a new approach to deal with eavesdropping. What makes physical layer security a promising alternative is that a perfect security can be achieved from mathematical point of view. Additionally, the achieved security can also be precisely quantified by characterizing the secrecy capacity, which is defined as the maximum reliable information rate at which the transmitted message cannot be decoded by eavesdroppers regardless of their computational power and knowledge of the encode scheme. Our first objective in this dissertation is precoding and artificial noise (AN) designs for enhancing secrecy capacity of MU-MIMO VLC systems.

In addition to the mentioned advantages, the spatial degrees of freedom introduced by MIMO enables supporting multiple users by means of precoding techniques. In reality, to support even more users in broad areas (e.g., supermarkets, airports), it is conceivable that the multi-cell configuration is also another natural progression in the development of VLC. Previous studies on multi-cell VLC systems mainly focused on the model composed of small atto-cells, where each individual cell is defined as the illuminated area of one LED array. Due to the small coverage of each cell, this model limits users' mobility. In this dissertation, we first propose a concept of multi-cell VLC networks, where each cell is composed of multiple LED arrays to cover a broader area. Each cell is essentially a MU-MIMO system in which multiple users are supported by precoding techniques. In such a multi-cell multi-user network, the main performance limiting factors are the intra-cell and inter-cell interferences. The second objective of the dissertation is to develop cell coordination/cooperation

strategies and their corresponding coordinated/cooperative precoding to alleviate (or possibly cancel out) these interferences.

1.5. Original Contributions

In accordance to the motivations and objectives described above, the contributions of the dissertation is twofold.

1. Firstly, we aim at improving the security of MU-MIMO VLC systems within the context of physical layer security. Specifically, we are interested in investigating the secrecy capacity performance with respect two different approaches: precoding and AN. As for the precoding approach, to ensure the confidentiality among legitimate users, ZF precoding is adopted. Then, optimal ZF precoding designs to maximize users' secrecy sum-rate are studied for two scenarios: known and unknown eavesdropper's CSI at the transmitter. In order to design ZF precoders with respect to user's secrecy capacity, a tractable formula for the VLC channel capacity should be known. Nevertheless, it is known that the input signal of VLC channels is amplitude constrained, for which no simple expressions for the channel capacity are available. To tackle this issue, we first derive closed-form expressions for the lower and upper bounds of the VLC channel capacity. It is revealed that at high signal-to-noise ratio (SNR) region (the condition that is usually available in VLC), the lower bound, which is simpler, is sufficient in characterizing the channel capacity due to its negligible gap to the exact one. The optimal ZF precoders are then designed with respect to the lower bound.

For the AN approach, the objective to guarantee max-min fairness of user's signal-to-interference-plus-noise ratios (SINR). In addition to that, the AN design also need to meet specific requirements depending on the availability of eavesdropper's CSI at the transmitter. In case the eavesdropper's CSI is unknown, the AN is designed in such a way that it does not interfere legitimate

users but possibly degrades the eavesdropper’s channel. In case the eavesdropper’s CSI is known, the AN design aims to limit the eavesdropper’s SINRs below a predefined threshold.

2. Secondly, we propose a multi-cell multi-user VLC network where each cell is an MU-MIMO VLC system, which is capable of supporting multiple users by means of precoding techniques. To reduce the impact of intra-cell and inter-cell interferences, we investigate three different cell cooperation/coordination strategies and their corresponding cooperative/coordinated precoding designs, namely: per-cell coordinated precoding, coordinated precoding and cooperative precoding with partial data sharing. In the considered multi-cell network, the VLC channels are subject to interferences, which are also amplitude constrained. Similar to the case with only amplitude constraint on the input signal mentioned previously, there are no closed-form expression for the channel capacity of such interference channels. Thus, we derive a lower and upper bound on the channel capacity of a scalar Gaussian interference channel in which both input signal and interference are amplitude constrained. The optimal cooperative/coordinated precoders to maximize users’ sum-rate are then designed based on the derived bounds. Finally, the performances of these strategies are evaluated and compared in terms of users’ sum-capacity.

1.6. Design Framework

Concisely, the central concern of this dissertation is precoding designs for MU-MIMO VLC systems (single and multiple cell fashions) with respect to optimizing users’ data rate-related performance criteria (i.e., sum-rate and secrecy sum-rate). Thus, the design framework essentially involves two fundamental issues: characterization of VLC channel capacity and constraints on the precoder design. First, let us revisit the concept of channel capacity, which was developed by C. E. Shannon in 1940s in his foundational work on information theory [59]. Consider a memoryless discrete-time

AWGN with channel input/output relationship

$$Y = X + N, \quad (1.6)$$

where X , Y , N denote channel input, output, and noise random variables, respectively. Shannon proved that the capacity of the channel in (1.6) is the maximum mutual information between X and Y over all possible input distribution of X

$$C = \max_{p(x)} I(X; Y) = \max_{p(x)} \sum_{x,y} p(x, y) \log \left(\frac{p(x, y)}{p(x)p(y)} \right), \quad (1.7)$$

where $p(x)$, $p(y)$ are the marginal probability distribution functions of X and Y , respectively, and $p(x, y)$ is the joint probability function of X and Y . For AWGN channels under an average signal power constraint, the maximizing input distribution $p(x)$ is found to be Gaussian, resulting in the following well-known equation

$$C = B \log \left(1 + \frac{P_s}{P_n} \right), \quad (1.8)$$

where B is the bandwidth of the channel, P_s is the average signal power and P_n is the average noise power. In case of VLC, due to the dynamic linear range of LEDs, the amplitude of input current signal should be constrained within a certain limit to ensure an efficient operation of LEDs. As a result, the input signal in VLC is subject to an amplitude constraint or equivalently peak power constraint and the formula in (1.8) may not hold for VLC channel (as the maximizing input distribution is not necessarily Gaussian). In fact, J.G. Smith showed that the capacity-achieving distribution for an amplitude-constrained additive white Gaussian noise (AWGN) channel is discrete with finite number of mass point [60]. Based on this observation, a relatively complicated numerical procedure was proposed to compute the capacity. Since it is challenging to incorporate the developed numerical procedure into the precoding design problems, simple analytical expressions are of importance in making the design tractable to solve. Therefore, the first step of our design framework is to

derive tractable closed-form expressions for the capacity of amplitude-constrained channels and use them as benchmarks for precoding designs. In particular, we aim at lower and upper bounds on the capacity in case of non-interference (Chapter 2 Section 2.1) and interference (Chapter 2 Section 2.1) channels.

Another aspect of the design framework is constraints on the precoders, which depend on design criteria and the transmit power. Though design criteria developed for RF systems (e.g., ZF, Regularized Zero-Forcing (RZF)) can be readily applied in VLC, the transmit power constraints in VLC are fundamentally different from those of RF due to unique characteristics of LEDs. Firstly, the input current of LEDs (i.e., drive current) must not be negative due to the lighting purpose. Secondly, it is known that LEDs exhibit a limited dynamic linear range where the output optical power increases linearly with an increase in the input current power. Hence, the second step of the framework is to formulate constraints on precoding designs with respect to these power requirements in VLC (Chapter 3 Section 3.3). The design framework is depicted in Fig. 1.4.

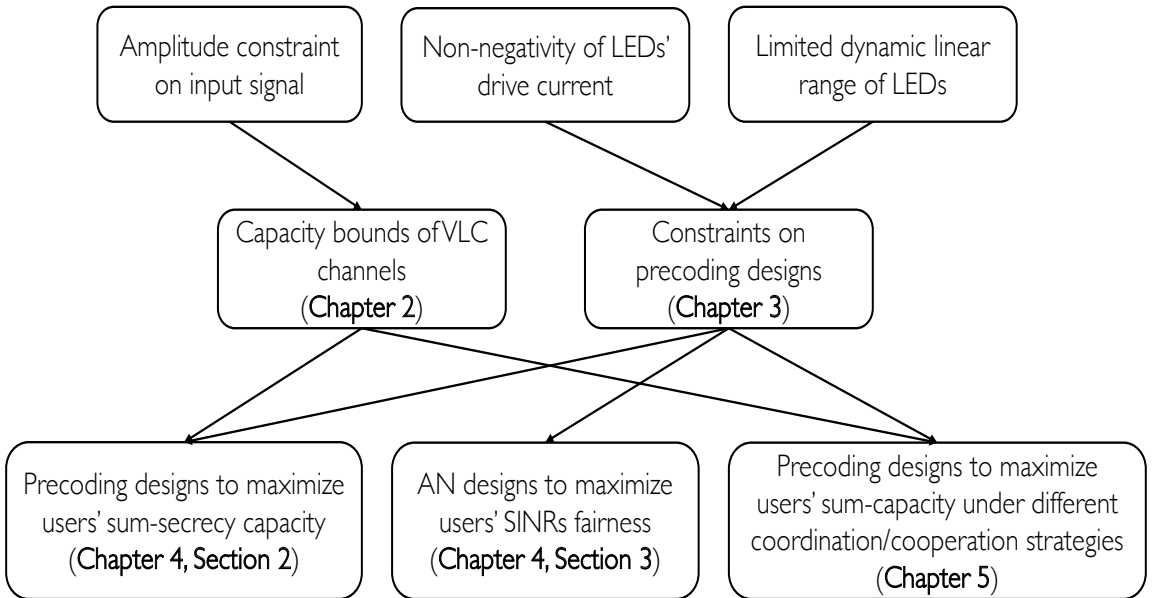


Figure 1.4: Design Framework

1.7. Thesis Organization

The reminder of the dissertation is organized into six chapters. In Chapter 2, we revisit the capacity analysis of classical scalar Gaussian channels with an amplitude constraint (i.e., peak power constraint) on the input signal for two different scenarios: with and without interferences, which are also amplitude-constrained. Due to the cumbersome in characterizing the capacities of such channels, this Chapter focuses on deriving their lower and upper bounds, which will be used as benchmarks for the precoding designs in the later parts of the dissertation. Asymptotic behaviors of the derived bounds at low and high SNR regimes are comprehensively investigated to confirm their validities. (giá trị) → ché đỗ

*Wardhiêm
còn (vì)*

Chapter 3 presents the concept of MU-MIMO VLC systems. Particularly, the broadcast transmission with linear precoding model is described in detail under unique constraints in VLC. Some common precoding techniques are also introduced in this chapter with a particular attention to the ZF precoding, which is the technique of interest in this dissertation. Chapter 4 and 5 focus on the our **key contributions** of the dissertation.

AN: artificial noise

In Chapter 4, we study the physical layer security of MU-MIMO VLC systems according to two different approaches: precoding and AN. For the precoding approach, we aim at designing optimal ZF precoding to maximize the users' secrecy sum-capacity under two scenarios: known and unknown eavesdropper's CSI at the transmitter. On the other hand, for the AN approach, the focus is on designing AN to ensure the max-min fairness of legitimate users's SINRs.

*tíng
đò
tín
để
cung cấp*

The second contribution of the dissertation is presented in Chapter 5. Firstly, the concept of multi-cell multi-user VLC network is introduced. Then, we investigate three different cell cooperation/coordination strategies and their corresponding cooperative/coordinated precoding designs, namely: per-cell coordinate precoding, coordinate precoding and partial cooperative precoding. Performances of these strategies are evaluated and compared in terms of users' sum-capacity.

*thiết kế nhiều nhân tố để đảm bảo công bằng fair
nghị định cho ứng dụng hợp lý?*

1.7 Thesis Organization

Finally, we conclude the dissertation in Chapter 6 with a summary and outlooks on the future research directions.

Chapter 2

Information Capacity of Amplitude-Constrained Scalar Gaussian Channels [61, 62]

In this chapter, we revisit the capacity of scalar Gaussian channels with an amplitude input signal constraint for two different scenarios: with and without interferences. For each scenario, simple closed-form expressions for the lower and upper bounds capacity are provided as benchmarks for the precoding designs in Chapter 4 and 5.

2.1. Amplitude-Constrained Scalar Gaussian Channels

In [60], J. G. Smith considered a scalar additive Gaussian noise channel, which is characterized by

$$Y = X + N, \quad (2.1)$$

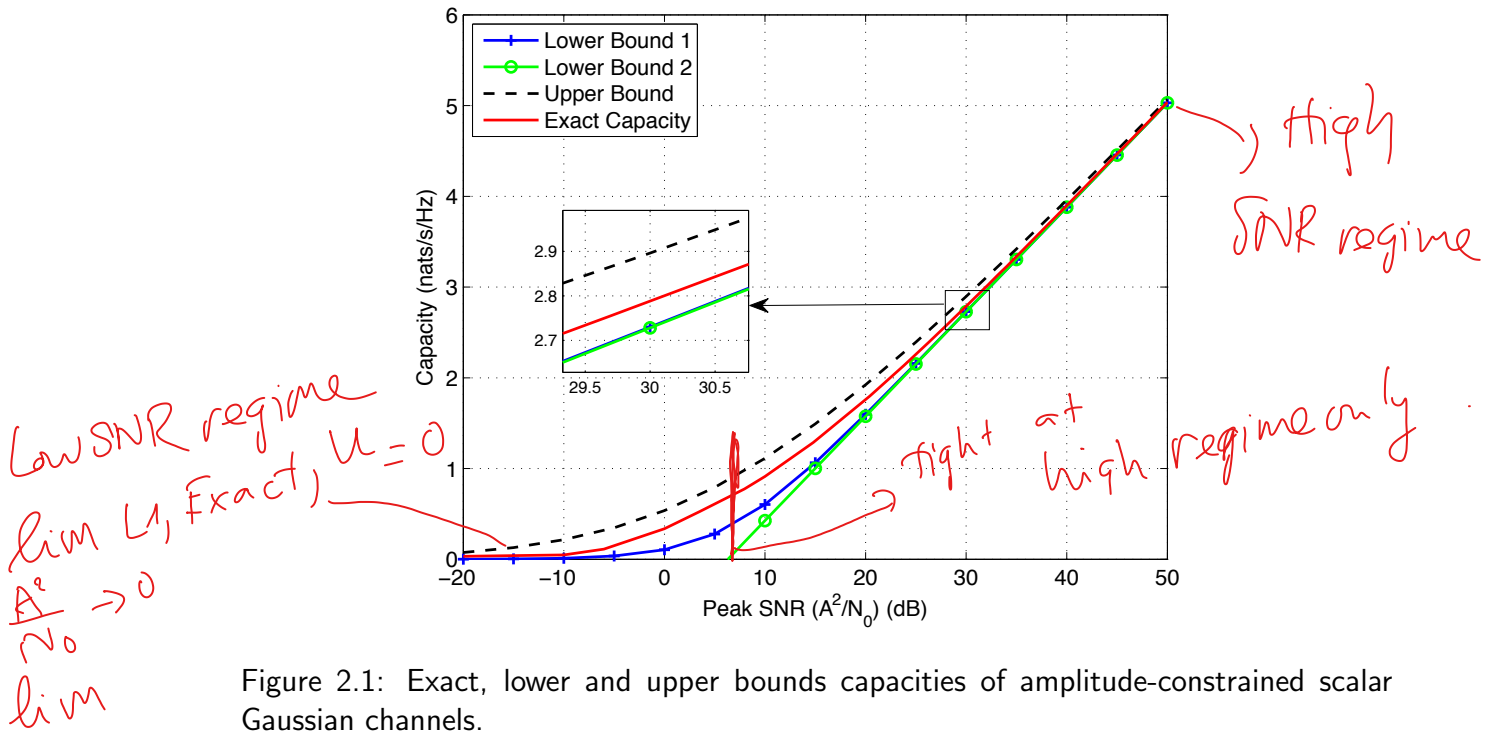


Figure 2.1: Exact, lower and upper bounds capacities of amplitude-constrained scalar Gaussian channels.

where X , N , and Y denote the channel input, noise, and output random variables, respectively. The input random variable X is assumed to be constrained to take on values on $[-A, A]$ for some arbitrary positive value of A ¹. The noise random variable N is assumed to be Gaussian with zero mean and variance N_0 . The capacity-achieving distribution of X for the channel in (2.1) is unique and discrete with a finite number of mass points. Necessary and sufficient conditions for the distribution were obtained and the capacity was computed numerically. Nevertheless, it is worth noting that the developed numerical procedure was quite computationally expensive especially for large value of $\frac{A}{N_0}$. Therefore, closed-form expressions for the capacity are of particular interest for system design purpose.

2.1.1. Lower Bound

For additive noise channels, a common way to derive a lower bound capacity is to use the Entropy Power Inequality (EPI) [59, 63] as

¹The channel in (2.1) is sometimes referred as the Gaussian channel with peak power constraint since the amplitude constraint $X < |A|$ is equivalent to the peak power constraint $X^2 < A^2$.

$$\begin{aligned}
 C_L^1 &= \mathbb{I}(X; Y) = h(Y) - h(Y|X) \\
 &= h(X + N) - h(N) \\
 &\stackrel{(EPI)}{\geq} \frac{1}{2} \log(e^{2h(X)} + e^{2h(N)}) - h(N) \\
 &= \frac{1}{2} \log\left(1 + \frac{e^{2h(X)}}{2\pi e N_0}\right). \tag{2.2}
 \end{aligned}$$

To make this bound as tight as possible, the distribution of X is chosen in such a way that it maximizes the differential entropy $h(X)$ under the amplitude constraint $X \leq |A|$. According to the maximum entropy theorem [64], it is well-known that the uniform distribution is the maximum entropy probability distribution for a random variable under no constraint other than it is contained in the distribution's support. It is thus reasonable to assume that X is uniformly distributed over $[-A, A]$, resulting in

$$C_L^1 = \frac{1}{2} \log\left(1 + \frac{2A^2}{\pi e N_0}\right). \tag{2.3}$$

From the above expression, it is straightforward to derive another lower bound by omitting the factor 1 as

$$\begin{aligned}
 C_L^2 &\geq \frac{1}{2} \log\left(1 + \frac{2A^2}{\pi e N_0}\right) > \frac{1}{2} \log\left(\frac{2A^2}{\pi e N_0}\right) \\
 &= \log\left(\frac{2A}{\sqrt{2\pi e N_0}}\right). \tag{2.4}
 \end{aligned}$$

2.1.2. Upper Bound

An upper bound for the capacity of a scalar Gaussian channel with an amplitude constraint is given by [65]

$$C_U = \max_{\alpha \in [0,1]} f(\alpha), \tag{2.5}$$

where $f(\alpha) = \alpha \log\left(\frac{2A}{\sqrt{2\pi e N_0}}\right) - \log\left(\alpha^\alpha (1-\alpha)^{\frac{3}{2}(1-\alpha)}\right)$. It is seen that $f(\alpha)$ is twice differentiable and is a concave function on its domain $\alpha \in [0, 1]$ due to the concavity of the logarithm function. Therefore, the maxima of $f(\alpha)$ can be found by finding the critical point α^* , (the point where $f'(\alpha^*) = 0$). In appendix A, we show that α^* exists and is unique. Moreover, α^* can be numerically found by using the bisection method, i.e., narrowing down the interval of α by halves over iteration by iteration [66]. With a predefined error tolerance $\nu = 10^{-3}$ and an initial interval of $[0, 1]$, α^* can be obtained after around 15 iterations.

Code cai hay

2.1.3. Numerical Example and Asymptotic Behaviors

Figure 2.1 shows the exact, the lower and the upper bounds capacity versus the peak SNR of an amplitude-constrained Gaussian channel. It is seen that the upper bound and the lower bound in (2.3) are tight at low and hight peak SNR regimes, whereas the lower bound in (2.4) is tight at high SNR region only. Obviously, for two lower bounds, $\lim_{\frac{A}{\sqrt{N_0}} \rightarrow 0} C_L^1 = 0$ and $\lim_{\frac{A}{\sqrt{N_0}} \rightarrow 0} C_L^2 = -\infty$. The following proposition proves the tightness of the upper bound at low and high peak SNR regimes.

Proposition 1. *Asymptotic behaviors of the upper bound*

$$\lim_{\frac{A}{\sqrt{N_0}} \rightarrow 0} C_U = 0, \quad (2.6)$$

$$\lim_{\frac{A}{\sqrt{N_0}} \rightarrow \infty} C_U = \log\left(\frac{2A}{\sqrt{2\pi e N_0}}\right). \quad (2.7)$$

Proof. See Appendix A.

2.2. Amplitude-Constrained Scalar Gaussian Interference Channels

In this section, we present two simple closed-form capacity bounds for a scalar Gaussian interference channel with amplitude constraints on the input signal and the interferences. Such a Gaussian interference channel with K interference sources is characterized by

$$Y = X + \sum_{i=1}^K I_i + N, \quad (2.8)$$

where X, I_i, N, Y denote the channel input, the i -th interference source, the noise, and channel output, respectively. The input X and the interference I_i are assumed to be constrained between $[-A, A]$ and $[-B_i, B_i]$, respectively, for some arbitrary positive values A, B_i . Similar to the case without interferences, the noise random variable N is assumed to be Gaussian with zero mean and variance N_0 .

2.2.1. Lower Bound

The channel capacity of (2.8) is defined as

$$\begin{aligned} C &= \max_{f_X(x)} \mathbb{I}(X; Y) \\ &= \max_{f_X(x)} h(Y) - h(Y|X) \\ &= \max_{f_X(x)} h\left(X + \sum_{i=1}^K I_i + N\right) - h\left(\sum_{i=1}^K I_i + N\right) \end{aligned} \quad (2.9)$$

Using the Entropy Power Inequality (EPI) and the inequality $h(Q) \leq \frac{1}{2} \log 2\pi e \sigma_Q^2$ for a random variable Q with its variance σ_Q^2 , a lower bound of C is given by

$$C_L = \frac{1}{2} \max_{f_X(x), f_{I_i}(i_i)} \log \left(e^{2h(X)} + \sum_{i=1}^K e^{2h(I_i)} + e^{2h(N)} \right) - \frac{1}{2} \log 2\pi e \left(\sum_{i=1}^K \sigma_{I_i}^2 + N_0 \right) \quad (2.10)$$

Following the same argument from the previous section, to make the bound as tight as possible, it is reasonable to assume that X and I_i are uniformly distributed over $[-A, A]$ and $[-B_i, B_i]$, resulting in

$$\begin{aligned} C_L &= \frac{1}{2} \log \left(4A^2 + 4 \sum_{i=1}^K B_i^2 + 2\pi e N_0 \right) - \frac{1}{2} \log 2\pi e \left(\frac{\sum_{i=1}^K B_i^2}{3} + N_0 \right) \\ &= \frac{1}{2} \log \frac{2 \left(A^2 + \sum_{i=1}^K B_i^2 \right) + \pi e N_0}{\pi e \left(\frac{\sum_{i=1}^K B_i^2}{3} + N_0 \right)}. \end{aligned} \quad (2.11)$$

It is straightforward to see that, without interferences, the above bound reduces to a lower bound in (2.3).

2.2.2. Upper Bound

Using the above mentioned entropy inequalities, an upper bound of C can be obtained from (2.9) by

$$C_U = \frac{1}{2} \log 2\pi e \left(\sigma_X^2 + \sum_{i=1}^K \sigma_{I_i}^2 + N_0 \right) - \frac{1}{2} \max_{f_{I_i}(i_i)} \log \left(\sum_{i=1}^K e^{2h(I_i)} + e^{2h(N)} \right). \quad (2.12)$$

Similar to the case of the lower bound, assume that X and I_i are uniformly distributed over $[-A, A]$ and $[-B_i, B_i]$, respectively. As a result, C_U is given by

$$\begin{aligned} C_U &= \frac{1}{2} \log 2\pi e \left(\frac{A^2 + \sum_{i=1}^K B_i^2}{3} + N_0 \right) - \frac{1}{2} \log \left(4 \sum_{i=1}^K B_i^2 + 2\pi e N_0 \right) \\ &= \frac{1}{2} \log \frac{\pi e \left(\frac{A^2 + \sum_{i=1}^K B_i^2}{3} + N_0 \right)}{2 \left(\sum_{i=1}^K B_i^2 \right) + \pi e N_0}. \end{aligned} \quad (2.13)$$

Without interference, the above upper bound reduces to

$$C_U^o = \frac{1}{2} \log \left(1 + \frac{A^2}{3N_0} \right). \quad (2.14)$$

2.2.3. Numerical Example and Asymptotic Behaviors

Figure 2.2 shows the lower and upper capacity bounds of the amplitude constrained

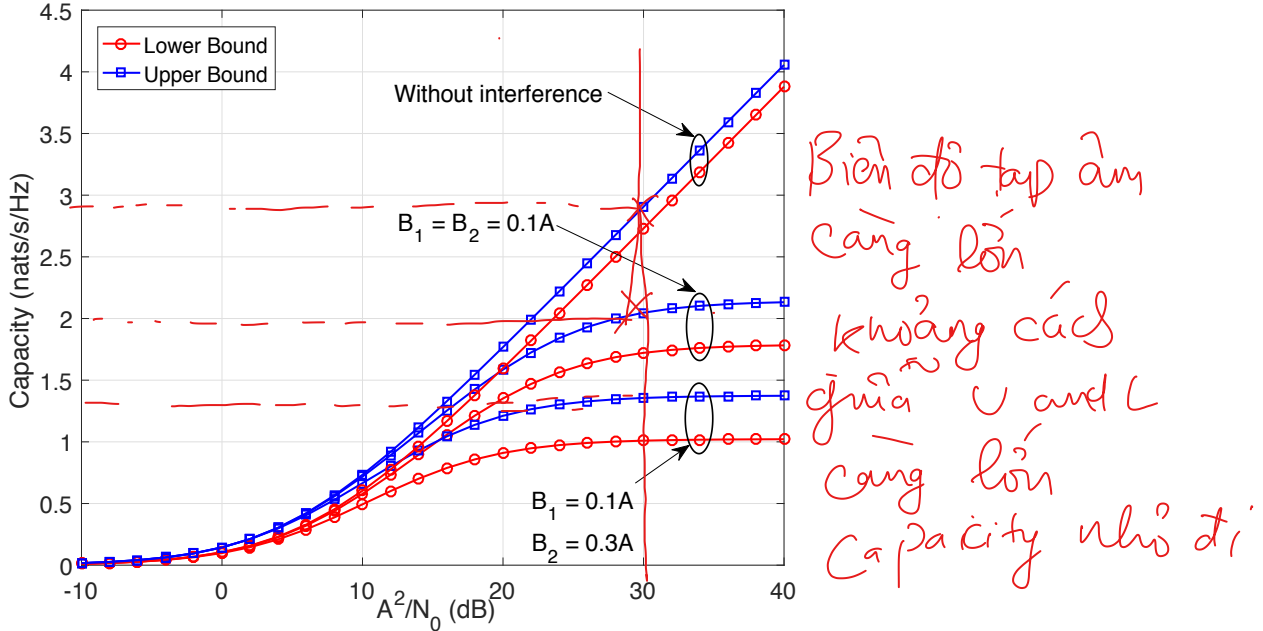


Figure 2.2: Lower and upper capacity bounds of amplitude constrained interference channels.

interference channels for $K = 2$ with different levels of interference power. It can be seen that the gap between the lower and upper bounds is relatively small in the case of no interference. Specifically, it is straightforward to see that

$$\lim_{\frac{A}{\sqrt{N_0}} \rightarrow 0} (C_U^o - C_L^o) = 0, \quad (2.15)$$

and

$$\lim_{\frac{A}{\sqrt{N_0}} \rightarrow \infty} (C_U^o - C_L^o) = \frac{1}{2} \log \left(\frac{\pi e}{6} \right) \approx 0.1765 \text{ nats}. \quad (2.16)$$

In general, let us assume that the interferences are proportional to the input power, i.e., $B_i = \alpha_i A$ for some $\alpha_i > 0$. This assumption is generally valid in multi-user broadcast systems, where the interferences seen by a user are the transmitted signals

nhiều tần số với cát và

for other users. Therefore, we can prove following asymptotic properties

$$\lim_{\frac{A}{\sqrt{N_0}} \rightarrow 0} (C_U - C_L) = 0, \quad (2.17)$$

and,

$$\lim_{\frac{A}{\sqrt{N_0}} \rightarrow \infty} (C_U - C_L) = \log \left(\frac{\pi e}{6} \right) \approx 0.353 \text{ nats}, \quad (2.18)$$

which are constant regardless of the interference power.

Chapter 3

Multi-user MIMO Visible Light Communications and Linear Precoding [61]

3.1. Introduction

Similar to other wireless technologies, supporting multiple users is an inevitable evolution of VLC systems. Figure 3.1 depicts a geographical configuration of a typical MU-MIMO VLC system, which comprises 4 LED arrays (i.e., LED transmitters) and 2 decentralized users. The signal processing is assumed to be done at a central processing unit (CPU), which is connected to the LED transmitters by wired connections, such as Ethernet, fiber or power-line communications. This configuration can also be regarded as a *coordinated multipoint* (CoMP) system for VLC communications [57]. The presence of multiple users, however, introduces the so-called multi-user interference (MUI), which can considerably degrade the system performance. Hence, research on MU VLC systems mainly focuses on methods to alleviate the MUI. It is generally challenging to deal with the MUI since there is usually no coordination among them. Hence, reducing the negative impact of MUI should be done at the transmitter. The

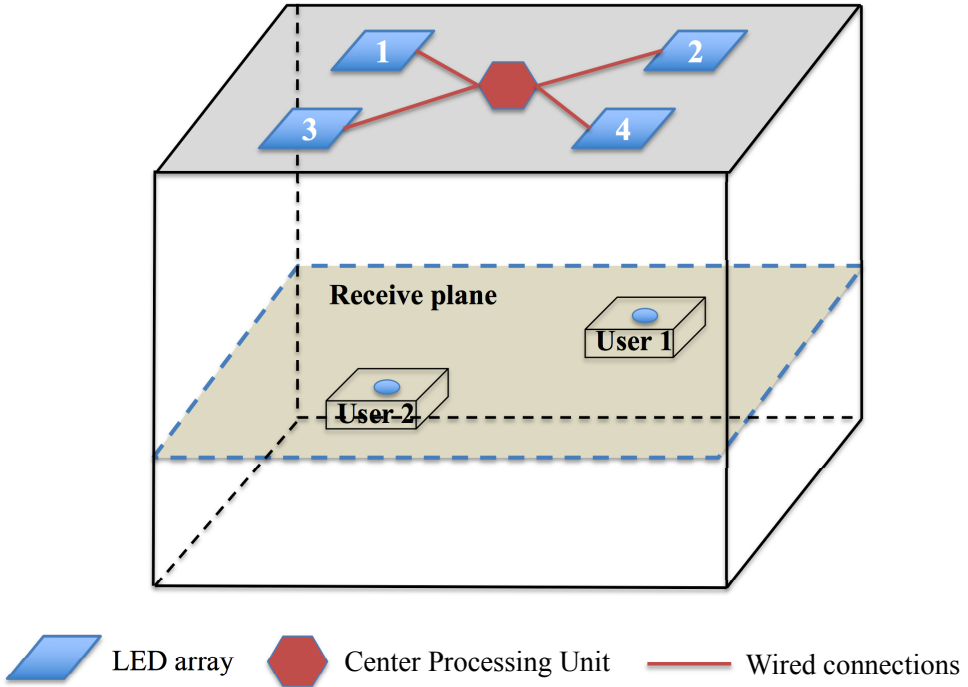


Figure 3.1: A geographical configuration of an MU-MIMO VLC system.

inherent MIMO configuration of indoor VLC systems introduces a spatial degrees of freedom, which can be utilized to support multiple users by means of precoding techniques. The fundamental idea of precoding is to pre-process the transmit signal based on the knowledge of user's CSI at the transmitters. Precoding techniques for RF broadcast channels have been extensively investigated [56, 67–71]. Nevertheless, adoption of those techniques for VLC is not straightforward because the RF signal is complex-valued, which is fundamentally different from the real and non-negative VLC signal.

This chapter focuses on linear precoding techniques for MU-MIMO VLC with a particular attention to ZF precoding thanks its simplicity and high performance at high SNR region. Since precoding designs require an availability of users' CSI at the transmitters, we assume throughout this dissertation that users' CSI are perfectly known at the transmitters through an uplink feedback (e.g., Wi-Fi). Practical constraints on the precoding design due to unique constraints of VLC are also described.

3.2. Linear Precoding for Multi-user MIMO Visible Light Communications

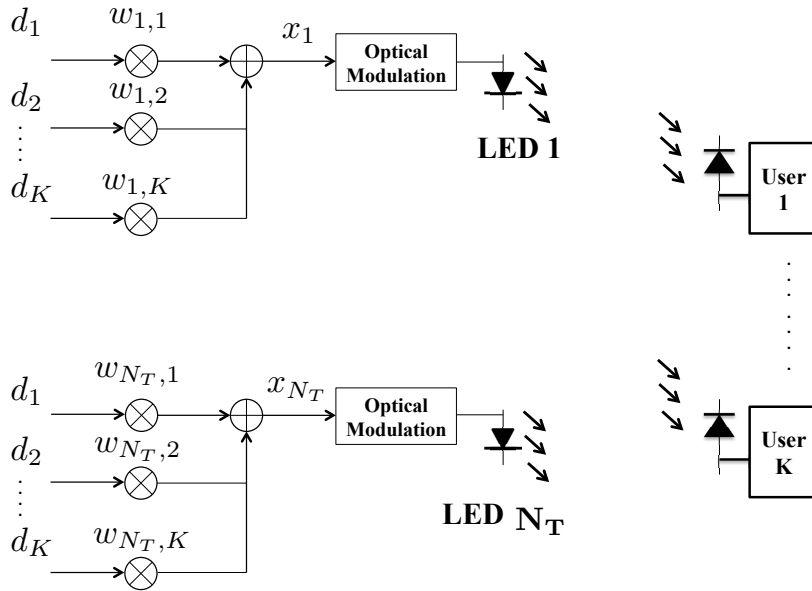


Figure 3.2: A schematic diagram of an MU-MIMO VLC system.

Figure 3.2 illustrates a schematic diagram of an MU-MIMO VLC system with N_T LED arrays as transmitters and K decentralized single-PD users. The N_T LED arrays cooperate to broadcast information to K users simultaneously. In our study, a direct current (DC)-biased Pulse Amplitude Modulation (PAM) scheme is employed. In such scheme, a DC bias current $I_{DC} \in \mathbb{R}_+$ which determines the brightness of the LEDs, is used to modulate a zero-mean data signal. Let $d_i \in \mathbb{R}$ be the data symbol intended for the i -th user, and $\mathbf{d} = [d_1 \ d_2 \ \dots \ d_K]^T \in \mathbb{R}^{K \times 1}$ be the data vector for all users. It is assumed that d_i is zero-mean, and without loss of generality, is normalized to the range of $[-1, 1]$. At the k -th LED array, the broadcast signal s_k which consists of data signals for all users, is generated from a linear combination of the data vector and the matrix $\mathbf{V}_k = [w_{k,1} \ w_{k,2} \ \dots \ w_{k,K}] \in \mathbb{R}^{1 \times K}$ as

$$s_k = \mathbf{V}_k \mathbf{d}, \quad (3.1)$$

As a result, the transmitted signal x_k can be expressed in the form of

$$x_k = s_k + I_{\text{DC}}^k, \quad (3.2)$$

where I_{DC}^k denotes the DC-bias for the k -th LED array. Since $\mathbb{E}[d_k] = 0$, the signal s_k does not affect the average illumination level of the LEDs. Instead, it is uniquely determined by the DC-bias I_{DC}^k . If we define $\mathbf{x} = [x_1 \ x_2 \ \dots \ x_K]^T \in \mathbb{R}^{K \times 1}$ as the transmitted signal vector and $\mathbf{I}_{\text{DC}} = [I_{\text{DC}}^1 \ I_{\text{DC}}^2 \ \dots \ I_{\text{DC}}^K]^T \in \mathbb{R}^{K \times 1}$ as the aggregate DC bias vector, the received optical signal at the k -th user can be written as

$$P_r^k = \mathbf{H}_k \mathbf{P}_s, \quad (3.3)$$

where $\mathbf{H}_k \in \mathbb{R}^{1 \times N_T}$ is the channel matrix between LED arrays and the k -th user

$$\mathbf{H}_k = [h_{k1} \ h_{k2} \ \dots \ h_{kN_T}], \quad (3.4)$$

where h_{ki} represents the channel response between the k -th user and the i -th LED array and is given in (1.3). $\mathbf{P}_s = [P_s^1 \ P_s^2 \ \dots \ P_s^{N_T}]^T \in \mathbb{R}^{N_T \times 1}$ is the transmitted optical power vector of the LED arrays whose element $P_s^k = \eta x_k$ is the transmitted optical power of the k -th LED arrays with η is the LED conversion factor. The received electrical signal at the k -th user after the optical-electrical conversion is therefore given by

$$\begin{aligned} y_k &= \gamma P_r^k + n_k = \gamma \eta \mathbf{H}_k \mathbf{x} + n_k \\ &= \gamma \eta \left(\mathbf{H}_k \mathbf{W}_k d_k + \mathbf{H}_k \sum_{i=1, i \neq k}^K \mathbf{W}_i d_i + \mathbf{H}_k \mathbf{I}_{\text{DC}} \right) + n_k, \end{aligned} \quad (3.5)$$

with γ is the PD responsivity, $\mathbf{W}_k = [w_{1,k} \ w_{2,k} \ \dots \ w_{N_T,k}]^T \in \mathbb{R}^{N_T \times 1}$ is the precoder for the k -th user. If we define $\mathbf{W} = [\mathbf{W}_1 \ \mathbf{W}_2 \ \dots \ \mathbf{W}_K]^T \in \mathbb{R}^{N_T \times K}$, it can be seen that \mathbf{W} can also be represented as $\mathbf{W} = [\mathbf{V}_1 \ \mathbf{V}_2 \ \dots \ \mathbf{V}_{N_T}]^T$, where

the k -th row vector is the *precoder* for the k -th LED array.

As seen in (5.6), the first term $\mathbf{H}_k \mathbf{W}_k d_k$ is the desired signal, while the second term $\mathbf{H}_k \sum_{i=1, i \neq k}^K \mathbf{W}_i d_i$ is the MUI. The third term $\mathbf{H}_k \mathbf{I}_{\text{DC}}$ represents the DC current for defining the illumination that carries no data and n_k denotes the receiver noise, which is assumed to be AWGN with zero mean and variance σ_k^2 , given by [37, 72]

$$\sigma_k^2 = 2e\overline{P_r^k}B + 4\pi e A_r \gamma \chi_{\text{amb}} (1 - \cos(\Psi_c)) B + i_{\text{amb}}^2 B, \quad (3.6)$$

where e is the elementary charge, B denotes the system bandwidth and $\overline{P_r^k} = \mathbb{E}[P_r^k] = \eta \mathbf{H}_k \mathbf{I}_{\text{DC}}$ is the average received optical power at the k -th user. i_{amp}^2 is the pre-amplifier noise current density, χ_{amp} is the ambient light photocurrent. After removing the DC term by Alternating Current (AC) coupling, the received signal can be written by

$$y_k = \gamma \eta \left(\mathbf{H}_k \mathbf{W}_k d_k + \mathbf{H}_k \sum_{i=1, i \neq k}^K \mathbf{W}_i d_i \right) + n_k. \quad (3.7)$$

3.2.1. Matched Filter Precoding

The matched filter (MF) precoder is simply a conjugate transpose of \mathbf{H}_k . In case of VLC, as \mathbf{H}_k is a real matrix, its conjugate transpose is identical to its transpose. The MF precoder is thus given by

$$0 \leq h_{k,i} \leq 1$$

$$\mathbf{W}_k = \mathbf{H}_k^T. \quad (3.8)$$

Substituting \mathbf{W}_k from (3.8) to (3.7), the received signal at the k -th user is written as $\mathbf{H}_k \cdot \mathbf{H}_k^T = [\mathbf{h}_{k,1} \ \mathbf{h}_{k,2} \dots \ \mathbf{h}_{k,N_T}] \cdot \begin{bmatrix} h_{k,1} \\ \vdots \\ h_{k,N_T} \end{bmatrix} = \|\mathbf{H}_k\|_2^2$

$$y_k = \gamma \eta \left(\mathbf{H}_k \mathbf{H}_k^T d_k + \mathbf{H}_k \sum_{i=1, i \neq k}^K \mathbf{H}_i^T d_i \right) + n_k. \Rightarrow y_k = \gamma n \|\mathbf{H}_k\|_2^2 \quad (3.9)$$

The MF precoding is known as the maximum ratio transmission, which maximizes the signal gain at the intended users [73, 74]. It is also known that MF precoding

performs very well when the number of transmitters is getting larger and is much greater the number of users [75].

3.2.2. Zero-Forcing Precoding

The ZF precoding algorithm aims to completely remove the MUI via the construction of the precoder \mathbf{W}_i in such a way that it is orthogonal to channel matrices of other users, that is

$$\mathbf{H}_k \mathbf{W}_i = 0, \quad \forall k \neq i. \quad (3.10)$$

In other words, if we define $\mathbf{H} = \begin{bmatrix} \mathbf{H}_1^T & \mathbf{H}_2^T & \dots & \mathbf{H}_K^T \end{bmatrix}^T$ as an aggregate channel matrix, the ZF constraint in (3.10) implies that

$$\mathbf{H}\mathbf{W} = \begin{bmatrix} \sqrt{q_1} & & & \\ & \sqrt{q_2} & & \\ & & \ddots & \\ & & & \sqrt{q_K} \end{bmatrix} = \text{diag}\{\sqrt{\mathbf{q}}\}, \quad (3.11)$$

where $\sqrt{\mathbf{q}} = \begin{bmatrix} \sqrt{q_1} & \sqrt{q_2} & \dots & \sqrt{q_K} \end{bmatrix}^T \in \mathbb{R}^{K \times 1}$ whose i -th element represents the channel gain of the i -th user. We thus can express \mathbf{W} in the form

$$\mathbf{W} = \mathbf{H}^{-} \text{diag}\{\sqrt{\mathbf{q}}\}, \quad (3.12)$$

where \mathbf{H}^{-} denotes the generalized inverse of \mathbf{H} , which can be any matrix that satisfies $\mathbf{H}\mathbf{H}^{-}\mathbf{H} = \mathbf{H}$. Generally, the generalized inverse \mathbf{H}^{-} is not unique. One of the special generalized inverse is the pseudo-inverse $\mathbf{H}^{\dagger} = \mathbf{H}^T(\mathbf{H}\mathbf{H}^T)^{-1}$, which is known to have minimal Frobenius norm among all the generalized inverses. Different from RF systems where the pseudo-inverse is the optimum precoder under the total average power constraint [70], for VLC systems, it is not necessary to be the optimal solution under amplitude constraint of VLC signals. Assume that \mathbf{H} is full row-rank, any

generalized inverse \mathbf{H}^- can be expressed by

$$\checkmark \quad \mathbf{H}^- = \mathbf{H}^\dagger + \mathbf{PQ}, \checkmark \quad (3.13)$$

where $\mathbf{P} = \mathbf{I} - \mathbf{H}^\dagger \mathbf{H}$ is the orthogonal projection onto the null space of \mathbf{H} and, \mathbf{Q} is an arbitrary matrix. Plugging (3.13) into (3.12), the general structure of any ZF precoding matrix \mathbf{W} is given by

Why \sqrt{q} ? instead q

$$\mathbf{W} = [\mathbf{H}^\dagger + \mathbf{PQ}] \text{diag}\{\sqrt{q}\}. \quad (3.14)$$

This reduces the beamformer design problem for a certain performance metric to an optimization problem with respect to the \mathbf{q} and the choice of generalized inverse \mathbf{H}^- via \mathbf{Q} .

beamformer design \rightarrow optimization { q | H }

3.2.3. Regularized Zero-Forcing Precoding [70]: Wiesel

The ZF precoding is known to achieve high performance at high SNR regime or when the number of users is sufficiently large [70]. However, it performs poorly when \mathbf{H} is ill-conditioned. The regularized zero-forcing (RZF) precoding is designed to overcome this disadvantage of the ZF. According to [67], the RZF precoder is given by

$$\mathbf{W} = \mathbf{H}^T (\mathbf{H} \mathbf{H}^T + \lambda \mathbf{I}_K)^{-1}, \quad (3.15)$$

*độc bai RZF
control như nào?*

where λ is the regularization vector, which controls the amount of interference among users.

The RZF can be considered as a generalization of MF and ZF schemes. It is seen that when $\lambda \rightarrow 0$, (3.15) becomes a pseudo-inverse ZF. On the other hand, a MF precoder can be obtained by setting $\lambda \rightarrow \infty$. More importantly, even when \mathbf{H} is ill-conditioned, the inverse in (3.15) can be made to behave as well as desired by choosing λ large enough.

Match filter

3.3. Optical Power Constraints (Done)

In this section, we briefly illustrate the amplitude constraint on VLC input signals,

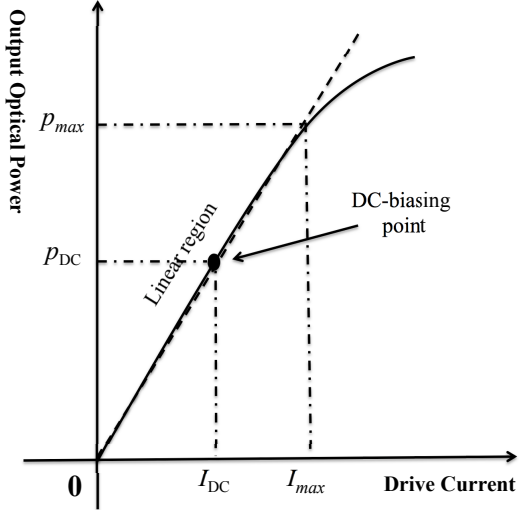


Figure 3.3: Nonlinear LED transfer characteristic.

which is fundamentally different from their RF counterpart. It should be noted that the constraint, in turn, affects significantly the precoder designs. As shown in Fig. 3.3, the LEDs exhibit a limited linear range, where the output optical power increases linearly from 0 to p_{max} in accordance with the input drive current from 0 to I_{max} . Hence, to guarantee normal operation of the LEDs, i.e., to avoid the overheating of the LEDs and the potential light intensity reduction, the drive current x_k for the k -th LED array must be constrained within the range of $[0, I_{max}]$ as

$$0 \leq s_k + I_{DC}^k \leq I_{max}. \quad (3.16)$$

From (3.1) and since $|d_k| \leq 1$, we get

$$-\|\mathbf{V}_k\|_1 \leq s_k \leq \|\mathbf{V}_k\|_1. \quad (3.17)$$

To ensure both (3.16) and (3.17), the following constraint should be imposed

$$\|\mathbf{V}_k\|_1 \leq \Delta_k, \quad (3.18)$$

where $\Delta_k = \min(I_{\text{DC}}^k, I_{\max} - I_{\text{DC}}^k)$. We can write the above constraint with respect to \mathbf{W}_i or \mathbf{W} as

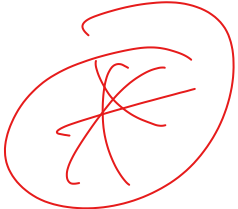
$$\sum_{i=1}^K \|[\mathbf{W}_i]_{k,:}\|_1 \leq \Delta_k, \quad (3.19)$$

or

$$\|[\mathbf{W}]_{k,:}\|_1 \leq \Delta_k. \quad (3.20)$$

In this dissertation, depending on the targeted performance metric, either the expression in (3.19) or (3.20) will be considered in the design of the optimal precoding matrices.

Chapter 4



Physical Layer Security in Multi-user MIMO Visible Light Communications [76, 77]

4.1. Introduction

In today's digital world, security and privacy are becoming two of the most important aspects of any communications systems. In wireless communications, the broadcast nature of wireless signals makes eavesdropping a possible threat as it is difficult to shield the transmitted signals from unintended users. Traditionally, in computer networking, the security of data transmission is performed at network and transport layers by means of key-based cryptographic techniques. Generally, key-based cryptography is divided into two categories: symmetric and asymmetric crypto-systems. The dynamic nature of wireless networks, however, poses difficulty in key distribution of symmetric crypto-system and computational complexity of asymmetric crypto-system. Moreover, all cryptographic algorithms work on an unproven premise that they can not be deciphered without the knowledge of the secret key in a reasonable time. With the advances in hardware and computational power, ciphers which were

believed to be unbreakable in the past are showing their vulnerabilities under various attacks. As a result, these drawbacks of traditional key-based cryptography has motivated research on new approaches for security in communications systems. In particular, security at physical layer (also known as physical layer security) has been emerging as a powerful measure over the past decade or so.

4.1.1. Physical Layer Security

Fundamentally different from security at upper layers, physical layer security exploits the randomness of noise and transmission media to prevent the transmitted information from being eavesdropped by malicious users. Most importantly, a perfect secrecy can be achieved regardless the computational power of the eavesdroppers or their network parameter knowledge. The foundational work on physical layer secu-

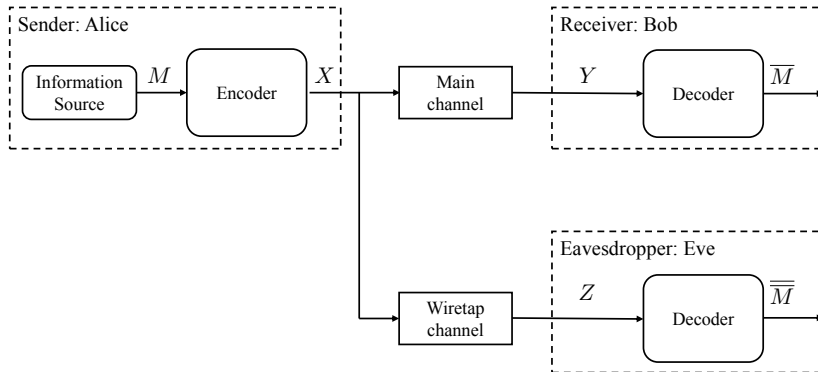


Figure 4.1: The wiretap channel [78] with three parties: a sender (Alice), a legitimate user (Bob) and an eavesdropper (Eve).

rity by A. D. Wyner introduced the concept of wiretap channel, which consists of a sender (Alice), a legitimate user (Bob) and an eavesdropper (Eve) as illustrated in Fig. (4.1) [78]. Here, Alice encodes her confidential message M to the information signal X , which is then transmitted to Bob wirelessly. Bob receives the transmitted signal X from Alice as Y , which is decoded to get an estimate message \bar{M} . The signal X is also observed as Z by Eve, who decodes it to get her own estimate message $\bar{\bar{M}}$. Under the assumption that the transmitter-eavesdropper channel (i.e., the wiretap channel) is a degraded version of the transmitter-legitimate user's one (i.e., the main channel), Wyner proved that it is possible to transmit the information signal X at a

positive data-rate R_s at which the eavesdropper is not able to extract any information from its received signal. R_s is termed as *secrecy capacity* or *secrecy rate* and is the fundamental performance metric in physical layer security. Then, subsequent works mainly focused on characterizing the secrecy capacity for different channel models and system configurations [79–87]. Specifically for the Gaussian channel, the secrecy capacity is shown to be the difference between the capacity of the main channel and that of the wiretap channels [80].

4.1.2. Physical Layer Security in Visible Light Communications

VLC has been considered to be inherently more secure than its RF counterpart due to the confinement of visible light by opaque surfaces. Nonetheless, the threat of eavesdropping is still visible especially in the scenario of large-scale VLC networks. Therefore, together with performance improvement, security enhancement is also an important criteria in designing MU VLC systems.

Compared to the extensive study on physical layer security in RF communications, there are only a few studies in VLC systems, which can be classified into two categories: single transmitter and multi-transmitter. Regarding the single transmitter configuration, a comprehensive analysis on the secrecy capacity was reported in [88] for the traditional wiretap channel (i.e., one transmitter, one legitimate user and one eavesdropper). For a scenario of multi-user multi-eavesdropper, the authors in [89] investigated the use of non-orthogonal multiple access (NOMA) as the method to improve the secrecy outage probability (SOP) performance. When multiple transmitter are deployed, their spatial degrees of freedom enables the use of precoding and AN in improving the secrecy capacity. On one hand, precoding techniques exploit the available spatial dimensions to improve users' capacity while controlling the capacity of the eavesdropper's channel (in case the transmitter has some knowledge of the eavesdropper's CSI). On the other hand, the AN technique is useful when the eavesdropper's CSI is unknown to the transmitter. the AN is created by the transmitter in

(Artificial
noise)

the hope that it degrades the eavesdropper's channel as much as possible while interfere the legitimate user's channel as little as possible. For a special scenario wherein a massive number, e.g., few thousands, of LEDs are deployed, an approach called *pattern synthesis* was proposed in [90]. By exploiting the excessive spatial degrees of freedom offered by the large number of LEDs and defining an insecurity zone, it is possible to shape a radiation pattern whose the main lobe is directed towards the legitimate user while achieving arbitrary small signal everywhere outside the insecurity zone.

In this dissertation, we focus on both precoding and AN approaches for physical layer security in MU-MIMO VLC systems with the presence of an eavesdropper. Specifically, precoding design aims at maximizing users' secrecy sum-capacity whereas the AN is designed with respect to the max-min fairness criterion of legitimate users' SINRs. It should be noted that the analyses in this dissertation can be readily extended to the case of multiple non-colluding eavesdroppers.

Signal to Interference plus noise Ratio

4.2. Precoding Design

4.2.1. Motivations and Objectives

In [91, 92], the typical wiretap channel, i.e., one legitimate user and one eavesdropper, was examined in the context of VLC channels. These studies utilized linear precoding approaches to improve the secrecy rate performance. Upper and lower bounds for the secrecy rate of single-input single-output (SISO) configuration were first derived as benchmarks. For MISO systems, ZF precoding was adopted to zero-force eavesdropper's reception and an achievable secrecy rate was obtained for both cases of perfect and imperfect CSI. The authors in [95] considered a more general configuration by examining an arbitrary number of eavesdroppers. The precoding strategy again was used. In addition to the precoding approach, *artificial noise* is another method to increase security level. Jamming signal, i.e., artificial noise, which causes no interference

X R_s

to the legitimate user is added to the transmitted signal for degrading eavesdropper's reception, thus increasing the secrecy rate. It should be noted that the input distribution of the jamming signal impacts considerably on the overall secrecy performance. Specifically, the uniform distribution was investigate in [93, 94]. On the other hand, the studies in [96, 97], respectively, showed that using the truncated Gaussian or the truncated generalized normal distribution for jamming signal can achieve better secrecy rate. It should be noted that previous studies mainly focused on the scenario of single legitimate user. Only the study in [90] considered the MU VLC systems, however, with the aforementioned special LEDs setup, and the confidentiality among users was also ignored.

In this study, we therefore focus on physical layer security issue in MU-MIMO VLC systems with confidential messages, i.e., messages among users must be kept confidential from each other and also from the eavesdropper. To achieve the goal of confidentiality among users, ZF precoding technique is adopted due to its computational advantage and very good performance at high SNR region. For this multiple legitimate user configuration, we are interested in characterizing the achievable secrecy sum-rate under the confidential message constraint. Specifically, we investigate lower bounds on the secrecy sum-rate of users for both cases of known and unknown eavesdropper's CSI at the transmitter based on the channel capacity bounds developed in Chapter 2. Based on the derived bound, the maximum secrecy sum-rate problems for two different scenarios: known and unknown eavesdropper's CSI at the transmitter, are then formulated as convex optimization problems, which can be solved efficiently by using standard optimization packages. Numerical results show that a positive secrecy sum-rate can always be achieved for the two scenarios, thus revealing that a completely secured communication between the transmitter and multiple users could be guaranteed with proper ZF precoding designs. Furthermore, it is found that due to the impact of channel correlation on the design of ZF precoding matrix, the position of eavesdropper has a significant effect on the secrecy performance.

4.2.2. System Model

Fig. 4.2 illustrates the schematic diagram of a MU-MISO VLC system with N_T

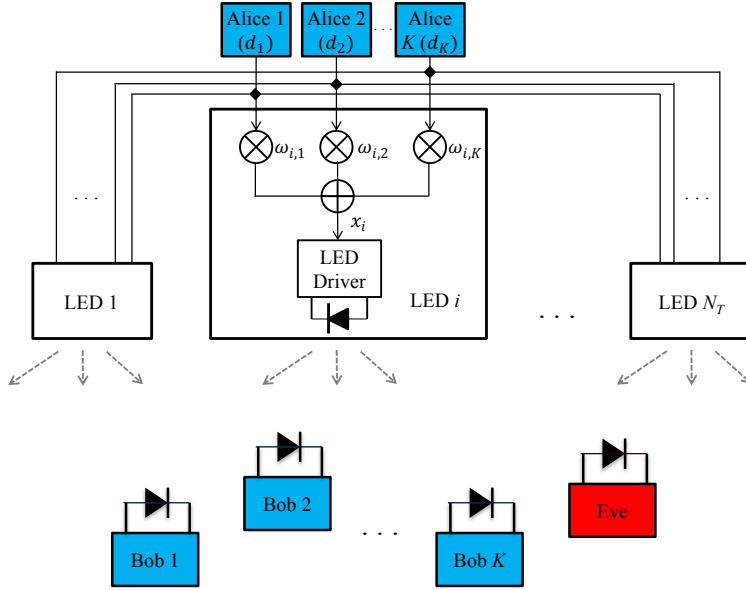


Figure 4.2: MU-MISO VLC system with N_T LED arrays for K non-cooperative legitimate pairs of user (Alice and Bob) with mutual confidentiality, and one Eavesdropper (Eve).

LED arrays (transmitting units) for K non-cooperative legitimate pairs of user (Alice and Bob) with mutual confidentiality, and one Eavesdropper (Eve). The system is generally identical with that described in Chapter 3 except the presence of Eve, who can be an active or a passive eavesdropper. Accordingly, Eve's CSI can be known and unknown to the transmitter. Following the notations in Chapter 3, we denote $\mathbf{H}_k \in \mathbb{R}^{1 \times N_T}$ and $\mathbf{H}_e \in \mathbb{R}^{1 \times N_T}$ as the channel matrices of the k -th user and Eve, respectively. Additionally, $\mathbf{W}_k \in \mathbb{R}^{N_T \times 1}$ is the ZF precoder for the k -th user. From (3.7), the received signals at the k -th user and Eve are given by

$$y_k = \gamma \eta \mathbf{H}_k \mathbf{W}_k d_k + n_k. \quad (4.1)$$

and

$$y_e = \gamma \eta \mathbf{H}_e \sum_{i=1}^K \mathbf{W}_i d_i + n_e, \quad (4.2)$$

4.2.3. Bound on Secrecy Sum-Capacity

In this section, we derive lower bounds on the secrecy sum-rate of the considered system for two scenarios: known and unknown eavesdropper's CSI \mathbf{H}_e at the transmitter. First, we define the secrecy sum-rate as a summation of the secrecy rates $C_{s,k}$ of all users, i.e.,

$$C_s \triangleq \sum_{i=1}^K C_{s,k} = \sum_{i=1}^K (C_k - C_{e,k}) = C_u - C_e, \quad (4.3)$$

where C_k is the rate of the k -th user and $C_{e,k}$ is the rate of the eavesdropper for the message d_k eavesdropping on the k -th user. Therefore, $C_u = \sum_{i=1}^K C_k$ is the sum rate of legitimate users and $C_e = \sum_{i=1}^K C_{e,k}$ is the sum rate of eavesdropper for the messages eavesdropping on all legitimate users.

For the rates of legitimate users, let us define $r_k = \gamma\eta\mathbf{H}_k\mathbf{W}_k d_k$, then Eq. (4.1) is rewritten as

$$y_k = r_k + n_k, \quad (4.4)$$

where r_k is constrained within $[-\gamma\eta\mathbf{H}_k\mathbf{W}_k, \gamma\eta\mathbf{H}_k\mathbf{W}_k]$. It is seem that (4.4) is an amplitude-constrained scalar Gaussian channel. Thus, the derived capacity bounds in Chapter 3 Section 2.1 can be applied for (4.4). However, as illustrated in Fig. 2.1, at the high SNR region (e.g., > 25 dB), the lower bound (2.4) is sufficient to characterize the the channel capacity due to a negligible gap between it and the exact capacity. As will be numerically showed in the later part, the condition of high users' SNR can always be achieved under our considered setup, making (2.4) valid to use. Thus, a lower bound on the rate of the channel (4.4) is given by

$$(2.4) \quad C_L^2 = \log \left(\frac{2A}{\sqrt{2\pi e N_0}} \right) C_k = \frac{1}{2} \log \left(\frac{2(\gamma\eta)^2 \mathbf{H}_k \mathbf{W}_k \mathbf{W}_k^T \mathbf{H}_k^T}{\pi e \sigma_k^2} \right) = \log (2\gamma\eta\mathbf{H}_k\mathbf{W}_k) - \log \left(\sqrt{2\pi e \sigma_k^2} \right). \quad (4.5)$$

4.2.4. Known \mathbf{H}_e

It is generally unrealistic to assume that eavesdropper's CSI is known to the transmitter since the eavesdropper is usually a malicious user who does not register on the network. However, the assumption of known eavesdropper's CSI still needs to be taken into account as it provides an upper bound on the secrecy performance compared with more reasonable scenarios. If \mathbf{H}_e is perfectly known to the transmitter, the ZF precoding can be applied to eliminate eavesdropper's reception. As a result, the communication between transmitter and legitimate users can be ensured to be completely secured. When the eavesdropper's reception is forced to zero, i.e., $C_e = 0$, any achievable rate of legitimate users is indeed the secrecy rate of the system. In other words, the secrecy sum-rate in this case is the achievable sum-rate of all users.

Using the bound in (4.5), the maximum secrecy sum-rate problem is given by

$$\begin{aligned} \mathcal{P}4.1 : \quad & \underset{\mathbf{W}_k}{\text{maximize}} \quad \sum_{i=1}^K \log (2\gamma\eta\mathbf{H}_k\mathbf{W}_k) - \log \left(\sqrt{2\pi e\sigma_k^2} \right) \\ & \text{subject to} \quad \mathbf{H}_i\mathbf{W}_k = 0 \quad \forall k \neq i, \\ & \quad \mathbf{H}_e\mathbf{W}_k = 0 \quad \forall k, \\ & \quad \sum_{i=1}^K \|[\mathbf{W}_i]_{k,:}\|_1 \leq \Delta_k \quad \forall k = 1, 2, \dots, N_T. \end{aligned} \tag{4.6}$$

It can be seen that the above problem is a standard determinant maximization (MAXDET) program subject to linear matrix inequalities [99]. This problem is convex and thus can be solved efficiently using standard optimization packages [100], [101].

4.2.5. Unknown \mathbf{H}_e

In practical scenarios when \mathbf{H}_e is completely unknown to the transmitter, e.g., a passive eavesdropper, it is generally impossible to suppress eavesdropper's reception. Therefore, the ZF technique is utilized for legitimate users only to guarantee confidential message transmission and to increase the achievable sum-rate, thus enhancing

the secrecy sum-rate as well. The secrecy sum-rate is then derived from the difference between C_u and C_e as in Eq. (4.3)

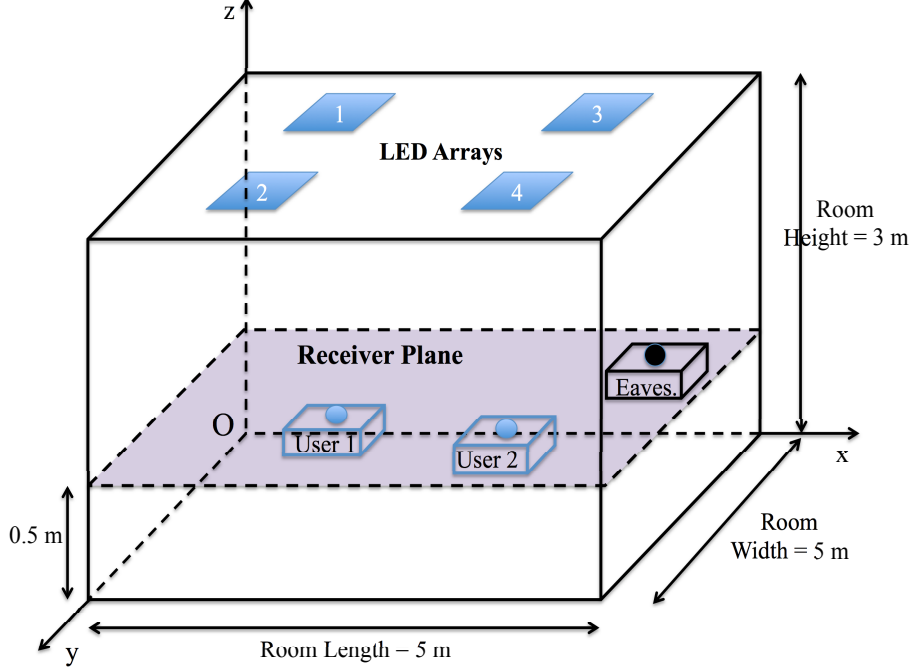


Figure 4.3: A geometrical configuration of the considered MU-MIMO VLC wiretap channel.

Theorem 1: A lower bound on the maximum secrecy sum-rate in this scenario is $\max(C_s, 0)$ where C_s is given by

$$C_s = C_u - C_e, \quad (4.7)$$

where C_u is the achievable sum-rate of legitimate users under ZF constraints, which is the solution to

$$\begin{aligned} \mathcal{P}4.2 : \quad & \underset{\mathbf{W}_k}{\text{maximize}} \quad \sum_{i=1}^K \log \left(2\gamma\eta \mathbf{H}_k \mathbf{W}_k \right) - \log \left(\sqrt{2\pi e \sigma_k^2} \right) \\ & \text{subject to} \quad \mathbf{H}_i \mathbf{W}_k = 0 \quad \forall k \neq i, \\ & \quad \sum_{i=1}^K \left\| [\mathbf{W}_i]_{k,:} \right\|_1 \leq \Delta_k \quad \forall i = 1, 2, \dots, N_T, \end{aligned} \quad (4.8)$$

and C_e is the maximum rate of the eavesdropper for the messages eavesdropping on legitimate users, which is given in Appendix B.

Proof: See Appendix B.

Similar to the previous scenario, the optimization problem **P4.2** is a MAXDET program subject to linear matrix inequalities. Thus, optimization packages can be used to solve the problem.

4.2.6. Numerical Results and Discussions

In this section, representative numerical results are provided to demonstrate the

Table 4.1: System Parameters

Parameter	Value
Room and LED configurations	
Room Dimension (Length \times Width \times Height)	5 (m) \times 5 (m) \times 3 (m)
Number of LED arrays, N_T	4
LED array size	0.1 (m) \times 0.1 (m)
Number of LED chips per array	36
LED array positions	array 1: [1.5, 1.5, 3] array 2: [1.5, 3.5, 3] array 3: [3.5, 1.5, 3] array 4: [3.5, 3.5, 3]
LED bandwidth, B	20 MHz
LED beam angle, ϕ (LED Lambertian order is 1)	120°
LED conversion factor, η	0.44 W/A
Users and eavesdropper photodiodes	
PD active area, D	1cm ²
PD responsivity, γ	0.53 A/W
PD field of view (FOV) semi-angle, Ψ_c	60°
Optical filter gain, $T_s(\psi)$	1
Refractive index of concentrator, κ	1.5
Other parameters	
Ambient light photocurrent, χ_{amb}	10.93 A/(m ² · Sr)
Pre-amplifier noise current density, i_{amb}	5 pA/Hz ^{-1/2}

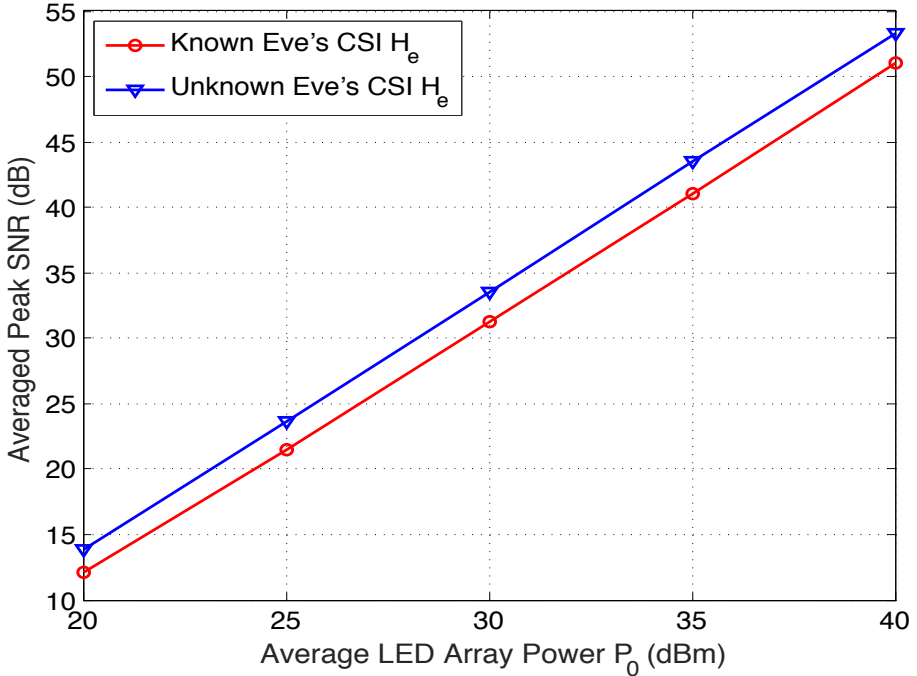


Figure 4.4: Averaged peak SNR of legitimate users: known and unknown \mathbf{H}_e .

maximum secrecy sum-rate performance derived in Sections 4.2.4 and 4.2.5. Fig. 4.3 shows the geometrical configuration of our considered MU-MISO VLC system with two legitimate users and one eavesdropper. We assume that users and eavesdropper are placed on the same receive plane, which is 0.5 m above the floor. Furthermore, a Cartesian coordinate system is set up for position specifications of LED arrays, legitimate users and the eavesdropper. For the sake of conciseness, all numerical results are obtained for the case of 2 legitimate users. Unless otherwise noted, parameters of the room, the transmitter, legitimate users and the eavesdropper are given in Table 4.1.

First, Fig. 4.4 illustrates the averaged peak SNRs of legitimate users versus the average radiated power P_0 of LED arrays for both cases: known and unknown \mathbf{H}_e . The average radiated power ranges from 20 to 40 dBm, which corresponds to 0.1 to 10 W. As will be shown later, the overall performance of the system depends on positions of the users and the eavesdropper. In this figure, we therefore average the results from 10,000 different channel realizations, i.e., 10,000 different positions of the users and the eavesdropper to evaluate the averaged performance. It is clearly shown that the averaged peak SNRs of higher than 25 dB can usually be achieved in

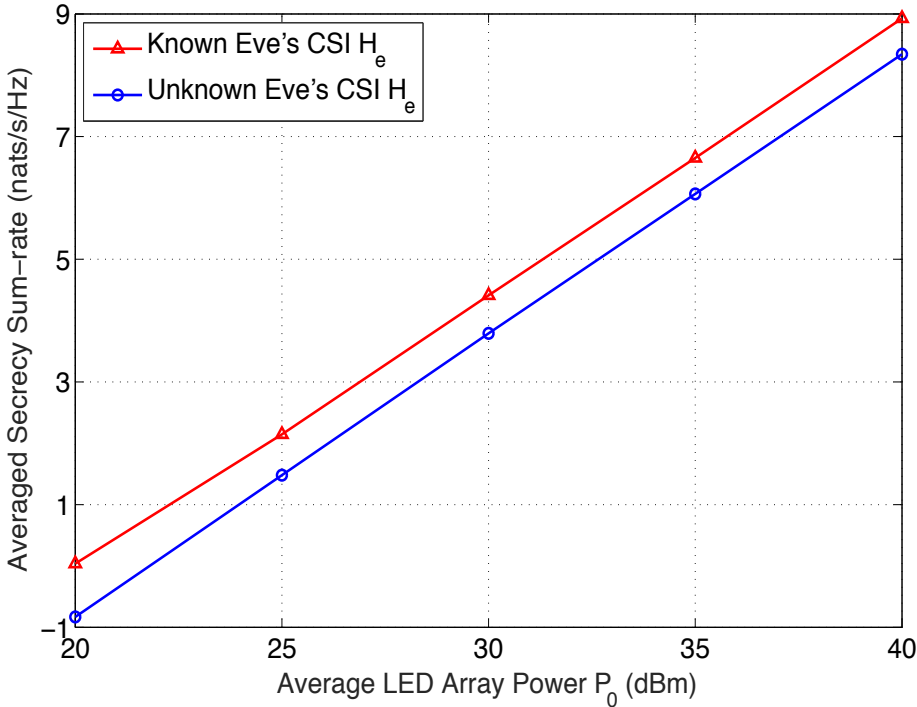


Figure 4.5: Averaged maximum secrecy sum-rate: known and unknown \mathbf{H}_e .

both cases in practical VLC systems, i.e., when the transmit power of LED arrays is higher than 30 dBm corresponding to 1 W. This validates the use of the bound in (2.4) in evaluating the secrecy capacity performance. In the case of known \mathbf{H}_e , due to the additional ZF constraint for canceling eavesdropper's reception, i.e., the second constraint of problem (4.6), the degrees of freedom in designing the precoding matrix is lower than that in the case of unknown \mathbf{H}_e , i.e., the feasible space for searching the optimal \mathbf{W}_k is smaller. As a result, the averaged user peak SNR in the scenario of unknown eavesdropper's CSI is better than that of the known one.

In Fig. 4.5, we show the averaged secrecy sum-rate performance versus the average radiated power P_0 by averaging 10,000 different channel realizations as in the previous figure. Though the sum-rate of legitimate users C_u , in the case of unknown \mathbf{H}_e is better (since the averaged peak SNR is better as shown in the previous figure), users must sacrifice a fraction of their communication rate C_e , which is considerable, to achieve perfectly secrecy. As a consequence, with the knowledge of \mathbf{H}_e at the transmitter, zero-forcing eavesdropper's reception can improve the averaged secrecy sum-rate by around 0.6 *nats* in comparison with the case of unknown \mathbf{H}_e . In addition,

4.2 Precoding Design

it is found that a positive secrecy sum-rate can be achieved in both scenarios for practical transmit power of LED arrays (typically, 4 – 5 W corresponding to around 35 dBm). That demonstrates the benefit of using precoding technique in improving the secrecy performance in MU-MISO VLC systems.

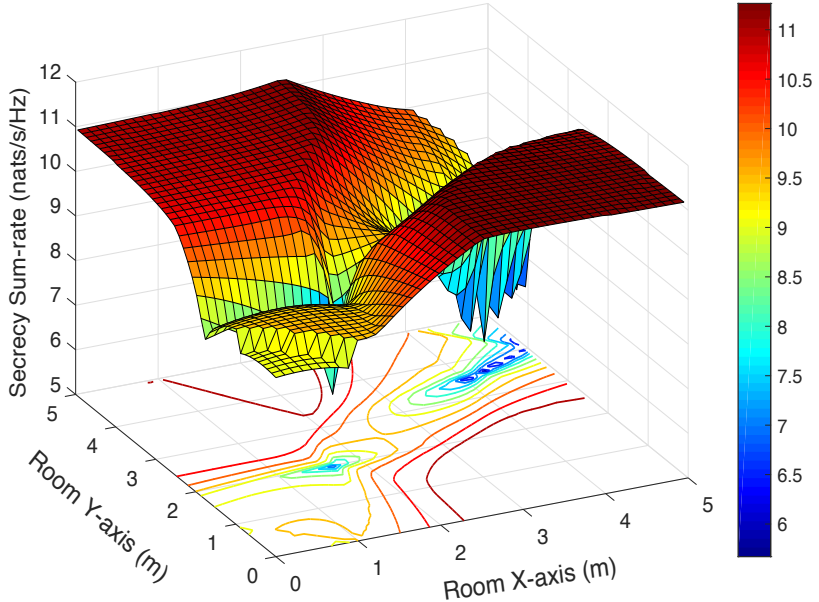


Figure 4.6: Maximum secrecy sum-rate for different positions of the eavesdropper: known \mathbf{H}_e .

Next, the distribution of the secrecy sum-rate with respect to eavesdropper's position when \mathbf{H}_e is known to the transmitter is depicted in Fig. 4.6. It is assumed that User 1 and User 2 are placed at [1.7, 2, 0.5], and [4.2, 3.6, 0.5], respectively. The average LED array transmit power P_0 is set to 40 dBm. As clearly illustrated in the figure, we observed a significant variation on the secrecy sum-rate performance according to the position of the eavesdropper. In general, the secrecy performance is relatively poor when the eavesdropper locates in the area around the line connecting the two users. Especially, it drops severely in the area nearby one of the two users. That is because when the eavesdropper is getting closer one of the legitimate users, its CSI becomes more similar, i.e., more correlated, to that of the user. As a consequence, the degrees of freedom in designing ZF precoding matrix is lower, leading to a degradation in the overall performance.

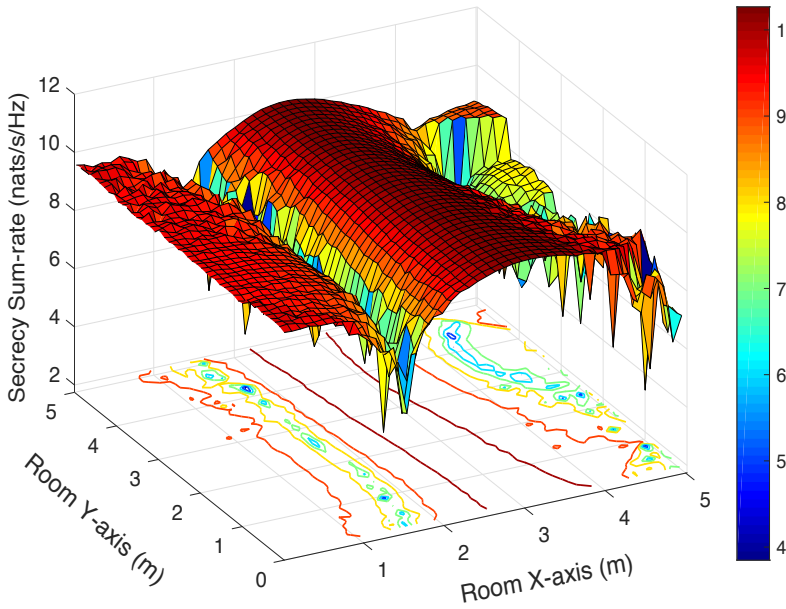


Figure 4.7: Maximum secrecy sum-rate for different positions of the eavesdropper: unknown \mathbf{H}_e .

Finally, in Fig. 4.7, we investigate the secrecy sum-rate distribution in the case of unknown \mathbf{H}_e at the transmitter. User's positions and LED power setup are the same as those in Fig. 4.6. Similar to the previous case, the secrecy sum-rate performance changes considerably in accordance to eavesdropper's position. However, because of the unawareness of the eavesdropper's channel, proper ZF precoding designs to suppress eavesdropper's CSI can not be achieved. Therefore, legitimate users must sacrifice a portion of their communication rates to ensure the confidentiality. As a result, there is a large area of the receive plane where the system suffers poor performance compared with the case of known \mathbf{H}_e .

4.3. Artificial Noise Design

4.3.1. Motivations and Objectives

As for the AN approach, to the best of our knowledge, all previous studies focused on the single legitimate user configuration only. Specifically, in [93] and [96], the AN was

generated by a set of LED transmitter to jam the eavesdropper’s channel. The rest of the LED transmitter were then used for transmitting the information-bearing signal to the legitimate user. On the other hand, the AN could also be added to the precoded information-bearing signal as studied in recent works [97, 115]. The combined signal was then transmitted by all LED transmitter. This approach (known as AN-aided precoding) involves both precoding designs for the AN and the information-bearing signals.

Due to the lack of the AN design approach for physical layer security in multi-user VLC wiretap channels, we attempt to fill this gap in this paper. It is known that the modulating signal in VLC is subject to amplitude constraint, which makes characterizing the channel capacity a challenging task [60]. In fact, closed-form expressions for the capacity of an amplitude constrained channel are not available. The AN-aided precoding design with respect to the secrecy capacity would be cumbersome, especially in the case of multiple users. In this paper, we therefore investigate an alternative approach for the AN-aided precoding design in multi-user VLC wiretap channels by considering the Quality of Service (QoS)-based perspective. In particular, we study the problem of max-min fairness SINR among multiple legitimate users under the presence of an eavesdropper whose CSI can be either known or unknown to the transmitter. In the case of unknown eavesdropper’s CSI, the AN is designed to lie in the null space of users’ channel matrices. We then investigate the impact of the AN noise power on the performances of users and the eavesdropper. In case the eavesdropper’s CSI is available, the AN-aided precoding is designed taking into account a constraint that the eavesdropper’s SINR is kept below a predefined threshold. In addition to the general design, a specific design, which adopts ZF technique as the underlaying precoding scheme for legitimate users, is also investigated.

4.3.2. AN-aided Precoding Model

Following the same notations in Chapter 3, let $d_k \in \mathbb{R}$ be the data symbol that is intended to the k -th user and $\mathbf{d} = \begin{bmatrix} d_1 & d_2 & \dots & d_K \end{bmatrix}^T \in \mathbb{R}^{K \times 1}$ be the data vector

of legitimate users. Without loss of generality, suppose that d_k is zero mean and is normalized to the range of $[-1, 1]$. At the k -th LED array, the information-bearing signal s_k is generated from a linear combination of the data vector and a precoding matrix $\mathbf{V}_k = \begin{bmatrix} w_{k,1} & w_{k,2} & \dots & w_{k,K} \end{bmatrix} \in \mathbb{R}^{1 \times K}$ as

$$s_k = \mathbf{V}_k \mathbf{d}. \quad (4.9)$$

In what follows, the AN-aided precoding models are explicitly described for two scenarios of unknown and known eavesdropper's CSI at the transmitter.

4.3.2.1. Unknown Eavesdropper's CSI

When the eavesdropper's CSI is not available at the transmitter, the AN should be

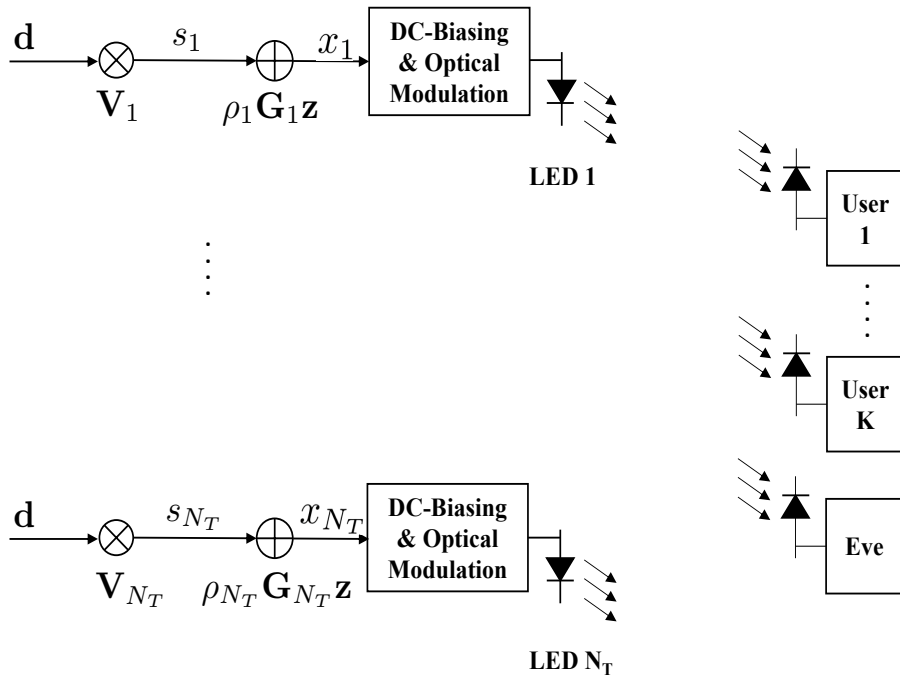


Figure 4.8: Schematic diagram of AN-aided precoding scheme: unknown \mathbf{H}_e .

designed in such a way that it is orthogonal to the information-bearing signal. By doing so, the AN would not interfere the legitimate users but potentially degrades the eavesdropper's channel. Let $\mathbf{H}_k = \begin{bmatrix} h_{1,k} & h_{2,k} & \dots & h_{N_T,k} \end{bmatrix} \in \mathbb{R}^{1 \times N_T}$ be the channel matrix of the k -th user, and $\mathbf{H} = \left[\mathbf{H}_1^T \quad \mathbf{H}_2^T \quad \dots \quad \mathbf{H}_K^T \right]^T \in \mathbb{R}^{K \times N_T}$ be the aggregated channel matrix.

gate matrix of all legitimate users. Assume that \mathbf{H} is full row-rank and let \mathbf{G} is an orthonormal basis for the null-space of \mathbf{H} . According the rank-nullity theorem, $\text{rank}(\mathbf{H}) + \dim(\mathbf{G}) = N_T$. Since $\text{rank}(\mathbf{H}) = K$, \mathbf{G} has a dimension of $(N_T - K)$. It can obviously seen that this AN design is not feasible when $N_T \leq K$. Throughout this paper, we thus assume that $N_T > K$. Figure 4.8 illustrates the AN-aided precoding model in this case where $\mathbf{z} = \begin{bmatrix} z_1 & z_2 & \dots & z_{N_T-K} \end{bmatrix}^T \in \mathbb{R}^{(N_T-K) \times 1}$ denotes the AN noise vector, which is added into the information-bearing signal s_n . It is also assumed that each element z_i is zero mean and is normalized to $[-1, 1]$. The broadcast signal at the n -th LED array can be written as

$$x_k = s_k + \rho_k \mathbf{G}_k \mathbf{z}, \quad (4.10)$$

where $\mathbf{G}_k \in \mathbb{R}^{1 \times (N_T - K)}$ is the k -th row vector of the orthonormal basic \mathbf{G} and ρ_k is a constant, which controls the amplitude of the AN signal at the k -th LED transmitter.

Since \mathbf{G} is an orthonormal basic for the null-space of \mathbf{H} , the received signal at the k -th user is written by

$$y_k = \gamma \eta \left(\mathbf{H}_k \mathbf{W}_k d_k + \mathbf{H}_k \sum_{i=1, i \neq k}^K \mathbf{W}_i d_i \right) + n_k. \quad (4.11)$$

Similarly, the received electrical signal at the eavesdropper is given by

$$y_e = \gamma \eta \left(\mathbf{H}_e \sum_{i=1}^K \mathbf{W}_i d_i + \mathbf{H}_e (\boldsymbol{\rho} \circ \mathbf{G}) \mathbf{z} \right) + n_e, \quad (4.12)$$

where \mathbf{H}_e is the channel matrix of the eavesdropper and $\boldsymbol{\rho} = \begin{bmatrix} \rho_1 & \rho_2 & \dots & \rho_{N_T} \end{bmatrix}^T$.

4.3.2.2. Known Eavesdropper's CSI

In case the eavesdropper's CSI is available at the transmitter, the AN is not necessary to be orthogonal to the information-bearing signal. By knowing eavesdropper's CSI, the transmitter optimally design the AN to meet the requirements on users' SINRs

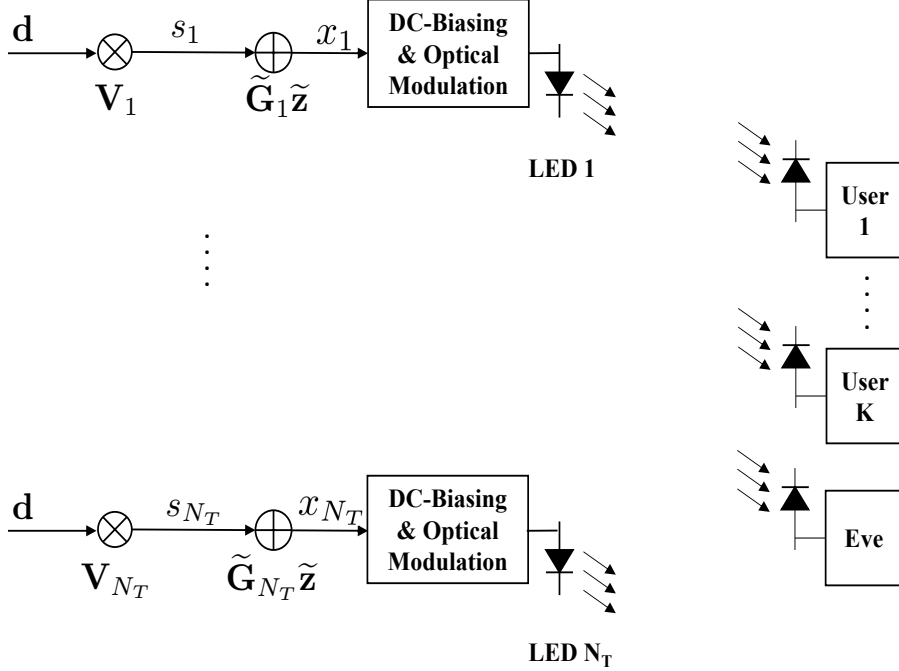


Figure 4.9: Schematic diagram of AN-aided precoding scheme: known \mathbf{H}_e .

while keeping the SINR of the eavesdropper below a pre-described threshold. In this case, let us denote $\tilde{\mathbf{z}} = \begin{bmatrix} \tilde{z}_1 & \tilde{z}_2 & \dots & \tilde{z}_{N_T} \end{bmatrix}^T \in \mathbb{R}^{N_T \times 1}$ as the AN noise vector and $\tilde{\mathbf{G}} \in \mathbb{R}^{N_T \times N_T}$ as its precoder, which can be an arbitrary matrix (Fig. 4.9). Similar to the case of unknown eavesdropper's CSI, each element \tilde{z}_i of $\tilde{\mathbf{z}}$ is assumed to be zero mean and normalized to $[-1, 1]$. The received signals at the k -th user and at the eavesdropper are then expressed by

$$y_k = \gamma\eta \left(\mathbf{H}_k \mathbf{W}_k d_k + \mathbf{H}_k \sum_{i=1, i \neq k}^K \mathbf{W}_i d_i + \mathbf{H}_k \tilde{\mathbf{G}} \tilde{\mathbf{z}} \right) + n_k, \quad (4.13)$$

and

$$y_e = \gamma\eta \left(\mathbf{H}_e \sum_{i=1}^K \mathbf{W}_i d_i + \mathbf{H}_e \tilde{\mathbf{G}} \tilde{\mathbf{z}} \right) + n_e, \quad (4.14)$$

respectively.

4.3.3. Optical Power Constraint

Similar to the arguments described in Chapter 3, Section 3.3, to guarantee normal operations of the LEDs and ensure energy efficiency, the drive current u_k must be constrained within the range $[0, I_{\max}]$ as

$$0 \leq x_k + I_k^{\text{DC}} \leq I_{\max}. \quad (4.15)$$

For the case of unknown eavesdropper's CSI, since $|d_i| \leq 1$ and $|z_i| \leq 1$, we get

$$-\left(\|\mathbf{V}_k\|_1 + \rho_n \|\mathbf{G}_k\|_1\right) \leq x_k \leq \left(\|\mathbf{V}_k\|_1 + \rho_k \|\mathbf{G}_k\|_1\right). \quad (4.16)$$

With respect to the precoding matrix \mathbf{W}_i and to ensure both (4.15) and (4.16), the following constraint should be imposed

$$\sum_{i=1}^K \left\| [\mathbf{W}_i]_{k,:} \right\|_1 + \rho_k \|\mathbf{G}_k\|_1 \leq \Delta_k, \quad (4.17)$$

where $\Delta_k = \min(I_k^{\text{DC}}, I_{\max} - I_k^{\text{DC}})$.

Similarly, in the case of known eavesdropper's CSI, we have the following constraint on precoders design

$$\sum_{i=1}^K \left\| [\mathbf{W}_i]_{k,:} \right\|_1 + \|\tilde{\mathbf{G}}_k\|_1 \leq \Delta_k, \quad (4.18)$$

where $\tilde{\mathbf{G}}_k$ is the k -th row vector of $\tilde{\mathbf{G}}$.

4.4. General AN-aided Precoding Design

4.4.1. Unknown Eavesdropper's CSI

It is known that the uniform distribution is the maximum entropy probability distribution for a random variable under no constraint other than it is contained in

the distribution's support. Hence, to maximize user's SINR as well as the interference caused by the AN at the eavesdropper, let us assume that d_k and z_k are both uniformly distributed over $[-1, 1]$. From (4.11) and (4.12), the SINR of the k -th legitimate user and the eavesdropper are then given by

$$\text{SINR}_k = \frac{\theta^2 |\mathbf{H}_k \mathbf{W}_k|^2}{\theta^2 \sum_{i=1, i \neq k}^K |\mathbf{H}_k \mathbf{W}_i|^2 + \sigma_k^2}, \quad (4.19)$$

and

$$\text{SINR}_{e,k} = \frac{\theta^2 |\mathbf{H}_e \mathbf{W}_k|^2}{\theta^2 \sum_{i=1, i \neq k}^K |\mathbf{H}_e \mathbf{W}_i|^2 + \theta^2 \|\mathbf{H}_e (\boldsymbol{\rho} \circ \mathbf{G})\|_F^2 + \sigma_e^2}, \quad (4.20)$$

respectively, where $\theta = \frac{1}{\sqrt{3}}\gamma\eta$. Note that $\text{SINR}_{e,k}$ is the SINR of the eavesdropper corresponding to the data symbol d_k it eavesdrops on the k -th user. In the considered system with K users, there are thus K values of the eavesdropper's SINRs for users' data symbols. Since \mathbf{H}_e is unknown to the transmitter, the precoding matrices \mathbf{W}_k are designed to solve the legitimate user SINR max-min fairness problem regardless of the eavesdropper's SINR. The problem is formulated as follows

$$\begin{aligned} \mathcal{P}4.3 : \quad & \underset{\mathbf{W}_k}{\text{maximize}} \quad \min_k \text{SINR}_k \\ & \text{subject to} \quad \sum_{i=1}^K \left\| [\mathbf{W}_i]_{k,:} \right\|_1 + \rho_k \|\mathbf{G}_k\|_1 \leq \Delta_k. \end{aligned} \quad (4.21)$$

To ensure the feasibility of $\mathcal{P}4.3$, ρ_k 's should be chosen to satisfy the inequality constraints. In principle, ρ_k 's are set individually depending on the AN power allocated in each LED transmitter. In fact, setting ρ_k 's individually can further improve the secrecy performance. For example, maximum AN power should be allocated to transmitter, which do not associate with any users. By doing so, the eavesdropper's channel can be considerably degraded. However, for the sake of simplicity, we assume that ρ_k 's are equal (i.e., $\rho_i = \rho_j = \rho$). Then, one can set $\rho = \frac{\bar{\rho} \min \Delta_n}{\max \|\mathbf{G}_n\|_1}$, where $\bar{\rho}$ ($0 \leq \bar{\rho} \leq 1$) is a constant which controls the amplitude of the AN in the sense that

the larger the \bar{p} is, the higher the AN amplitude (i.e., power) becomes. By introducing a slack variable t , **P4.3** can be rewritten as

$$\begin{aligned} \mathcal{P}4.4 : \quad & \underset{\mathbf{W}_k, t}{\text{maximize}} \quad t \\ & \text{subject to} \quad \frac{|\mathbf{H}_k \mathbf{W}_k|^2}{\sum_{i=1, i \neq k}^K |\mathbf{H}_k \mathbf{W}_i|^2 + \sigma_k'^2} \geq t \\ & \quad \sum_{i=1}^K \|[\mathbf{W}_i]_{k,:}\|_1 \leq \Delta_{\bar{\rho},k}, \end{aligned} \quad (4.22)$$

where $\sigma_k'^2 = \sigma_k^2/\theta^2$ and $\Delta_{\bar{\rho},k} = \Delta_k - \frac{\bar{p} \min \Delta_n}{\max \|\mathbf{G}_k\|_1} \|\mathbf{G}_k\|_1$. It can be seen that the first constraint of **P4.4** is not convex, thus it is difficult to solve. A standard approach to handle the problem is to reformulate it to a convex optimization for a fixed t and then using the bisection method to solve the reformulated problem. Following the same procedure in [104], let $\mathbf{W} = [\mathbf{W}_1 \ \mathbf{W}_2 \ \dots \ \mathbf{W}_K] \in \mathbb{R}^{N_T \times K}$, $\mathbf{w} = \text{vec}(\mathbf{W}^T)$, and \mathbf{I}_K^k be the matrix obtained from the identity matrix of size K by setting the (k, k) -th element be zero. Now, for a fixed value of t , we solve the following feasibility problem

$$\begin{aligned} \mathcal{P}4.5 : \quad & \text{find} \quad \mathbf{w} \\ & \text{subject to} \quad \|\mathbf{B}_k \mathbf{w} + \boldsymbol{\sigma}'_k\|_F \leq \frac{1}{\sqrt{t}} \mathbf{H}_k (\mathbf{I}_{N_T} \otimes \mathbf{e}_k^T) \mathbf{w} \\ & \quad - \mathbf{a} \leq \mathbf{w} \leq \mathbf{a}, \\ & \quad \mathbf{U} \mathbf{a} \leq \Delta_{\bar{\rho}}, \end{aligned} \quad (4.23)$$

where $\mathbf{B}_k = \begin{bmatrix} \mathbf{H}_k \otimes \mathbf{I}_K^k \\ \mathbf{0}_{1 \times N_T K} \end{bmatrix}$, $\boldsymbol{\sigma}'_k = \begin{bmatrix} \mathbf{0}_{1 \times K} & \sigma'_k \end{bmatrix}^T$, $\mathbf{U} = \mathbf{I}_{N_T} \otimes \mathbf{1}_K^T$, $\mathbf{a} = \begin{bmatrix} a_1 & a_2 & \dots & a_{N_T K} \end{bmatrix}^T$ is a new optimization variable and $\Delta_{\bar{\rho}} = \begin{bmatrix} \Delta_{\bar{\rho},1} & \Delta_{\bar{\rho},2} & \dots & \Delta_{\bar{\rho},N_T} \end{bmatrix}^T$. The above problem is a second-order cone program (SOCP) [103], which is convex and can be solved efficiently using off-the-self optimization packages [100, 101]. The optimal t is the maximum value for which \mathbf{w} exists and satisfies the constraints in **P4.5**. Therefore, the optimal value of t can be found by bisection algorithm as described in detail in [104]. The algorithm is presented here for the sake of convenience.

Algorithm 1 Bisection algorithm for solving problem $\mathcal{P}4.5$

1. Estimate channel matrices \mathbf{H}_k , \mathbf{H}_e and noise variances σ_k^2 , σ_e^2 .
2. Initialize t_1 and t_2 ($t_1 < t_2$) so that $\mathcal{P}4.5$ is infeasible when $t = t_2$ and feasible when $t = t_1$.
3. Initialize a tolerance parameter ϵ .

while $t_2 - t_1 > \epsilon$ **do**

$$t = (t_1 + t_2)/2.$$

Solve the feasibility of $\mathcal{P}4.5$ by CVX toolbox.

if the problem is feasible **then** $t_1 = t$.

else $t_2 = t$.

end if

end while

The optimal precoder \mathbf{W}_k^* is given by $\mathbf{W}_k^* = (\mathbf{I}_{N_T} \otimes \mathbf{e}_k^T) \tilde{\mathbf{w}}$, where $\tilde{\mathbf{w}}$ is the last feasible solution to $\mathcal{P}4.5$ (i.e., the solution to $\mathcal{P}4.5$ for $t = t_1$).

4.4.2. Known Eavesdropper's CSI

In this case, the SINRs of the k -th legitimate user and the eavesdropper are given by

$$\text{SINR}_k = \frac{|\mathbf{H}_k \mathbf{W}_k|^2}{\sum_{i=1, i \neq k}^K |\mathbf{H}_k \mathbf{W}_i|^2 + \left\| \mathbf{H}_k \tilde{\mathbf{G}} \right\|_F^2 + \sigma_k'^2}, \quad (4.24)$$

and

$$\text{SINR}_{e,k} = \frac{|\mathbf{H}_e \mathbf{W}_k|^2}{\sum_{i=1, i \neq k}^K |\mathbf{H}_e \mathbf{W}_i|^2 + \left\| \mathbf{H}_e \tilde{\mathbf{G}} \right\|_F^2 + \sigma_e'^2}, \quad (4.25)$$

respectively, where $\sigma_e'^2 = \sigma_e^2/\theta^2$. Different from the previous case, since the eavesdropper's CSI is available at the transmitter, the eavesdropper's SINR can be taken into account in the optimal precoders design. The max-min fairness problem is then

formulated as follows

$$\begin{aligned} \mathcal{P}4.6 : \quad & \underset{\mathbf{W}_k, \tilde{\mathbf{G}}}{\text{maximize}} \quad \min_k \text{SINR}_k \\ & \text{subject to} \quad \text{SINR}_{e,k} \leq \lambda_k, \\ & \quad \sum_{i=1}^K \left\| [\mathbf{W}_i]_{k,:} \right\|_1 + \left\| \tilde{\mathbf{G}}_k \right\|_1 \leq \Delta_k, \end{aligned} \quad (4.26)$$

where λ_k is the maximum allowable SINR threshold imposed on the eavesdropper. Obviously, problem $\mathcal{P}4.6$ is more complex than $\mathcal{P}4.3$ due to an additional non-convex constraint on the eavesdropper's SINR and the optimization is over both precoding matrices \mathbf{W}_k and $\tilde{\mathbf{G}}$. However, the same procedure can be applied to solve the problem. Similar to the previous case, we transform it to the following equivalent form

$$\begin{aligned} \mathcal{P}4.7 : \quad & \underset{\mathbf{W}_k, \tilde{\mathbf{G}}, t}{\text{maximize}} \quad t \\ & \text{subject to} \quad \text{SINR}_k \geq t, \\ & \quad \text{SINR}_{e,k} \leq \lambda_k, \\ & \quad \sum_{i=1}^K \left\| [\mathbf{W}_i]_{k,:} \right\|_1 + \left\| \tilde{\mathbf{G}}_k \right\|_1 \leq \Delta_k. \end{aligned} \quad (4.27)$$

Next, let us define $\mathbf{W} = [\mathbf{W}_1 \ \mathbf{W}_2 \ \dots \ \mathbf{W}_K]$, $\mathbf{Q} = [\mathbf{W} \ \tilde{\mathbf{G}}] \in \mathbb{R}^{N_T \times (N_T+K)}$, and $\mathbf{q} = \text{vec}(\mathbf{Q}^T)$. With the same manner, for a fixed value of t , we solve the feasibility of the following problem

$$\begin{aligned} \mathcal{P}4.8 : \text{find} \quad & \mathbf{q} \\ \text{subject to} \quad & \|\mathbf{B}_k \mathbf{q} + \boldsymbol{\sigma}'_k\|_F \leq \frac{1}{\sqrt{t}} \mathbf{H}_k (\mathbf{I}_{N_T} \otimes (\mathbf{e}_k^T \mathbf{V})) \mathbf{q}, \\ & \|\mathbf{B}_{e,k} \mathbf{q} + \boldsymbol{\sigma}'_e\|_F \geq \frac{1}{\sqrt{\lambda_k}} \mathbf{H}_e (\mathbf{I}_{N_T} \otimes (\mathbf{e}_k^T \mathbf{V})) \mathbf{q}, \\ & -\mathbf{a} \leq \mathbf{q} \leq \mathbf{a}, \\ & \mathbf{U} \mathbf{a} \leq \Delta, \end{aligned} \quad (4.28)$$

where $\mathbf{B}_k = \begin{bmatrix} \mathbf{H}_k \otimes \mathbf{I}_{N_T+K}^k \\ \mathbf{0}_{1 \times N_T(N_T+K)} \end{bmatrix}$, $\mathbf{B}_{e,k} = \begin{bmatrix} \mathbf{H}_e \otimes \mathbf{I}_{N_T+K}^k \\ \mathbf{0}_{1 \times N_T(N_T+K)} \end{bmatrix}$, $\mathbf{V} = \begin{bmatrix} \mathbf{I}_K & \mathbf{0}_{K \times N_T} \end{bmatrix}$, $\mathbf{U} = \mathbf{I}_{N_T} \otimes \mathbf{1}_{N_T+K}^T$, $\Delta = \begin{bmatrix} \Delta_1 & \Delta_2 & \dots & \Delta_{N_T} \end{bmatrix}^T$, $\boldsymbol{\sigma}'_k = \begin{bmatrix} \mathbf{0}_{1 \times (N_T+K)} & \sigma'_k \end{bmatrix}^T$, $\boldsymbol{\sigma}'_e = \begin{bmatrix} \mathbf{0}_{1 \times (N_T+K)} & \sigma'_e \end{bmatrix}^T$, and $\mathbf{a} = \begin{bmatrix} a_1 & a_2 & \dots & a_{N_T(N_T+K)} \end{bmatrix}^T$ is a new optimization variable. Unlike $\mathcal{P}4.5$, the above problem is not convex due to the nonconvexity of the constraint on the eavesdropper's SINR. To overcome this issue, we utilize the convex-concave procedure (CCCP) to find a local optimal solution [105, 106]. The CCCP involves an iterative process where at the i -th iteration of the procedure, we approximately linearize the convex term $\|\mathbf{B}_{e,k}\mathbf{q} + \boldsymbol{\sigma}'_e\|$ using its Taylor expansion as $\|\mathbf{B}_{e,k}\mathbf{q}^{(i)} + \boldsymbol{\sigma}'_e\| \approx \|\mathbf{B}_{e,k}\mathbf{q}^{(i-1)} + \boldsymbol{\sigma}'_e\| + \frac{[\mathbf{B}_{e,k}\mathbf{q}^{(i-1)} + \boldsymbol{\sigma}'_e]^T \mathbf{B}_{e,k}}{\|\mathbf{B}_{e,k}\mathbf{q}^{(i-1)} + \boldsymbol{\sigma}'_e\|} (\mathbf{q}^{(i)} - \mathbf{q}^{(i-1)})$, where $\mathbf{q}^{(i-1)}$ is the value of \mathbf{q} obtained from the previous iteration. As a result, at each iteration of the procedure, problem $\mathcal{P}4.8$ is approximated to the following convex optimization problem

$$\begin{aligned}
 \mathcal{P}4.9 : \quad & \text{find} && \mathbf{q}^{(i)} \\
 & \text{subject to} && \|\mathbf{B}_k \mathbf{q}^{(i)} + \boldsymbol{\sigma}'_k\|_F \leq \frac{1}{\sqrt{t}} \mathbf{H}_k (\mathbf{I}_{N_T} \otimes (\mathbf{e}_k^T \mathbf{V})) \mathbf{q}^{(i)}, \\
 & && \|\mathbf{B}_{e,k} \mathbf{q}^{(i-1)} + \boldsymbol{\sigma}'_e\|_F + \frac{[\mathbf{B}_{e,k} \mathbf{q}^{(i-1)} + \boldsymbol{\sigma}'_e]^T \mathbf{B}_{e,k}}{\|\mathbf{B}_{e,k} \mathbf{q}^{(i-1)} + \boldsymbol{\sigma}'_e\|_F} (\mathbf{q}^{(i)} - \mathbf{q}^{(i-1)}) \\
 & && \geq \frac{1}{\sqrt{\lambda_k}} \mathbf{H}_e (\mathbf{I}_{N_T} \otimes (\mathbf{e}_k^T \mathbf{V})) \mathbf{q}^{(i)}, \\
 & && -\mathbf{a} \leq \mathbf{q}^{(i)} \leq \mathbf{a}, \\
 & && \mathbf{U} \mathbf{a} \leq \Delta.
 \end{aligned} \tag{4.29}$$

The detailed iterative algorithm for solving $\mathcal{P}4.8$ is summarized as follows

Algorithm 2 Iterative algorithm for solving problem $\mathcal{P}4.8$

1: **Initialization**

1. Estimate channel matrices \mathbf{H}_k , \mathbf{H}_e and noise variances σ_k^2 , σ_e^2 .
2. Initialize $\mathbf{q}^{(0)}$ to be sufficiently small.

2: **Iteration:** At the i -th iteration

1. Update $\mathbf{q}^{(i)}$ given $\mathbf{q}^{(i-1)}$ from previous iteration by solving problem $\mathcal{P}4.9$ using CVX toolbox .
2. $i = i + 1$.

3: **Termination:** terminate the iteration when

1. $\|\mathbf{q}^{(i)} - \mathbf{q}^{(i-1)}\| \leq \epsilon$, where $\epsilon = 10^{-3}$ is the predefined threshold, or
 2. $i = L$, where $L = 10$ is the predefined maximum number of iterations.
-

4.5. AN-Aided ZF Precoding

In this section, a specific designs for the proposed AN-aided precoding scheme using ZF technique are described. ZF aims at decoupling the multi-user channel into multiple independent sub-channels, thus simplifies the AN design and ensure confidentiality among legitimate users.

4.5.1. Unknown Eavesdropper's CSI

Using the notations in Chapter 3 Section 3.2.2, with ZF precoding, the SNR of the k -th user is given by

$$\text{SNR}_k^{\text{ZF}} = \frac{|\mathbf{H}_k \mathbf{W}_k|^2}{\sigma_k'^2} = \frac{q_k}{\sigma_k'^2}, \quad (4.30)$$

The max-min fairness problem is formulated as

$$\begin{aligned} \mathcal{P}4.10 : \quad & \text{maximize}_{\mathbf{W}_k} \quad \min_k \frac{q_k}{\sigma'^2_k} \\ & \text{subject to} \quad \mathbf{HW} = \text{diag}\{\sqrt{\mathbf{q}}\}, \\ & \quad \sum_{i=1}^K \left\| [\mathbf{W}_i]_{k,:} \right\|_1 + \rho_k \|\mathbf{G}_k\|_1 \leq \Delta_k. \end{aligned} \quad (4.31)$$

Similar to the case of optimal design, we assume that ρ_k 's are set equally at all LED transmitter. Let us define $\boldsymbol{\sigma}'^2 = \begin{bmatrix} \sigma'_1 & \sigma'_2 & \dots & \sigma'_K \end{bmatrix}^T$ and $\text{diag}\{\mathbf{q}'\} = \text{diag}\{\mathbf{q}\} \text{diag}\{\boldsymbol{\sigma}'^2\}$ where $\mathbf{q}' = [q'_1 \quad q'_2 \quad \dots \quad q'_K]$. Then, $\mathcal{P}4.10$ can be rewritten as

$$\begin{aligned} \mathcal{P}4.11 : \quad & \text{maximize}_{\mathbf{W}_k} \quad \min_k q'_k \\ & \text{subject to} \quad \mathbf{HW} = \text{diag}\{\sqrt{\mathbf{q}'}\} \text{diag}\{\boldsymbol{\sigma}'\}, \\ & \quad \sum_{i=1}^K \left\| [\mathbf{W}_i]_{k,:} \right\|_1 \leq \Delta_{\bar{\rho},k}. \end{aligned} \quad (4.32)$$

Following the similar argument in [70], we can search the optimal solution of the form $\mathbf{q}' = q' \mathbf{1}$ for some q' is optimal. To see this, let \mathbf{W}^* and \mathbf{q}^* be the optimal solution to $\mathcal{P}4.11$ and we define new variables $\mathbf{q}' = \bar{q} \mathbf{1}$ and $\mathbf{W} = \mathbf{W}^* \text{diag}\left\{ \begin{bmatrix} \sqrt{\bar{q}/q_1^*} & \dots & \sqrt{\bar{q}/q_K^*} \end{bmatrix} \right\}$, where $\bar{q} = \min_k q_k^*$. Then, it holds that

$$\begin{aligned} \mathbf{HW} &= \mathbf{HW}^* \text{diag}\left\{ \begin{bmatrix} \sqrt{\bar{q}/q_1^*} & \dots & \sqrt{\bar{q}/q_K^*} \end{bmatrix} \right\} \\ &= \text{diag}\{\sqrt{\mathbf{q}^*}\} \text{diag}\{\sqrt{\boldsymbol{\sigma}}\} \text{diag}\left\{ \begin{bmatrix} \sqrt{\bar{q}/q_1^*} & \dots & \sqrt{\bar{q}/q_K^*} \end{bmatrix} \right\} \\ &= \text{diag}\{\sqrt{\mathbf{q}'}\} \text{diag}\{\sqrt{\boldsymbol{\sigma}}\}, \end{aligned} \quad (4.33)$$

and

$$\begin{aligned} \left\| [\mathbf{W}]_{k,:} \right\|_1 &= \left\| \left[\mathbf{W}^* \text{diag}\left\{ \begin{bmatrix} \sqrt{\bar{q}/q_1^*} & \dots & \sqrt{\bar{q}/q_K^*} \end{bmatrix} \right\} \right]_{k,:} \right\|_1 \\ &\leq \left\| [\mathbf{W}^*]_{k,:} \right\|_1, \end{aligned} \quad (4.34)$$

since $\bar{q}/q_k^* \leq 1$ for all k . That is, \mathbf{W} and \mathbf{q}' are also feasible and offer the same objective. We thus can reduce **P4.11** to

$$\begin{aligned} \mathcal{P}4.12 : \quad & \underset{q' \geq 0, \mathbf{Q}}{\text{maximize}} \quad q' \\ & \text{subject to} \quad \sqrt{q' \sigma_k^2} \left\| [\mathbf{H}^\dagger + \mathbf{PQ}]_{k,:} \right\|_1 \leq \Delta_k \quad \forall k. \end{aligned}$$

It is easy to see that the optimal solution q'_{opt} is given by

$$q'_{\text{opt}} = \min_k \frac{\Delta_{\bar{\rho},k}^2}{\sigma_n' \left\| [\mathbf{H}^\dagger + \mathbf{PQ}]_{k,:} \right\|_1^2}, \quad (4.35)$$

where \mathbf{Q} is the solution to

$$\begin{aligned} \mathcal{P}4.13 : \quad & \underset{\mathbf{Q}, t}{\text{minimize}} \quad t \\ & \text{subject to} \quad \sigma_k' \left\| [\mathbf{H}^\dagger + \mathbf{PQ}]_{k,:} \right\|_1^2 \leq t. \end{aligned}$$

It can be seen that the above problem is a linear programming, which has been well studied in literature and can be solved efficiently using off-the-self optimization packages.

4.5.2. Known Eavesdropper's CSI

In this case, the SINR of the k -user is simplified as

$$\text{SINR}_k^{\text{ZF}} = \frac{|\mathbf{H}_k \mathbf{W}_k|^2}{\left\| \mathbf{H}_k \tilde{\mathbf{G}} \right\|_F^2 + \sigma_k'^2}. \quad (4.36)$$

Since ZF is only applied to legitimate users, the expression for the SINR of the eavesdropper is the same to that in (4.25). The max-min fairness problem is then

given by

$$\begin{aligned}
 \mathcal{P}4.14 : \quad & \underset{\mathbf{W}_k, \tilde{\mathbf{G}}}{\text{maximize}} \quad \min_k \text{SINR}_k^{\text{ZF}} \\
 & \text{subject to} \quad \text{SINR}_{e,k}^{\text{ZF}} \leq \lambda_k, \\
 & \quad \mathbf{H}_i \mathbf{W}_k = 0 \quad \forall k \neq i, \\
 & \quad \sum_{i=1}^K \left\| [\mathbf{W}_i]_{k,:} \right\|_1 + \left\| \tilde{\mathbf{G}}_k \right\|_1 \leq \Delta_k,
 \end{aligned} \tag{4.37}$$

It can be seen that it is difficult to handle the above problem by using of the expression in (3.13) due to the involvement of \mathbf{G} in both objective function and constraints. Instead, we follow the same procedure as in the case of the optimal design described in Section 4.4.2 to reformulate $\mathcal{P}4.13$ to a convex optimization problem. With the same variable transformations as in $\mathcal{P}4.8$, we solve the feasibility of the following problem

$$\begin{aligned}
 \mathcal{P}4.15 : \quad & \text{find} \quad \mathbf{q} \\
 & \text{subject to} \quad \left\| \mathbf{B}_k \mathbf{q} + \boldsymbol{\sigma}'_k \right\|_F \leq \frac{1}{\sqrt{t}} \mathbf{H}_k (\mathbf{I}_{N_T} \otimes (\mathbf{e}_k^T \mathbf{V})) \mathbf{q}, \\
 & \quad \left\| \mathbf{B}_{e,k} \mathbf{q} + \boldsymbol{\sigma}'_e \right\|_F \geq \frac{1}{\sqrt{\lambda_k}} \mathbf{H}_e (\mathbf{I}_{N_T} \otimes (\mathbf{e}_k^T \mathbf{V})) \mathbf{q}, \\
 & \quad \mathbf{H}_k (\mathbf{I}_{N_T} \otimes (\mathbf{e}_i^T \mathbf{V})) \mathbf{q} = 0, \quad \forall k \neq i, \\
 & \quad -\mathbf{a} \leq \mathbf{q} \leq \mathbf{a}, \\
 & \quad \mathbf{U} \mathbf{a} \leq \boldsymbol{\Delta}.
 \end{aligned} \tag{4.38}$$

Similar to $\mathcal{P}4.8$, the CCCP can be used to solve the above problem.

4.6. Numerical Results and Discussions

In this section, numerical results are presented to demonstrate the performances of the optimal and suboptimal AN aided precoding designs presented in previous Sections. System configurations and parameters are the same with those used in the precoding approach. All results are obtained through averaging 5,000 different

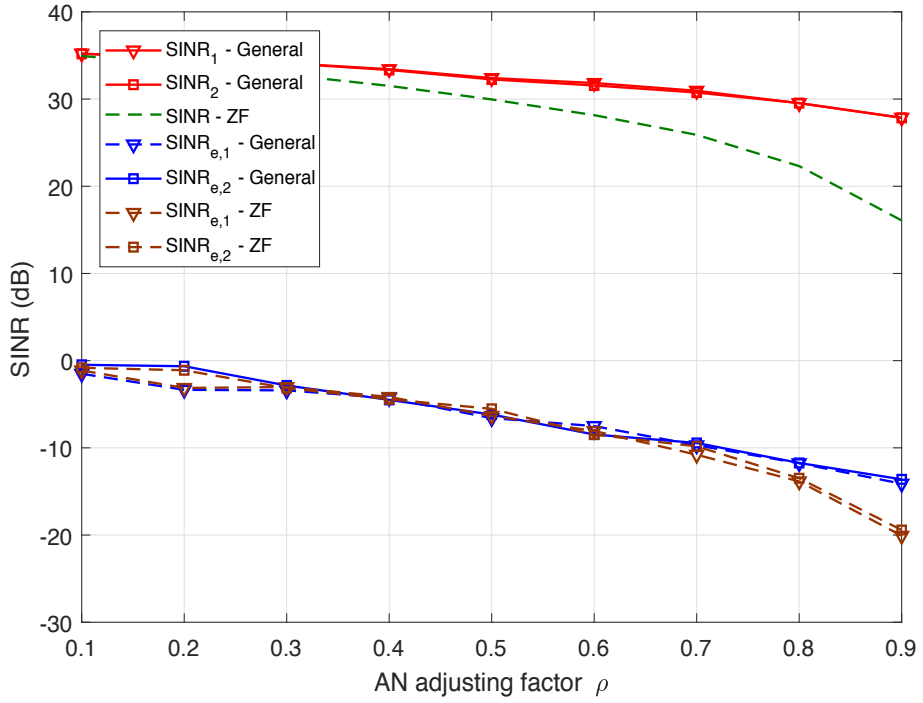


Figure 4.10: Max-min fairness of users' SINRs with respect to AN adjusting factor: unknown \mathbf{H}_e

channel realizations of users and the eavesdropper. Furthermore, for the sake of conciseness, results are presented for the case of 2 users.

In case of unknown \mathbf{H}_e , Fig. 4.10 shows the max-min fairness of users' SINRs with respect to the AN adjusting factor ρ for both general and ZF designs. The average LED array transmit power is set to 35 dBm. Similar to the ZF design, the general design has the optimal solution where users' SINRs are equal. It is also observed that significant gaps between users' and eavesdropper's SINRs are achieved in both designs, thus ensuring high secrecy capacity performances. For example at $\rho = 0.9$, the performance gaps are 40 dB and 36 dB in case of general and ZF designs, respectively.

In Fig. 4.11, the fairness performances versus average LED transmit power are illustrated. The AN adjusting factor is set to $\rho = 0.5$. It is seen that the general design, which optimizes users' SINRs output, outperforms the ZF design, especially at lower transmit power. At high transmit power regimes, the performance of the ZF design approaches that of the general one. This reflects the fact that ZF precoding

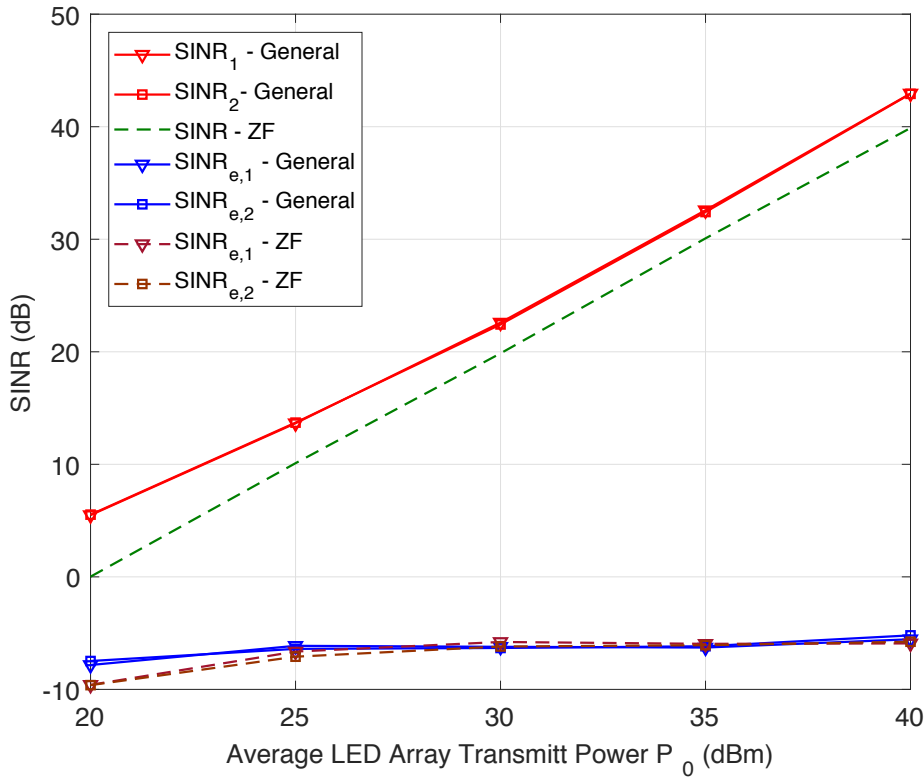


Figure 4.11: Max-min fairness of users's SINRs with respect to average LED array transmit power: unknown \mathbf{H}_e , $\rho = 0.5$.

achieves good performance at high transmit power [70]. It is also seen that the eavesdropper's SINRs in case of ZF design are lower than those of the general one at the low transmit power region. However, they are almost the same when the transmit power increases.

For the case of active eavesdropper, Fig. 4.12 depicts the max-min fairness performances in accordance with the average LED transmit power for different values of eavesdropper's SINR threshold. For simplicity, assume that $\lambda_k = \lambda_j = \lambda$ ($\forall k \neq j$). It should be noted that it is only meaningful to choose the thresholds if large differences between users' and eavesdropper's SINR could be guaranteed. On the other hand, if λ is set too low (i.e., too demanding constraints on the eavesdropper's SINR), the optimization problems $\mathcal{P}4.6$ and $\mathcal{P}4.14$ may not be feasible. As such, $\lambda = -5$ and -10 dB are chosen for simulations. Similar to the case of unknown \mathbf{H}_e , we also observed significant gaps between users' and eavesdropper' SINR in both general and ZF designs. Interestingly, while the eavesdropper's SINRs are kept almost

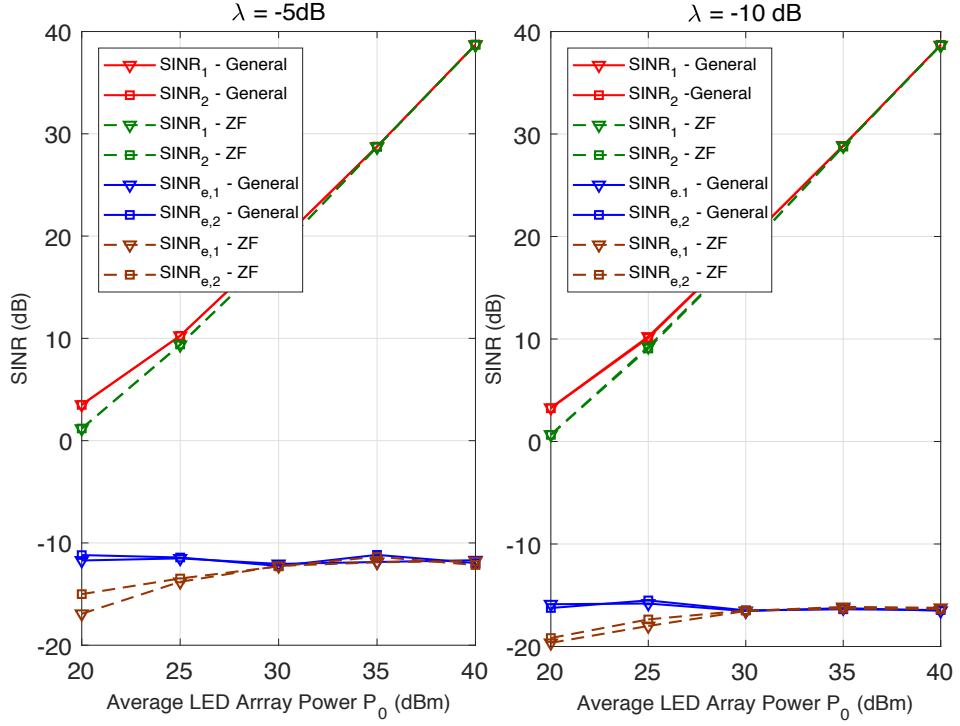


Figure 4.12: Max-min fairness of users's SINR with respect to average LED array transmit power: known \mathbf{H}_e .

constant in case of general design, they increase according to an increase in the transmit power in case of ZF design. Moreover, it is seen that users' performances in case $\lambda = -10 \text{ dB}$ are negligibly worse than those when $\lambda = -5 \text{ dB}$ (i.e., more relaxing threshold on eavesdropper's SINR).

4.7. Conclusions

This chapter studied precoding and AN designs for physical layer security in MU-MIMO VLC systems. The precoding design was based on ZF technique to ensure confidentiality among users. The maximum secrecy sum-rate problems were formulated and solved for two different scenarios: known and unknown eavesdropper's CSI at the transmitter. Numerical results showed that performance in the case of known eavesdropper's CSI is slightly better than that of unknown CSI and positive secrecy performances can always be achieved for both scenarios. Additionally, it was seen that the position of eavesdropper has a significant impact on the secrecy performance.

On the other hand, the objective of the AN designs was to guarantee a max-min fairness of users' SINRs. In case the eavesdropper's CSI is not available, the AN was designed to lie on the null-space of the users' channel. When the eavesdropper's CSI is available, the design aimed at limiting the eavesdropper's SINR below a certain threshold. A specific An design, which utilized ZF was also examined. In case of unknown eavesdropper's CSI, numerical results showed that, for the both designs (i.e., general and ZF), significant gaps between users' and eavesdropper's SINR were achieved. In case of known eavesdropper's CSI and general design, it was observed that, the eavesdropper' SINR was kept almost constant regardless of the transmitted power. In case of ZF design, the eavesdropper's SINR increased in accordance to an increase of the transmitted power. Similar to the case of unknown eavesdropper's CSI, both designs provided sufficient secrecy level.

Chapter 5

Multi-cell Multi-user Visible Light Communications Networks [62]

5.1. Introduction

The expected ubiquity of the future VLC means that it should be able to support multiple users in large public areas, such as supermarkets, stations or airports. Considering the fact that the illuminating coverage of LEDs is limited, this requirement essentially makes multi-cell configuration an inevitable progression in the development of future VLC networks.

5.1.1. Motivations

Initial research on multi-cell VLC networks focused on the model composed of small optical atto-cells, where each individual cell is illuminated by a LED array (LED luminaire) which is also known as an optical Access Point (AP). Nevertheless, if the same frequency resources are used across all cells, the inter-cell interference, which severely degrades the signal to interference plus noise ratio (SINR) of cell-edge users, is inevitable. As a result, methods for mitigating or eliminating the impact of inter-cell interference are of particular importance in the design of multi-cell VLC networks.

In fact, several approaches have been proposed to deal with the problem. In [25], the concept of joint transmission (JT) in RF was adapted to the atto-cell VLC networks. The proposed JT scheme was developed based on a specific structure of the APs in which each AP was composed of multiple clusters with different beam directions. Two transmission regions, namely: single point transmission region and multipoint transmission region were then defined according to the position of the user. Users within the single point transmission region were served by a cluster by means of OFDM. On the other hand, users in the multipoint transmission region were served by multiple clusters from different APs and the traditional frequency-partitioning approach was utilized to avoid the inter-cell interference. The same authors in [26] proposed a fractional frequency reuse (FFR) strategy to avoid the inter-cell interference at the expense of reduced bandwidth efficiency. Furthermore, the atto-cell configuration with FFR limits the mobility of user since switching frequencies during user movement degrades the user experience, which is a critical measure to some quality-sensitive services, such as video streaming and voice over IP (VoIP) [27]. Aside from the frequency partition approach, several works focused on cooperative transmission and signal design. Specifically, a cooperative transmission and reception based on On-Off Keying (OOK) and Pulse Position Division Multiplexing (PPDM) have been proposed [107]. While enabling a relatively simple transmission scheme, the proposed method required the receiver to have some information about the transmitter, which increases the complexity of the system. Efficient signal designs based on phase-shifted superposition and time superposition to mitigate interference have also been recently explored in [108, 109]. These design, however, still compromised the system bandwidth efficiency.

Due to the fact that commercial LEDs have limited modulation bandwidth (up to 20 MHz for the popular phosphorescent LEDs), the unity frequency reuse (UFR) strategy is more favorable as it allows users to make use of the full available spectrum. Precoding techniques then can be employed at the transmitters to alleviate the impact of inter-cell interference together with improved user mobility. This ap-

proach essentially combines neighboring atto-cells into a larger mutli-AP cell, which is termed as CoMP cell as we described in detail in Chapter 3.

5.1.2. Objectives

Building upon the well-established single CoMP cell configuration, we extend the concept to a multiple cell fashion to realize large-scale VLC networks². ZF precoding is utilized as the underlaying precoding scheme to support multiple users in one cell. Due to the above mentioned advantages of improved user mobility and enhanced bandwidth efficiency, the UFR strategy is adopted across all CoMP cells. Consequently, desired signals for users in one cell can be severely interfered by both intra-cell and inter-cell interferences. While the intra-cell interference could be handled effectively by means of precoding techniques in much the same way as in the case of single cell, it is challenging to deal with the inter-cell one. Different from the widely used frequency partition approach in atto-cell networks, the underlaying precoding scheme used in each CoMP cell introduces another way to overcome the challenge. That is by allowing coordination and/or cooperation, i.e., coordinated/cooperative precoding design³, among cells, it is possible to jointly design their precoders. The inter-cell interference, therefore, can be alleviated (or eliminated) by the coordinated/cooperative precoders.

In parallel to our study in this dissertation, the authors in [110] studied a coordinated precoding scheme for multi-cell VLC systems where, similar to this work, each cell is composed multiple luminaire transmitters. With the assumption that users downlink CSI is exchanged through a backbone network among cells, the weighted sum mean square error (WSMSE) is adopted as the performance criterion for the purpose of coordinated beamforming design. Different from that work, in this thesis, capitalizing on the underlay ZF precoding, we extensively examine different coordinated/cooperative precoding designs in multi-user multi-cell VLC, namely: per cell

²In this dissertation, we use the term multi-cell for referring to the multi-CoMP cell configuration.

³Since cell coordination/cooperation are realized through coordinated/cooperative precoding designs, they are used interchangeably.

coordinated precoding, coordinated precoding, and cooperative precoding with partial data sharing. For each design, the objective is to maximize users' sum-rate. In the considered multi-cell network, the VLC channels are subject to interferences, which are amplitude constrained. Thus, we utilize the lower and upper bound on the channel capacity of a scalar Gaussian interference channel in which both input signal and interference are amplitude constrained, which were derived in Chapter 2 Section 2.2. The optimal cooperative/coordinated precoders are then designed with respect to these bounds.

5.2. Network Model

We consider multi-user multi-cell CoMP VLC broadcast networks consisting of M cells ($M > 1$) whose primary purpose is the illumination of large areas. Each cell is formed by N_T LED arrays, which jointly serve K users⁴ simultaneously by means of precoding techniques; and it is assumed that all signal processing is done by a CPU. Fig. 5.1a illustrates a 4-cell VLC network, where $N_T = 4$ and LED arrays are arranged in a rectangular shape. Wired connections, such as Ethernet, fiber or power-line communications, can be used between CPUs for inter-cell cooperation as well as cells to/from gateway transmissions. As the primary purpose of the system is illumination, a proper lighting design is required to provide an uniform illumination over the target plane. Therefore, it is inevitable that there are overlapping illuminated areas, which are referred as inter-cell interference areas, at the edges of each cell as shown in Fig. 5.1b.

We assume that each user is equipped with a single-PD receiver. Therefore, each cell can be essentially regarded as a MU-MIMO VLC system. In such a multi-user broadcast system, the dominant performance-limiting factor is the multi-user interference (also known as intra-cell interference in the context of multi-cell networks). To alleviate the impact of the intra-cell interference, different linear precoding schemes

⁴For mathematical descriptions, it is assumed that the number of users is the same for every cell. For numerical simulations, however, we also examine the case that cells have different numbers of users.

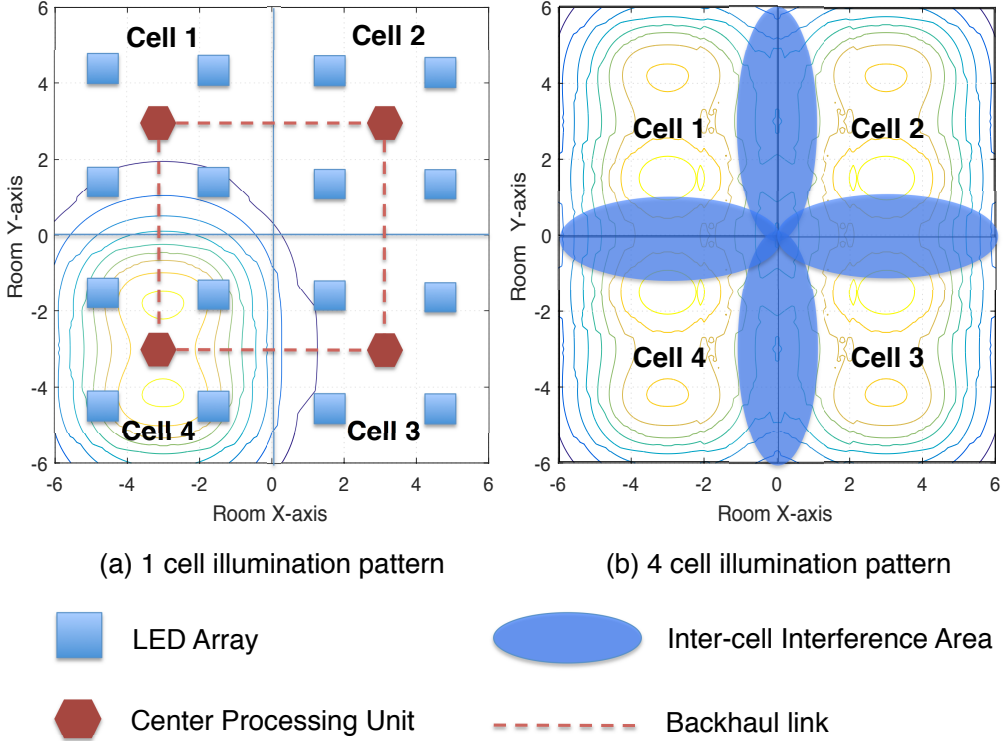


Figure 5.1: Multi-user multi-cell VLC network and illumination area.

were considered and optimally solved under the unique constraints of visible light signal [53–55, 57, 58, 111, 112, 114–118]. This paper, as we mentioned, deals with the multi-cell configuration, where, in addition to the intra-cell interference, the desired signals for users in one cell are also affected by the signals for users of the adjacent cells, i.e., inter-cell interference. For the sake of notation, throughout the paper, we denote $\mathcal{N}_c = \{N_{c,1}, N_{c,2}, \dots, N_{c,N_T}\}$ be the set of N_T LED arrays which belong to the c -th cell and $\mathcal{U}_c = \{U_{c,1}, U_{c,2}, \dots, U_{c,K}\}$ be the set of K users located in this cell. It is also assumed that $N_T \geq K$.

5.2.1. Precoding Model and Broadcast Transmission

Let $d_{c,i} \in \mathbb{R}$ be the data symbol that is intended to user $U_{c,i}$ and $\mathbf{d}_c = \begin{bmatrix} d_{c,1} & d_{c,2} & \dots & d_{c,K} \end{bmatrix}^T \in \mathbb{R}^{K \times 1}$ be the data vector for all users of the c -th cell. Suppose that $d_{c,i}$ is zero mean and normalized to the range of $[-1, 1]$. At the LED array $N_{c,i}$, the broadcast signal $s_{c,i}$ for users of \mathcal{U}_c is generated from a linear combination of the data vector and the

matrix $\mathbf{V}_{c,i} = \begin{bmatrix} w_{c,i,1} & w_{c,i,2} & \dots & w_{c,i,K} \end{bmatrix} \in \mathbb{R}^{1 \times K}$ as

$$s_{c,i} = \mathbf{V}_{c,i} \mathbf{d}_c. \quad (5.1)$$

Since $s_{c,i}$ can take on a negative value, which is not valid for IM/DD used in VLC, a DC-bias $I_{c,i}^{\text{DC}}$ should be added to $s_{c,i}$ to ensure the non-negativity of the input signal, i.e.,

$$x_{c,i} = s_{c,i} + I_{c,i}^{\text{DC}} \geq 0. \quad (5.2)$$

As $\mathbb{E}[\mathbf{d}_c] = \mathbf{0}$, the signal $s_{c,i}$ does not effect the average illumination level of the LEDs. Instead, it is uniquely determined by the DC-bias $I_{c,i}^{\text{DC}}$. If we define $\mathbf{P}_c^s = \begin{bmatrix} P_{c,1}^s & P_{c,2}^s & \dots & P_{c,N_T}^s \end{bmatrix}^T \in \mathbb{R}^{N_T \times 1}$ is the transmitted power vector for the LED arrays of the c -th cell whose element $P_{c,i}^s = \eta x_{c,i}$ is the transmitted optical power of the k -th LED array with η being the LED conversion factor, the received optical signal at user $U_{c,k}$ can be written as

$$P_{c,k}^r = \left[\mathbf{H}_{1,c,k} \quad \mathbf{H}_{2,c,k} \quad \dots \quad \mathbf{H}_{M,c,k} \right] \left[\mathbf{P}_1^s \quad \mathbf{P}_2^s \quad \dots \quad \mathbf{P}_M^s \right]^T \quad (5.3)$$

where $\mathbf{H}_{i,c,k} = \begin{bmatrix} h_{i,1,c,k} & h_{i,2,c,k} & \dots & h_{i,N_T,c,k} \end{bmatrix} \in \mathbb{R}^{1 \times N_T}$ is the channel matrices between \mathcal{N}_i and $U_{c,k}$.

If we denote $\mathbf{x}_c = \begin{bmatrix} x_{c,1} & x_{c,2} & \dots & x_{c,N_T} \end{bmatrix}^T \in \mathbb{R}^{N_T \times 1}$ as the transmitted signal vector and $\mathbf{I}_c^{\text{DC}} = \begin{bmatrix} I_{c,1}^{\text{DC}} & I_{c,2}^{\text{DC}} & \dots & I_{c,N_T}^{\text{DC}} \end{bmatrix}^T \in \mathbb{R}^{N_T \times 1}$ as the aggregated DC bias vector for users at the c -th cell, the received electrical signal at user $U_{c,k}$, after the optical-

electrical conversion, is given by

$$\begin{aligned}
 y_{c,k} &= \gamma P_r^{c,k} + n_{c,k} = \gamma \eta \left[\mathbf{H}_{1,c,k} \quad \mathbf{H}_{2,c,k} \quad \dots \quad \mathbf{H}_{M,c,k} \right] \left[\mathbf{x}_1 \quad \mathbf{x}_2 \quad \dots \quad \mathbf{x}_M \right]^T + n_{c,k} \\
 &= \gamma \eta \left(\underbrace{\mathbf{H}_{c,c,k} \mathbf{W}_{c,k} d_{c,k} + \mathbf{H}_{c,c,k} \sum_{i \in \mathcal{U}_c, i \neq k} \mathbf{W}_{c,i} d_{c,i}}_{\text{intra-cell interference}} + \underbrace{\sum_{c' \neq c} \sum_{j \in \mathcal{U}_{c'}} \mathbf{H}_{c',c,k} \mathbf{W}_{c',j} d_{c',j}}_{\text{inter-cell interference}} \right. \\
 &\quad \left. + \underbrace{\sum_{i=1}^M \mathbf{H}_{i,c,k} \mathbf{I}_i^{\text{DC}}}_{\text{DC current}} \right) + n_{c,k}, \tag{5.4}
 \end{aligned}$$

with γ being the PD responsivity and $\mathbf{W}_{c,k} = \begin{bmatrix} w_{c,1,k} & w_{c,2,k} & \dots & w_{c,N_T,k} \end{bmatrix}^T \in \mathbb{R}^{N_T \times 1}$ being the *precoder* for user $U_{c,k}$. As seen from Eq. (5.4), the first term $\mathbf{H}_{c,c,k} \mathbf{W}_{c,k} d_{c,k}$ is the desired signal, the second and the third terms $\mathbf{H}_{c,c,k} \sum_{i \in \mathcal{U}_c, i \neq k} \mathbf{W}_{c,i} d_{c,i}$, $\sum_{c' \neq c} \sum_{j \in \mathcal{U}_{c'}} \mathbf{H}_{c',c,k} \mathbf{W}_{c',j}$ represent the intra-cell and inter-cell interferences, respectively. $\sum_{i=1}^M \mathbf{H}_{i,c,k} \mathbf{I}_i^{\text{DC}}$ is the DC current that carries no data, $n_{c,k}$ denotes the receiver noise, which is assumed to be AWGN with zero mean and variance $\sigma_{c,k}^2$, and is given as in (3.6)

$$\sigma_{c,k}^2 = 2\gamma e \overline{P_{c,k}^r} B + 4\pi e A_r \gamma \chi_{\text{amp}} (1 - \cos(\Psi)) B + i_{\text{amp}}^2 B, \tag{5.5}$$

where $\overline{P_{c,k}^r} = \mathbb{E}[P_{c,k}^r] = \eta \left(\sum_{i=1}^M \mathbf{H}_{i,c,k} \mathbf{I}_i^{\text{DC}} \right)$ is the average received optical power at user $U_{c,k}$. After removing the DC current by AC coupling, the received signal can be written by

$$y_{c,k} = \gamma \eta \left(\mathbf{H}_{c,c,k} \mathbf{W}_{c,k} d_{c,k} + \mathbf{H}_{c,c,k} \sum_{i \in \mathcal{U}_c, i \neq k} \mathbf{W}_{c,i} d_{c,i} + \sum_{c' \neq c} \sum_{j \in \mathcal{U}_{c'}} \mathbf{H}_{c',c,k} \mathbf{W}_{c',j} d_{c',j} \right) + n_{c,k}. \tag{5.6}$$

5.2.2. ZF Precoding and Optical Power Constraint

As seen from Eq. (5.6), the desired signal of user $U_{c,k}$ can be greatly degraded by the inter-cell and the intra-cell interferences where the former is generally more severe since it comes from the signals intended to users in the same cell which are stronger

than that from the other cells. The intra-cell interference, however, can be effectively suppressed by utilizing ZF precoding technique whose idea is to construct the precoder $\mathbf{W}_{c,i}$ in such a way that it is orthogonal to $\mathbf{H}_{c,c,k}$, that is

$$\mathbf{H}_{c,c,k} \mathbf{W}_{c,i} = 0 \quad \forall i \in \mathcal{U}_c, i \neq k. \quad (5.7)$$

If we define $\mathbf{H}_c = \begin{bmatrix} \mathbf{H}_{c,c,1}^T & \mathbf{H}_{c,c,2}^T & \dots & \mathbf{H}_{c,c,K}^T \end{bmatrix}^T$ and $\mathbf{W}_c = \begin{bmatrix} \mathbf{W}_{c,1} & \mathbf{W}_{c,2} & \dots & \mathbf{W}_{c,K} \end{bmatrix}$, the ZF constraint in (5.7) implies that

$$\mathbf{H}_c \mathbf{W}_c = \begin{bmatrix} \sqrt{q_{c,1}} \\ & \sqrt{q_{c,2}} \\ & & \ddots \\ & & & \sqrt{q_{c,K}} \end{bmatrix} = \text{diag}\{\sqrt{\mathbf{q}_c}\}, \quad (5.8)$$

where $\sqrt{\mathbf{q}_c} = \begin{bmatrix} \sqrt{q_{c,1}} & \sqrt{q_{c,2}} & \dots & \sqrt{q_{c,K}} \end{bmatrix}^T$ whose i -th element represents the channel gain of user $U_{c,k}$.

With the constraint in (5.7), the received signal at $U_{c,k}$ is rewritten as

$$y_{c,k} = \gamma \eta \left(\mathbf{H}_{c,c,k} \mathbf{W}_{c,k} d_{c,k} + \sum_{c' \neq c} \sum_{j \in \mathcal{U}_{c'}} \mathbf{H}_{c',c,k} \mathbf{W}_{c',j} d_{c',j} \right) + n_{c,k}, \quad (5.9)$$

which contains the inter-cell interference term only. In addition to the ZF constraint in (5.7), one always must take the transmit power constraint into consideration when formulating optimal precoding designs as we described in Chapter 2 for the case of single cell. Similarly, in this multi-cell configuration, the input current signal of the LEDs is non-negative and is amplitude constrained to a certain threshold, i.e., $0 \leq x_{c,i} \leq I_{\max}$ with I_{\max} being the maximum input current for the LEDs to maintain their linear operating range. Since $d_{c,i}$ is assumed to be normalized within $[-1, 1]$,

these two constraints lead to the following constraint on the precoder design

$$\sum_{k=1}^K \left\| [\mathbf{W}_{c,k}]_{:,i} \right\|_1 \leq \Delta_{c,i}, \quad (5.10)$$

where $\Delta_{c,i} = \min(I_{c,i}^{\text{DC}}, I_{\max} - I_{c,i}^{\text{DC}})$.

In the following section, we investigate different cell coordination/cooperation strategies to mitigate the impact of the inter-cell interference. With respect to the derived lower and upper capacity bounds in Section II, the optimal coordinated/cooperative ZF precoding to maximize the users' sum-rate is then designed for each strategy accordingly.

5.3. Cell Coordination/Cooperation Strategies

5.3.1. Per-Cell Coordinated Precoding

We first examine the simplest cell coordination level where all signal processing are performed on a per-cell basis. Nonetheless, cell coordination by sharing precoding designs are allowed. That is each cell designs its own precoders taking into account the precoders of other cells. Following (2.11) and (2.13), the lower and upper capacity bounds of user $U_{c,k}$ are respectively given by

$$C_{c,k}^L = \frac{1}{2} \log \left(\frac{2(\gamma\eta)^2 \left((\mathbf{H}_{c,c,k} \mathbf{W}_{c,k})^2 + \sum_{c' \neq c} \sum_{j \in \mathcal{U}_{c'}} (\mathbf{H}_{c',c,k} \mathbf{W}_{c',j})^2 \right) + \pi e \sigma_{c,k}^2}{\pi e \left(\frac{(\gamma\eta)^2 \sum_{c' \neq c} \sum_{j \in \mathcal{U}_{c'}} (\mathbf{H}_{c',c,k} \mathbf{W}_{c',j})^2}{3} + \sigma_{c,k}^2 \right)} \right), \quad (5.11)$$

and

$$C_{c,k}^U = \frac{1}{2} \log \left(\frac{\pi e \left(\frac{(\gamma\eta)^2 ((\mathbf{H}_{c,c,k} \mathbf{W}_{c,k})^2 + \sum_{c' \neq c} \sum_{j \in \mathcal{U}_{c'}} (\mathbf{H}_{c',c,k} \mathbf{W}_{c',j})^2)}{3} + \sigma_{c,k}^2 \right)}{2(\gamma\eta)^2 \sum_{c' \neq c} \sum_{j \in \mathcal{U}_{c'}} (\mathbf{H}_{c',c,k} \mathbf{W}_{c',j})^2 + \pi e \sigma_{c,k}^2} \right). \quad (5.12)$$

In this coordinated scheme, the goal is to design precoders, i.e., $\mathbf{W}_{c,k}$, to maximize the lower and upper sum-rate (sum-capacity) of all users in the c -th cell. Moreover, it is straightforward to see that the optimal precoders to the problem of maximizing the lower sum-rate is the same with that of the upper bound. Therefore, finding the optimal solution to maximize the lower sum-rate is sufficient.

$$\begin{aligned} \mathcal{P}5.1 : \quad & \underset{\mathbf{W}_{c,k}}{\text{maximize}} \quad \sum_{k=1}^K C_{c,k}^L \\ & \text{subject to} \quad \mathbf{H}_{c,c,k} \mathbf{W}_{c,i} = 0 \quad \forall k \neq i, \\ & \quad \sum_{k=1}^K \left\| [\mathbf{W}_{c,k}]_{i,:} \right\|_1 \leq \Delta_{c,i}. \end{aligned} \quad (5.13)$$

It is important to note that, different from the single-cell setting, the choice of precoders at each cell affects the inter-cell interference at the neighboring cells, and that, in turn also affects their precoding design. As a result, the optimal solution to $\mathcal{P}5.1$ needs to be found in an iterative manner until the sum-rate of each cell achieves its maximal value. Specifically for the c -th cell, at each iteration, we solve $\mathcal{P}5.1$ to find $\mathbf{W}_{c,k}$ while all other $(M-1)K$ precoders $\mathbf{W}_{c',j}$ are fixed, i.e., the inter-cell interference term $\sum_{c' \neq c} \sum_{j \in \mathcal{U}_{c'}} (\mathbf{H}_{c',c,k} \mathbf{W}_{c',j})^2$ is constant. However, even fixing the inter-cell interference, it can be seen that $\mathcal{P}5.1$ is not a convex optimization problem due to the non-convexity of the objective function. Thus, it is generally difficult to find its optimal solution.

Here, we develop an iterative algorithm based on the CCCP to find a local optimal solution to the problem. First, let us denote $\theta_{c,k} = \sum_{c' \neq c} \sum_{j \in \mathcal{U}_{c'}} (\mathbf{H}_{c',c,k} \mathbf{W}_{c',j})^2$. By introducing a slack variable $\lambda_{c,k}$ and expressing $\mathbf{H}_{c,k} \mathbf{W}_{c,k} = \sqrt{q_{c,k}}$, $\mathcal{P}5.1$ is then

rewritten as

$$\begin{aligned}
 \mathcal{P}5.2 : \quad & \underset{\mathbf{W}_{c,k}, q_{c,k}, \lambda_{c,k}}{\text{maximize}} \quad \frac{1}{2} \sum_{k=1}^K \log \left(\frac{2(\gamma\eta)^2 (\lambda_{c,k} + \theta_{c,k}) + \pi e \sigma_{c,k}^2}{\pi e \left(\frac{(\gamma\eta)^2 \theta_{c,k}}{3} + \sigma_{c,k}^2 \right)} \right) \\
 & \text{subject to} \quad \mathbf{H}_c \mathbf{W}_c = \text{diag} \left\{ \begin{bmatrix} \sqrt{q_{c,1}} & \sqrt{q_{c,2}} & \dots & \sqrt{q_{c,K}} \end{bmatrix} \right\}, \\
 & \quad \sum_{k=1}^K \left\| [\mathbf{W}_{c,k}]_{i,:} \right\|_1 \leq \Delta_{c,i}, \\
 & \quad q_{c,k} \geq \lambda_{c,k}, \\
 & \quad q_{c,k} \geq 0.
 \end{aligned} \tag{5.14}$$

The objective function of $\mathcal{P}5.2$ is now concave, yet the first constraint is not convex since $\mathbf{H}_c \mathbf{W}_c$ is affine while $\text{diag} \left\{ \begin{bmatrix} \sqrt{q_{c,1}} & \sqrt{q_{c,2}} & \dots & \sqrt{q_{c,K}} \end{bmatrix} \right\}$ is concave. The CCCP involves an iterative process to find a local maximal of $\mathcal{P}5.2$ by, at the i -th iteration of the procedure, approximately linearizing the concave term $\sqrt{q_{c,k}^{(i)}}$ by its Taylor expansion as $\sqrt{q_{c,k}^{(i)}} \approx \sqrt{q_{c,k}^{(i-1)}} + \frac{1}{2\sqrt{q_{c,k}^{(i-1)}}} (q_{c,k}^{(i)} - q_{c,k}^{(i-1)})$ where $q_{c,k}^{(i-1)}$ is the obtained from the previous iteration. From this approximation, $\mathcal{P}5.2$ is transformed to a convex optimization problem which can be solved efficiently by using standard optimization packages. Capitalizing on the process for solving $\mathcal{P}5.2$, we are now able to develop an iterative algorithm for solving $\mathcal{P}5.1$ as follows

5.3.2. Coordinated Precoding

As can be seen from (5.9), the inter-cell interference can be problematic, especially for cell-edge users and in the case of populous cells. In the per-cell coordinated scheme, each cell designs precoders for its own users considering the interferences from other cells. The inter-cell interference, therefore, is minimized but not completely eliminated. From this observation, a natural way to cancel out the inter-cell interference is to *extend* the ZF precoder design in such a way that it takes into account the channels of users in other cells. This requires, for every cell, the availability of out-of-cell users' CSI through CSI sharing among cells. Different from the per-cell coordinated

Algorithm 3 Iterative algorithm for solving problem **P5.1**

1: Initialization

1. Estimate channel matrices $\mathbf{H}_{c,c,k}$ and noise variances $\sigma_{c,k}^2$.
2. Initialize $\mathbf{W}_{c',k}^{(0)}$ to satisfy the constraint in (5.10).

2: Iteration: At the i -th iteration

1. Given $\mathbf{W}_{c',k}^{(i-1)}$, solve **P5.2** using CCCP to find the optimal $\mathbf{W}_{c,k}^{(i)}$, denoted as $\mathbf{W}_{c,k}^{*(i)}$.
2. Use the obtained $\mathbf{W}_{c,k}^{*(i)}$ to solve **P5.2** for other cells.
3. $i = i + 1$.

3: Termination: terminate the iteration when

1. $|\mathbf{W}_{c,k}^{(*i)} - \mathbf{W}_{c,k}^{*(i-1)}| \leq \epsilon$, where $\epsilon = 10^{-3}$ is a predefined threshold, or
 2. $i = L$, where $L = 10$ is the predefined maximum number of iterations.
-

scheme, once the inter-cell interference is eliminated, maximizing the sum-rate of users in all cells reduces to maximizing the sum-rate of users in each individual cell.

With respect to the lower bound capacity from (2.3), the optimal precoding design is then formulated as

$$\begin{aligned} \mathcal{P}5.3 : \quad & \underset{\mathbf{W}_{c,k}}{\text{maximize}} \quad \sum_{k=1}^K \log \left(1 + \frac{2(\gamma\eta)^2 \mathbf{H}_{c,c,k} \mathbf{W}_{c,k} \mathbf{W}_{c,k}^T \mathbf{H}_{c,c,k}^T}{\pi e \sigma_{c,k}^2} \right) \\ & \text{subject to} \quad \mathbf{H}_{c,c,k} \mathbf{W}_{c,i} = 0 \quad \forall k \neq i, \{k, i\} \in \mathcal{U}_c \\ & \quad \mathbf{H}_{c,c',k} \mathbf{W}_{c,i} = 0 \quad \forall c' \neq c, \forall k \in \mathcal{U}_{c'} \\ & \quad \sum_{k=1}^K \left\| [\mathbf{W}_{c,k}]_{n,:} \right\|_1 \leq \Delta_{c,n}, \quad \forall n = 1, 2, \dots, N_T. \end{aligned} \tag{5.15}$$

Although the second ZF constraint in **P5.3** reduces the degrees of freedom on designing $\mathbf{W}_{c,k}$, it essentially removes the inter-cell interference introducing to users in other cells, thus significantly improve the overall sum-rate performance. Similar to problem **P5.1**, the above problem can be solved using the CCCP.

It should be noted that **P5.3** is not always feasible. To see this, let $\bar{\mathbf{H}}_c = \left[\mathbf{H}_{c,c',k}^T \right]_{\forall c' \neq c, \forall k \in \mathcal{U}_{c'}}^T$ and $\tilde{\mathbf{H}}_{c,k} = \left[\mathbf{H}_{c,c,1}^T \cdots \mathbf{H}_{c,c,k-1}^T \cdots \mathbf{H}_{c,c,k+1}^T \mathbf{H}_{c,c,K}^T \right]^T$. A non-zero solution for the precoder of $U_{c,k}$ requires that the null space of $\left[\tilde{\mathbf{H}}_{c,k}^T \quad \bar{\mathbf{H}}_c^T \right]^T$ has a

dimension greater than 0, which is satisfied when $N_T > \text{rank} \left(\begin{bmatrix} \tilde{\mathbf{H}}_{c,k}^T & \bar{\mathbf{H}}_c^T \end{bmatrix}^T \right)$. Thus, the feasibility of $\mathcal{P}5.3$ is equivalent to the condition that $N_T > \max \left\{ \text{rank} \left(\begin{bmatrix} \tilde{\mathbf{H}}_{c,k}^T & \bar{\mathbf{H}}_c^T \end{bmatrix}^T \right) \right\}_{\forall c,k}$. This, however, is not always possible when $\begin{bmatrix} \tilde{\mathbf{H}}_{c,k}^T & \bar{\mathbf{H}}_c^T \end{bmatrix}^T$ is full row rank and the number of its row is larger than or equal to N_T . As a consequence, to ensure the feasibility of $\mathcal{P}5.3$, every cell should accommodate at most N_T users. Since the first ZF constraint always needs to be satisfied as the intra-cell interference is generally more severe than the inter-cell one, the number of out-of-cell users being taken into account for the precoder design of one cell is then $(N_T - K)$. The problem now is how to select those $(N_T - K)$ out-of-cell users to maximize the overall sum-rate performance. One can immediately realize that those users should be selected from different cells as their channel are more spatially uncorrelated. In this paper, as we consider the simplest 2-cell configuration for numerical results, out-of-cell users are chosen randomly for the sake of simplicity. Once the set of out-of-cell users is determined for every cell, the optimal precode design problem is essentially the same as $\mathcal{P}5.1$ with an additional ZF constraint for the selected out-of-cell users. The optimal solution can then be found by an iteration algorithm.

5.3.3. Partial Cooperative Precoding with Data Sharing

Despite the previous coordinated precoding design helps to overcome the problem of inter-cell interference, one can further improve the sum-rate performance by allowing data sharing among cells to enhance users' SNR. With this assumption, one can immediately think of a full cooperation among all cells, i.e., cells act as a large single cell. This type of cooperation is essentially equivalent to the MU-MIMO VLC broadcast systems with MN_T LED arrays and MK users discussed in [119–121]. In the context of RF communications, this full cell cooperation is sometimes referred as *multi-cell processing (MCP)*. The MCP imposes further signal processing constraints on the precoding design, especially when there are more cells and large number of users and in case of multi-cell VLC systems it is not always effective. That is because

of the following two reasons. Firstly, with a proper lighting design, the inter-cell interference at a given cell can only come from its neighboring cells. Consequently, data symbols for users in one cell should only be shared to the neighboring cells. Secondly, due to the limited FOV of the LEDs, the inter-cell interference is mainly caused by the cell-edge LED arrays of the neighboring cells. Therefore, sharing data to all LED arrays of the neighboring cells might not help to improve the performance much. From these two observations, in this work, we thus consider a partial cooperation strategy, which requires relatively lower complexity compared to the full cooperation approach. In this scheme, the data symbols for users in \mathcal{N}_c is only shared to the cell-edge LED arrays of the neighboring cells, which contribute the majority of the inter-cell interference. Those selected LED arrays in the neighboring cells cooperate with \mathcal{N}_c to form a new set of LED arrays, denoted as $\mathcal{N}_{\bar{c}}$, which now transmits signal to the users in the c -th cell. Hence, there are possibly several LED arrays which serve users in different cells. For mathematical convenience, let us denote

1. $\bar{\mathcal{N}}_{c',c}$ be the set of the cell-edge LED arrays of the c' -th cell, which borders to the c -th cell. As a result, $\mathcal{N}_{\bar{c}} = \mathcal{N}_c \bigcup_{\forall c'} \bar{\mathcal{N}}_{c',c}$.
2. $\bar{\mathcal{N}}_c = \bigcup_{\forall c'} \bar{\mathcal{N}}_{c',c}$ be the set of the cell-edge LED arrays of all adjacent cells of the c -th cell.
3. $\mathbf{H}_{\bar{c},c,k}$ be the channel matrix from $\mathcal{N}_{\bar{c}}$ to user $U_{c,k}$.
4. $\mathbf{W}_{\bar{c},c,k}$ be the precoder for user $U_{c,k}$.

With these notations, the received signal at user $U_{c,k}$ can then be written as

$$y_{c,k} = \gamma \eta \left(\mathbf{H}_{\bar{c},c,k} \mathbf{W}_{\bar{c},c,k} d_{c,k} + \mathbf{H}_{\bar{c},c,k} \sum_{i \in U_c, i \neq k} \mathbf{W}_{\bar{c},c,i} d_{c,i} + \sum_{c' \neq c} \sum_{j \in U_{c'}} \mathbf{H}_{\bar{c}',c,k} \mathbf{W}_{\bar{c}',c,j} d_{c',j} \right) + n_{c,k}. \quad (5.16)$$

Since each LED array can transmit data to users of different cells, the power constraint in (5.10) needs to be reformulated. Assume that the LED array $N_{c,k}$ in the c -th cell

is indexed as $N_{c',k_{c'}}$ in the neighboring c' -th cell. The LED power constraint is then written as

$$\sum_{i \in U_c} \left\| [\mathbf{W}_{\bar{c},c,i}]_{k,:} \right\|_1 + \sum_{c'} \sum_{i \in U_{c'}} \left\| [\mathbf{W}_{\bar{c}',c,i}]_{k_{c'},:} \right\|_1 \leq \Delta_{\bar{c},c,k}. \quad (5.17)$$

Assume also that the data sharing process is done through a backhaul link connecting cells with unlimited capacity and no delay constraints, the optimal ZF precoder design problem for this cooperative form is given by

$$\begin{aligned} \mathcal{P}5.4 : \quad & \underset{\mathbf{W}_{\bar{c},c,k}}{\text{maximize}} \quad \sum_{c=1}^M \sum_{k \in U_c} \log \left(1 + \frac{2(\gamma\eta)^2 \mathbf{H}_{\bar{c},c,k} \mathbf{W}_{\bar{c},c,k} \mathbf{W}_{\bar{c},c,k}^T \mathbf{H}_{\bar{c},c,k}^T}{\pi e \sigma_{c,k}^2} \right) \\ & \text{subject to} \quad \mathbf{H}_{\bar{c},c,k} \mathbf{W}_{\bar{c},c,i} = 0 \quad \forall k, i \in U_c, k \neq i, \\ & \quad \mathbf{H}_{\bar{c},c',k} \mathbf{W}_{\bar{c},c,i} = 0 \quad \forall c \neq c', k \in U_{c'}, i \in U_c \\ & \quad \sum_{i \in U_c} \left\| [\mathbf{W}_{\bar{c},c,i}]_{k,:} \right\|_1 + \sum_{c'} \sum_{i \in U_{c'}} \left\| [\mathbf{W}_{\bar{c}',c,i}]_{k_{c'},:} \right\|_1 \leq \Delta_{\bar{c},c,k}. \end{aligned} \quad (5.18)$$

It should be noted that selecting all LED arrays in $\mathcal{N}_{c'}$ which have LoS link to $U_{c,k}$ may not be optimum since a certain selection of LED arrays in $\mathcal{N}_{c'}$ will affect the precoder design for users in this cell. It, in turn, has an impact on the sum-rate performance. For the sake of conciseness, we leave the problem of optimally selecting LED arrays for a future investigation.

5.4. Numerical Results and Discussions

In this section, numerical results are presented to demonstrate the effectiveness of different cell cooperation strategies. For the sake of illustration, we consider a two-cell CoMP VLC network with two users in each cell as depicted in Fig. 5.2. Additionally, a Cartesian coordinate system whose origin is in the center of the ceiling is used for specifying the positions of users and the LED arrays. We assume that all users are placed on the same receive plane, which is 0.6 m above the floor. Unless otherwise noted, the parameters of the room, LED arrays and optical receivers are given in

Table 5.1: Multi-Cell VLC System Parameters

Parameter	Value
Room and LED configurations	
Room Dimension (Length \times Width \times Height)	12 (m) \times 6 (m) \times 3 (m)
Number of LED arrays, M	8
LED array size	0.1 (m) \times 0.1 (m)
Number of LED chips per array	36
LED array positions	Array 1: (-4, -1.5, 0) Array 3: (-2, 1.5, 0) Array 5: (2, -1.5, 0) Array 7: (4, 1.5, 0) Array 2: (-2, -1.5, 0) Array 4: (-4, 1.5, 0) Array 6: (4, -1.5, 0) Array 8: (2, 1.5, 0)
LED bandwidth, B	20 MHz
LED beam angle, ϕ (LED Lambertian order is 1)	120°
LED conversion factor, η	0.44 W/A
Receiver photodetectors	
PD active area, A_r	1 cm ²
PD responsivity, γ	0.54 A/W
PD field of view (FOV), Ψ	60°
Optical filter gain, $T_s(\psi)$	1
Refractive index of the concentrator, κ	1.5
Other parameters	
Ambient light photocurrent, χ_{amp}	10.93 A/(m ² · Sr)
Preamplifier noise current density, i_{amp}	5 pA/Hz ^{-1/2}

Table I.

Firstly, the benefit of cell coordination/cooperation in reducing the impact of inter-cell interference is illustrated. To do this, we examine the performance of each coordination/cooperation strategy with respect to a user's position while fixing other users' positions. Specifically, we fix the positions of User 1, 2, and 3 as follows

- User 1: $\text{UT1} = \begin{pmatrix} -3.2, & -1.8, & 2.4 \end{pmatrix}$

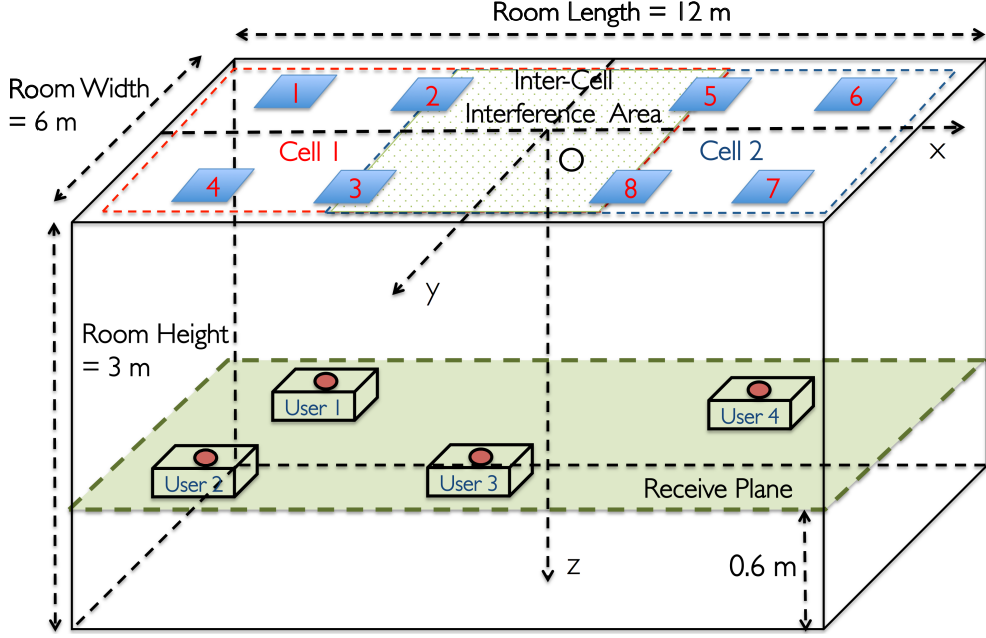


Figure 5.2: Geometrical configuration of a multi-user multi-cell MU-MIMO VLC systems with 8 LEDs arrays.

- User 2: $\text{UT2} = \begin{pmatrix} -0.5, & 1.2, & 2.4 \end{pmatrix}$
- User 3: $\text{UT3} = \begin{pmatrix} 3.5, & -1.5, & 2.4 \end{pmatrix}$

and let User 4 moves within Cell 2. Fig. 5.3 shows the lower bound maximum sum-rate performances of the considered schemes in accordance with User 4's position. The transmitted LED array power P_s is set to 35 dBm. As clearly seen from the figure, the per-cell coordinated precoding suffers from poor performance especially when User 4 is in cell-edge area, i.e., the inter-cell interference area. On the other hand, the coordinated and partial cooperative schemes generally perform well as the inter-cell interference is effectively eliminated. Moreover, we also observe that the partial cooperative precoding offer a slightly better performance than the coordinated one does, especially when User 4 is close to either User 2 or User 3. That is because when users are close to each other, their channels become more correlated. The partial cooperative precoding with data sharing helps to improve users' received signal quality, thus reduce the impact of channel correlation.

Next, we present the averaged maximum sum-rate performance versus the average LED array transmitted power for the considered cooperative schemes with dif-

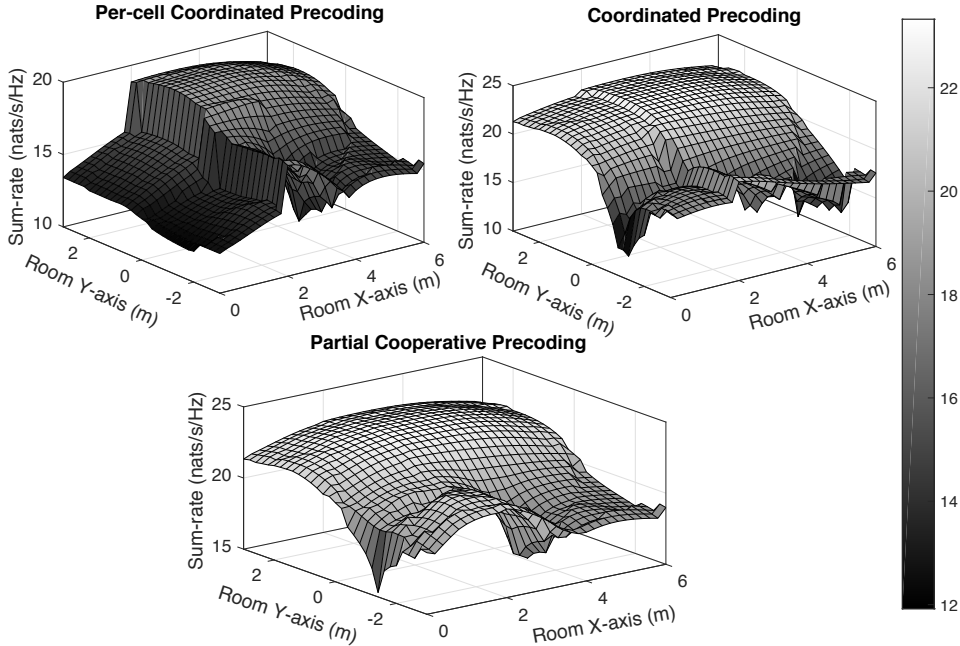


Figure 5.3: Maximum sum-rate distribution for different cooperative schemes.

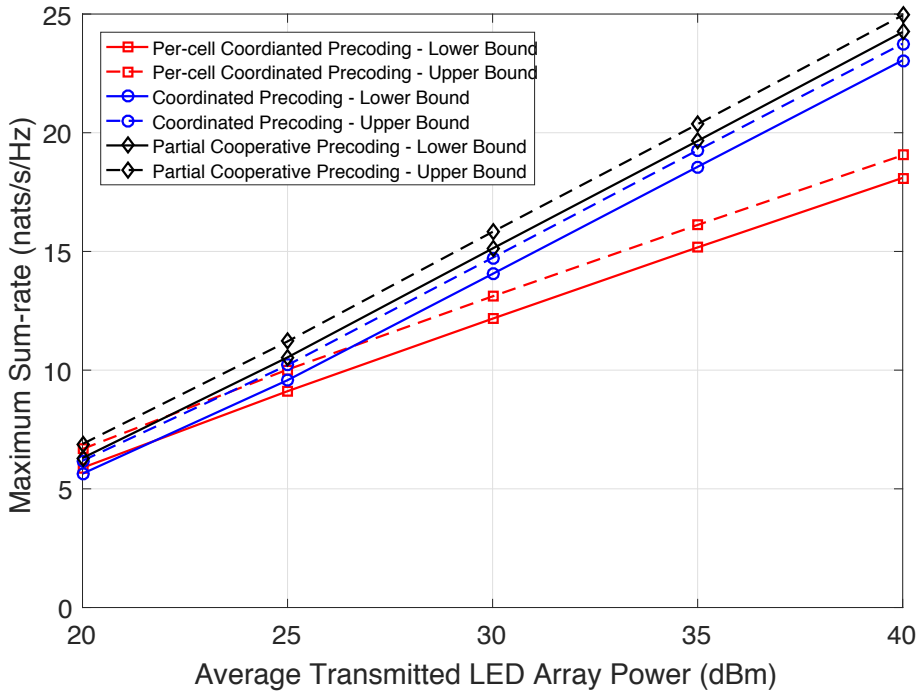


Figure 5.4: Average maximum sum-rate versus average LED array transmitted power: 2-by-2.

ferent numbers of users. All the results are obtained through 10,000 different channel realizations, i.e., 10,000 different positions of users uniformly located in their cell. First, we examine the case of having 4 users in total which corresponds to two dif-

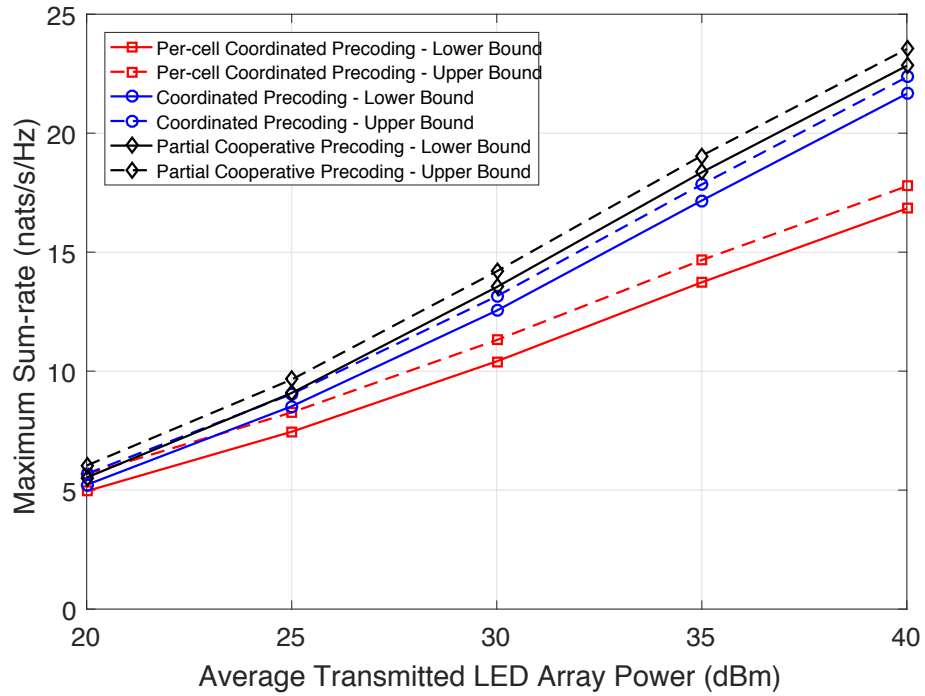


Figure 5.5: Average maximum sum-rate versus average LED array transmitted power:1-by-3.

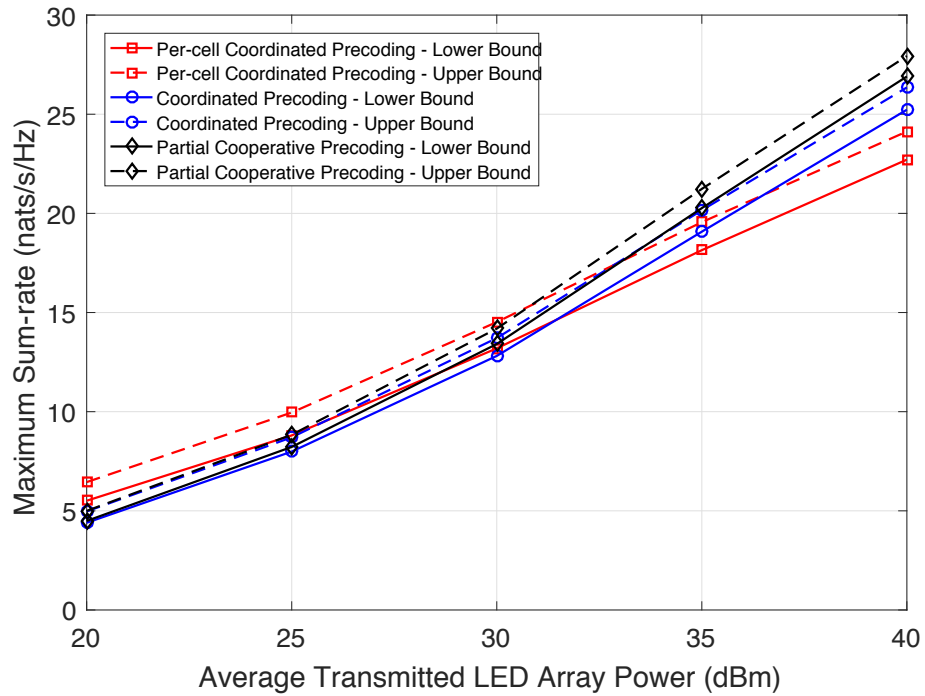


Figure 5.6: Average maximum sum-rate versus average LED array transmitted power: 3-by-3.

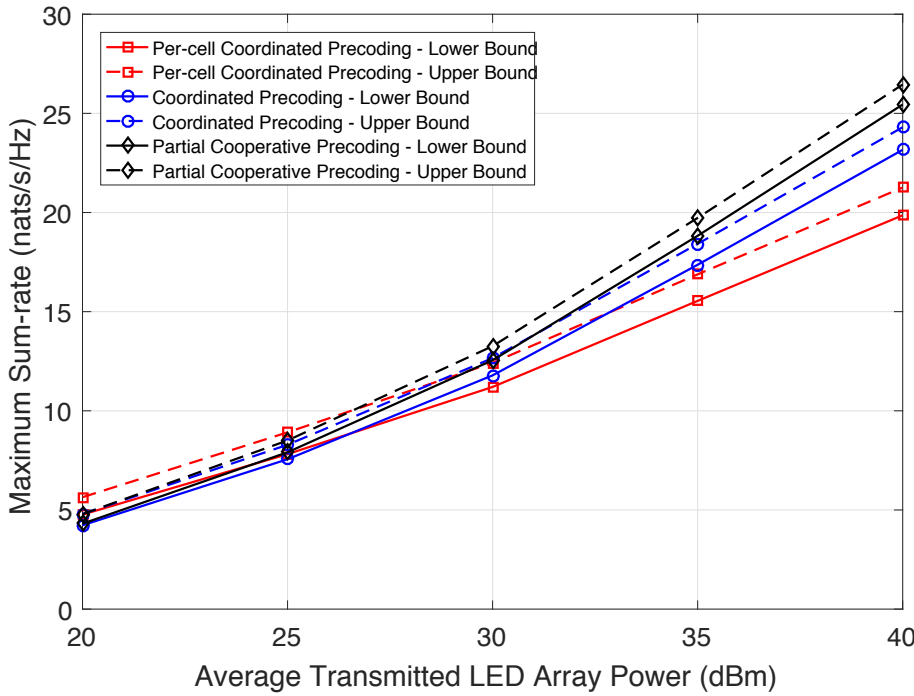


Figure 5.7: Average maximum sum-rate versus average LED array transmitted power: 2-by-4.

ferent configurations: 2-by-2 (2 users in each cell) and 1-by-3 (1 users in the first cell and 3 users in the second cell). Figures 5.4 and 5.5 show the two cases of 2-by-2 and 1-by-3, respectively. The average LED array power ranges from 20 to 40 dBm, which corresponds from 0.1 to 10 Watt. In both cases of user configuration, we observe significant performance improvements of the coordinated and partial cooperative precoding schemes over the per-cell coordinated one. Additionally, as the inter-cell interference is proportional to the LED transmitted power, these improvements increase in accordance with an increase in the LED transmitted power as well. Particularly, for both configuration at 40 dBm transmitted power, the performance gains of the coordinated and partial cooperative schemes are 5 and 6.2 nats, respectively. It is interesting to note that the partial cooperative precoding does not outperform the coordinated scheme much, thus revealing that cell coordination without data sharing is sufficient enough to reduce the impact of inter-cell interference. Additionally, it is seen that the overall performance of the 2-by-2 configuration is slightly better than the 1-by-3 one. That is because with a relatively small number of LED arrays per cell,

5.4 Numerical Results and Discussions

i.e., 4, the performance loss, on average, due to channel correlation in the 3-user-cell over the 2-user-cell is higher than that of 2-user-cell over the 1-user-cell.

In the case of more users per cell, Figs. 5.6 and 5.7 illustrate performances of 3-by-3 and 2-by-4 configurations, respectively. Compared to from the previous scenarios, the improvements of the coordinated precoding and partial cooperative precoding over the per-cell coordinated scheme are lower. At 40 dBm transmitted power, these improvements are 2.5, 4.2 nat in the 3-by-3 configuration and 3.3, 5.6 nat in the 2-by-4 one. Even at lower transmitted power, we observe that the per-cell coordinated scheme performs better than the two coordinated/cooperative schemes. The reason is when more users are involved in the coordinated/cooperative precoder designs (the number of uses per cell is large compared to the number of LED arrays per cell), the impact of channel correlation gets larger, i.e., there are less dimensions available for interference cancelation. Therefore, when the transmitted power is low the impact of the the inter-cell interference, which is weak, is not as high as that of the channel correlation.

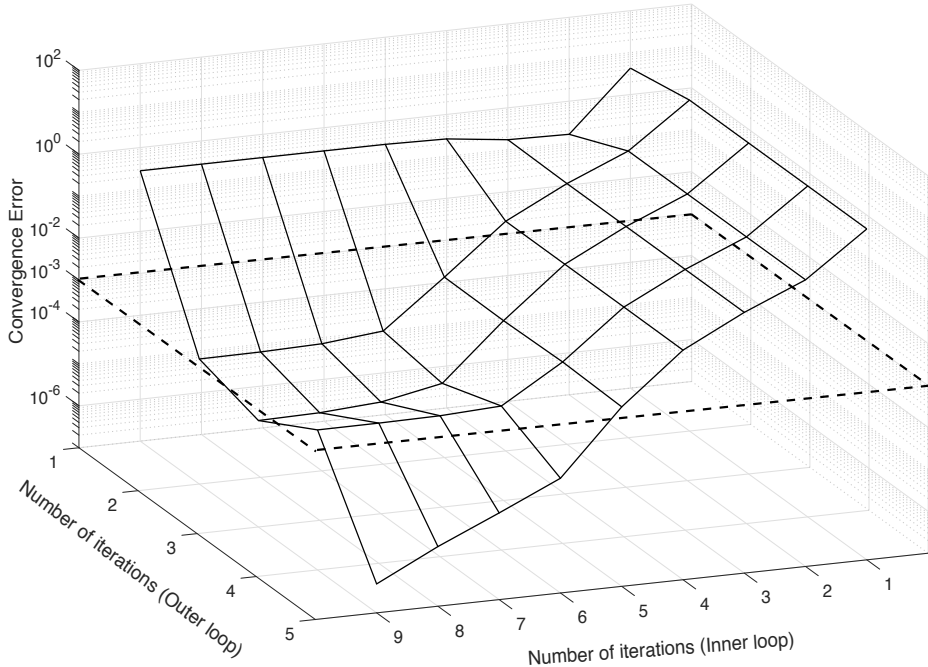


Figure 5.8: Convergence behavior of Algorithm 3: 2-by-2.

In Figs. 5.8 and 5.9, the convergence behaviors of Algorithm 3 for 2-by-2 and 3-

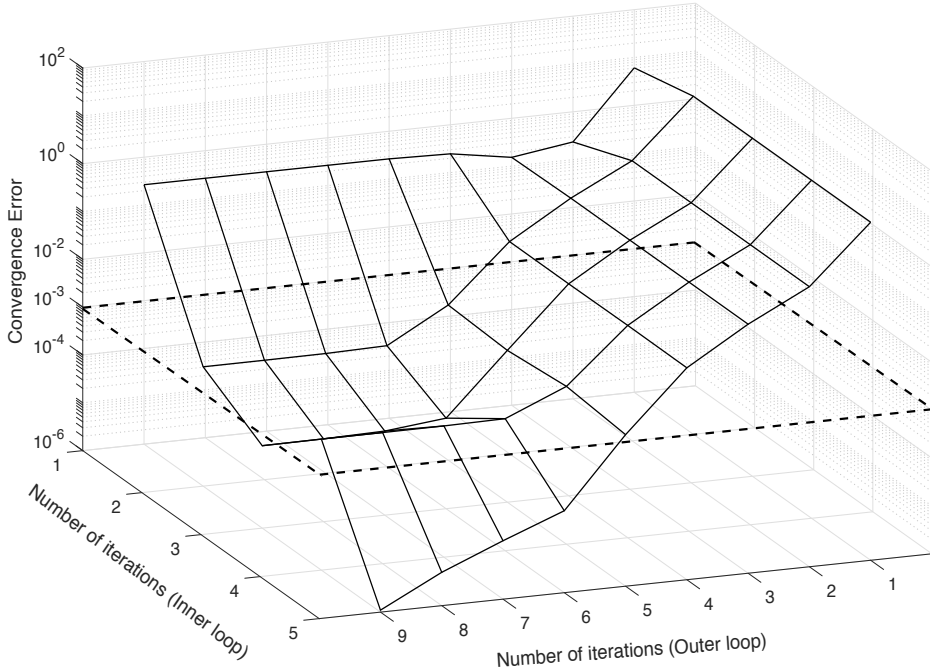


Figure 5.9: Convergence behavior of Algorithm 3: 3-by-3.

by-3 scenarios are presented, respectively. The average LED array transmit power is set to 35 dBm. It should be noted that Algorithm 3 involves two iterative procedures, namely: an inner iterative loop to solve **P5.2** using CCCP and an outer iterative loop of the algorithm itself. In both cases, it is observed that at a target convergence error (i.e., convergence of the users sum-rate) $\epsilon_{\text{convergence}} = 10^{-3}$, the algorithm requires on average 5 inner and 2 outer iterations, thus 10 iterations in total. As the speed of users movement is typically slow in indoor scenarios, this low complexity of the algorithm confirms its practicality in case of time-varying VLC channels.

5.5. Conclusions

In this chapter, we have investigated several strategies of cell coordination/cooperation for a multi-user multi-cell CoMP VLC network. The optimal ZF precoder was designed to maximize the achievable sum-rate of users for each strategy. Numerical results showed that the partial cooperative precoding scheme, due to data sharing among cells, generally achieved the best performance while the coordinated precod-

5.5 Conclusions

ing with less signal processing overhead also performed relative well. Interestingly, in the case when the number of users per cell is large compared to the number of LED arrays, the coordinated and partial cooperative precoding did not outperform much the per-cell coordinated precoding which even obtained better performance at lower transmitted power region.

Chapter 6

Summary and Future Research

6.1. Summary

The exponentially increasing demand of global data traffic over the past decade has posed serious challenges to the existing wireless communications technologies. In contrast, the radio spectrum is a limited resource and is increasingly congested due to increases in number of applications and users. This has motivated researchers to look at new spectrum resources. Operating over a nearly unlimited and license-free spectrum, VLC effectively addresses these above problems. Building upon of the widespread lighting infrastructure, VLC is also expected to play an important role in the future ubiquitous networks.

This dissertation focuses on a precoding design framework for MU-MIMO VLC systems (single and multiple cell fashions) with respect to enhancing physical layer security and optimizing performance. Essentially, the framework involves two fundamental issues in VLC: characterization of VLC channel capacity and constraints on precoding design imposed by practical LED power requirements. Unlike their RF counterpart, VLC channels are subject to amplitude constraint on the channel input, resulting in the unavailability of analytical expressions for the channel capacity. Thus, the first step of our framework is to derive simple lower and upper bound expressions

6.1 Summary

for the VLC channel capacity. Then, the derived bounds are used as benchmarks for the precoding designs. Due to unique characteristics of LEDs, transmit power constraints in VLC are also different from those in RF. As a result, the second step of the framework is formulate constraints on precoding designs in accordance to power constraints in VLC.

The broadcast nature of visible light signal makes eavesdropping a potential threat since any users located within the illuminated area can receive the signals that are intended for other users. In addition to the traditional security measures at network and transport layers, security at the physical layer (i.e., physical layer security) provides a completely new way to prevent eavesdropping. In this dissertation, our first objective is to investigate the designs of two methods, namely: precoding and AN to enhance physical layer security in multi-user VLC systems. First, we aim at optimizing ZF precoding designs to maximize users' secrecy sum-capacity for two scenarios: known and unknown eavesdropper's CSI at the transmitter. It is shown that performance in the case of known eavesdroppers CSI is slightly better than that of unknown CSI and positive sum secrecy-capacity performances can always be achieved for both scenarios. For the second approach on AN, the design purpose is to guarantee a max-min fairness of users' SINRs subject to specific constraints imposed on the eavesdropper. In case the eavesdropper's CSI is unknown, the AN should not interfere legitimate users but possibly degrades the eavesdroppers channel as much as possible. In case the eavesdropper's CSI is known, the AN design aims to limit the eavesdropper's SINR below a predefined threshold. Numerical results reveal that significant gaps between users' and eavesdropper's SINRs can always be achieved in both scenarios of eavesdropper's CSI, thus confirming the benefit of using AN to improve the secrecy level in MU-MIMO VLC systems.

In practical deployments, to support a larger number of users in broad areas, multi-cell configurations are natural progression of VLC. We introduce in this thesis a concept of multi-cell VLC networks, where each cell composes of multiple LED transmitters to support multiple users by means of precoding techniques. In such

multi-cell multi-user networks, the presence of intra-cell and inter-cell interferences are the main performance-limiting factors. Therefore, the second objective of the thesis is to design cell coordination/cooperation strategies and their corresponding coordinated/cooperative precoding to alleviate, or possibly, to cancel out the intra-cell and inter-cell interferences. The performances of the proposed strategies in terms of users sum-capacity are extensively evaluated and compared.

6.2. Future Research

As one of its contributions, this dissertation proposed the concept of muti-CoMP cell for VLC and studied different cell cooperation/coordination strategies as the approaches to reduce to negative impact of intra-cell and inter-cell interferences. The design objective was to maximize the all-cell user's sum-capacity. Our future research will continue exploring another aspects in the design of the proposed multi-CoMP cell VLC. Specifically, we aim at cell cooperation/coordination strategies to address the following issues

6.2.1. User Max-main Fairness

Aside from maximizing users' sum-capacity, ensuring fairness among users is also an important criterion in any multi-user systems. In the single-cell configuration, the fairness designs have been considered in [58,113,118] in terms of user's capacity, MSE and SINR, respectively. In our proposed multi-cell configuration, there are two levels of user fairness, namely: fairness among users in one cell and fairness among cells. In this research direction, our first target is to design cell coordination/cooperation strategies to guarantee both fairness levels. However, depending on the system configuration, this might not be feasible. In that case, considering cell fairness is of higher priority, our next target is a design for the fairness among cells while taking account a tolerance on the fairness of users.

6.2.2. Physical Layer Security with the Presence of Multiple Eavesdroppers

In multi-cell scenarios, from the perspective of users in one cell, users of the other cells are untrusted. Therefore, different from the study in this dissertation where a single eavesdropper was assumed, a multi-eavesdropper scenario should be considered. Here, we are interested in cell coordination/cooperation strategies to ensure a mutual confidentiality among cells while the users' secrecy sum-capacity is maximized for each cell. Cell coordination/cooperation strategies can be realized by, similar in this study, coordinated/cooperative precoding designs or coordinated/cooperative AN, which is potentially interesting approach.

Appendices

A. A Proof of Proposition 1 in Chapter 2

The first derivative of $f(\alpha)$ is given by

$$f'(\alpha) = \log\left(\frac{2A}{\sqrt{2\pi e N_0}}\right) - \log(\alpha) + \frac{3}{2} \log(1-\alpha) + \frac{1}{2}. \quad (\text{A.1})$$

Since $f'(\alpha)$ is continuous, monotonically decreasing over $(0, 1)$, $\lim_{\alpha \rightarrow 0} f'(\alpha) = \infty$ and $\lim_{\alpha \rightarrow 1} f'(\alpha) = -\infty$, the critical point α^* exists and is unique. At the critical point

$$f_1(\alpha^*) = \log(\alpha^*) - \frac{3}{2} \log(1-\alpha^*) = \log\left(\frac{2A}{\sqrt{2\pi e N_0}}\right) + \frac{1}{2}. \quad (\text{A.2})$$

As

$$\lim_{\frac{A}{\sqrt{N_0}} \rightarrow 0} \log\left(\frac{2A}{\sqrt{2\pi e N_0}}\right) + \frac{1}{2} = -\infty, \quad (\text{A.3})$$

$$\lim_{\frac{A}{\sqrt{N_0}} \rightarrow \infty} \log\left(\frac{2A}{\sqrt{2\pi e N_0}}\right) + \frac{1}{2} = \infty, \quad (\text{A.4})$$

$$\lim_{\alpha^* \rightarrow 0} f_1(\alpha^*) = -\infty, \quad (\text{A.5})$$

$$\lim_{\alpha^* \rightarrow 1} f_1(\alpha^*) = \infty \quad (\text{A.6})$$

and $f_1(\alpha^*)$ is continuous, monotonically increasing, we deduce to

$$\lim_{\frac{A}{\sqrt{N_0}} \rightarrow 0} \alpha^* = 0 \text{ and } \lim_{\frac{A}{\sqrt{N_0}} \rightarrow \infty} \alpha^* = 1. \quad (\text{A.7})$$

As a result

$$\lim_{\frac{A}{\sqrt{N_0}} \rightarrow 0} C_U = f(0) = 0, \quad (\text{A.8})$$

$$\lim_{\frac{A}{\sqrt{N_0}} \rightarrow \infty} C_U = f(1) = \log \left(\frac{2A}{\sqrt{2\pi e N_0}} \right). \quad (\text{A.9})$$

This completes the proof.

B. A Proof of Theorem 1 in Chapter 4

B.1. Differential Entropy of the Sum of Uniform Random Variables

Let $\{X_i\}_{i=1}^N$ be N independent uniform random variables and assume that the support of X_i is $[-A_i, A_i]$ for some $A_i > 0$. If we define a random variable $Y = \sum_{i=1}^N X_i$, then the probability density function (PDF) of Y is given by [102]

$$f_Y^{(N)}(y) = U_n \left[\sum_{\vec{\epsilon} \in \{-1, 1\}^N} \left(y + \sum_{i=1}^N \epsilon_i A_i \right)^{N-1} \times \text{sign} \left(y + \sum_{i=1}^N \epsilon_i A_i \right) \prod_{i=1}^N \epsilon_i \right], \quad (\text{B.1})$$

where $U_n = \frac{1}{(N-1)! 2^{N+1} \prod_{i=1}^N A_i}$. The summation is over all 2^N vectors of signs

$$\vec{\epsilon} = (\epsilon_1, \epsilon_2, \dots, \epsilon_N) \in \{-1, 1\}^N \text{ where } \epsilon_i = \pm 1$$

and

$$\text{sign}(x) \stackrel{\Delta}{=} \begin{cases} 1 & \text{if } x > 0, \\ 0 & \text{if } x = 0, \\ -1 & \text{if } x < 0. \end{cases}$$

Hence, the differential entropy of Y is written as

$$h(Y) = - \int f_Y^{(N)}(y) \log f_Y^{(N)}(y) dy. \quad (\text{B.2})$$

It is generally difficult to obtain a closed-form expression for $h(Y)$ due to the complexity of the PDF function in Eq. (B.1). However, for the simplest case when $N = 2$, $f_Y^{(N)}(y)$ can be expressed as

$$f_Y^{(N)}(y) = \begin{cases} \frac{y+A_1+A_2}{4A_1A_2} & -A_1 - A_2 \leq y \leq -|A_1 - A_2|, \\ \min\left(\frac{1}{2A_1}, \frac{1}{2A_2}\right) & -|A_1 - A_2| \leq y \leq |A_1 - A_2|, \\ \frac{-y+A_1+A_2}{4A_1A_2} & |A_1 - A_2| \leq y \leq A_1 + A_2, \\ 0 & \text{otherwise.} \end{cases}$$

The differential entropy $h(Y)$ is then given in closed-form as follows

$$h(Y) = \min \left(\log(2A_1) + \frac{A_2}{2A_1}, \log(2A_2) + \frac{A_1}{2A_2} \right). \quad (\text{B.3})$$

B.2. Data Processing Inequality [64, Theorem 2.8.1]

Random variables X, Y, Z are said to form a Markov chain in that order (denoted by $X \rightarrow Y \rightarrow Z$) if the conditional distribution of Z depends only on Y and is conditionally independent of X , i.e.,

$$p(x, y, z) = p(x)p(y|x)p(z|y) \quad (\text{B.4})$$

The *Data Processing Inequality* states that: if $X \rightarrow Y \rightarrow Z$, then $\mathbb{I}(X; Y) \geq \mathbb{I}(X; Z)$

B.3. Derivation of Eq. (4.7)

Let us define $r_{e,i} = \gamma\eta\mathbf{H}_e\mathbf{W}_i d_i$ where \mathbf{W}_i is the solution to problem (4.8) and $r_e = \sum_{i=1}^K r_{e,i}$, respectively. Denoting that $A_i = \gamma\eta\mathbf{H}_e\mathbf{W}_i$, then $r_{e,i}$ is uniformly distributed over the interval $[-A_i, A_i]$. Hence, the sum rate for messages eavesdropping on legitimate users of the eavesdropper can be expressed by

$$C_e = \sum_{i=1}^K C_{e,i} = \sum_{i=1}^K \mathbb{I}(r_{e,1}; y_e). \quad (\text{B.5})$$

By the definition, it is easy to prove that $r_{e,i} \rightarrow r_e \rightarrow y_e$. Following the *Data Processing Inequality*, we thus obtain

$$\begin{aligned} C_e &\leq \sum_{i=1}^K \mathbb{I}(r_{e,1}; r_e) = \sum_{i=1}^K (h(r_e) - h(r_{e,i}|r_e)) \\ &= K \times h(r_e) - \sum_{i=1}^K h(\overline{r}_{e,i}), \end{aligned} \quad (\text{B.6})$$

where $\overline{r}_{e,i} = \sum_{j=1, j \neq i}^K r_{e,j}$ is the sum of $K - 1$ independent uniform random variables. Therefore, using the results in Eqs. (B.1) and (B.2), C_e can be derived leading to a completion of the proof. Specifically for the case $K = 2$, C_e is given by

$$\begin{aligned} C_e &\leq 2 \min \left(\log(2A_1) + \frac{A_2}{2A_1}, \log(2A_2) + \frac{A_1}{2A_2} \right) - \log(2A_1) - \log(2A_2) \\ &= \min \left(\log \left(\frac{A_1}{A_2} \right) + \frac{A_2}{A_1}, \log \left(\frac{A_2}{A_1} \right) + \frac{A_1}{A_2} \right). \end{aligned} \quad (\text{B.7})$$

Bibliography

- [1] GSMA Intelligence, *Global Mobile Trend 2017*, September 2017. [Online]. Available: <https://regmedia.co.uk/2017/09/12/gsma-mobile-trends-2017.pdf>
- [2] Cisco Systems Inc., *Cisco Visual Networking Index: Global Mobile Data Traffic Forecast Update, 2016-2021 White Paper*. [Online]. Available: <https://www.cisco.com/c/en/us/solutions/collateral/service-provider/visual-networking-index-vni/mobile-white-paper-c11-520862.pdf>
- [3] D. C. O'Brien, L. Zeng, H. L-Minh, G. Faulkner, J. W. Walewski, S. Randel, “Visible light communications: Challenges and possibilities,” *In Proc. of the 2008 IEEE 19th International Symposium on Personal, Indoor and Mobile Radio Communications*, Cannes, France, September 2008.
- [4] Lucible, *LiFi: Enlightening Communications, White Paper*, December 2017. [Online]. Available: <http://www.lucibel.io/documents/6980376/6980618/LiFi+White+Paper/390b2011-8cb4-4312-abe6-66fd741395e7>.
- [5] LuminLink, *White Paper*, 2009. [Online]. Available: bemri.org/visible-light-communication/documents-and.../368...white-paper/file.html.
- [6] A. Jovicic, L. Junyi, T. Richardson, “Visible light communication: opportunities, challenges and the path to market,” *IEEE Commun. Mag.*, vol. 51, no. 12, pp. 26–32, December 2013.
- [7] P. H. Pathak, X. Feng, P. Hu, and P. Mohapatra, “Visible light communication, networking, and sensing: a survey, potential and challenges,” *IEEE Commun. Surveys Tuts.*, vol. 17, no. 4, pp. 2047–2077, September 2015.
- [8] A. G. Bell, W. G. Adams, Tyndall, and W. H. Preece, “Discussion on the photo-phone and the conversion of radiant energy into sound,” *J. Soc. Telegraph Eng.*, vol. 9, no. 34, pp. 375–383, 1880.
- [9] Y. Tanaka, T. Komine, S. Haruyama, M. Nakagawa, “Indoor visible light data transmission system utilizing white LED lights,” *IEICE Trans. Commun.*, vol. E86-B, no.8, pp.2440–2454, August 2003.

BIBLIOGRAPHY

- [10] T. Komine, M. Nakagawa, "Fundamental analysis for visible-light communication system using LED lights," *IEEE Trans. Consum. Electron.*, vol. 50, no. 1, pp. 100–107, February 2004.
- [11] C. Liu, B. Sadeghi, E. W. Knightly, "Enabling vehicular visible light communication (V2LC) network," *In Proc. of the Eighth ACM international workshop on Vehicular inter-networking*, pp. 41–50, September 2011.
- [12] M.Uysal, Z. Ghassemlooy, A. Bekkali, A. Kadri, H. Menouar, "Visible light communication for vehicular networking: performance study of a V2V system using a measured headlamp beam pattern model," *IEEE Veh. Technol. Mag.*, vol. 10, no. 4, December 2015.
- [13] P. Ji, H-M. Tsai, C. Wang, F. Liu, "Vehicular visible light communications with LED taillight and rolling shutter camera," *In Proc. of the 2014 IEEE 79th Vehicular Technology Conference (VTC Spring)*, Seoul, South Korea, May 2014.
- [14] A. Nuwanpriya, S-W. Ho, C. S. Chen, "Indoor MIMO visible light communications: novel angle diversity receivers for mobile users," *IEEE J. Sel. Areas Commun.*, vol. 33, no. 9, pp. 1780–1792, May 2015
- [15] B. Zhang, K. Ren, G. Xing, X. Fu, C. Wang, "SB VLC: secure barcode-based visible light communication for smartphones," *IEEE Trans. Mobile Comput.*, vol. 15, no. 2, pp. 432–446, March 2015.
- [16] Z. Ong, W-Y. Chung, "Long range VLC temperature monitoring system using CMOS of mobile device camera," *IEEE Sensors J.*, vol. 16, no. 6, pp. 1508–1509, March 2015.
- [17] Visible Light Communication Consortium (VLCC). [Online]. Available: <http://www.vlcc.net>
- [18] Visible Light Communication Association (VLCA). [Online]. Available: <http://vlca.net>
- [19] Home Gigabit Access Project (OMEGA). [Online]. Available: <http://www.ict-omega.eu>
- [20] Smart Lighting Engineering Research Center, Boston University. [Online]. Available: <http://www.bu.edu/smarterlighting>
- [21] Center on Optical Wireless Applications, Pennsylvania State University, [Online]. Available: <http://photonics.psu.edu>
- [22] IEEE Std 802.15.7, IEEE Standard for Local and metropolitan area networks - Part 15.7: Short-range wireless optical communication using visible light, Mar. 2011
- [23] A. H. Azhar, T-A. Tran, D. O'Brien, "A gigabit/s indoor wireless transmission using MIMO-OFDM visible-light communications," *IEEE Photon. Technol. Lett.*, vol. 25, no. 2, pp. 171–174, January 2013.

- [24] D. Tsonev, H. Chun, S. Rajbhandari, J. J. D. McKendry, S. Videv, E. Gu, M. Haji, S. Watson, A. E. Kelly, G. Faulkner, M. D. Dawson, H. Haas, D. O'Brien, "A 3-gb/s single-LED OFDM-based wireless VLC link using a gallium nitride *muLED*," *IEEE Photon. Technol. Lett.*, vol. 26, no. 7, pp.637–640, April 2014.
- [25] C. Chen, D. Tsonev, and H. Haas, "Joint transmission in indoor visible light communication downlink cellular networks," *In Proc. of the IEEE Global Communications Conference (GLOBECOM), Workshop on Optical Wireless Communications*, pp. 1127–1132, December 2013,
- [26] C. Chen, S. Videv, D. Tsonev, and H. Haas, "Fractional frequency reuse in DCO-OFDM-based optical attocell networks," *J. Lightw. Technol.*, vol. 33, no. 19, pp. 3986–4000, October 2015.
- [27] X. Li, R. Zhang, L. Hanzo, "Cooperative load balancing in hybrid visible light communications and wifi," *IEEE Trans. Commun.*, vol. 63, no. 4, pp. 1319–1329, March 2015.
- [28] I. Otomo, T. Fujihashi, Y. Hirota, T. Watanabe, "Cooperative Wi-Fi and visible light communication for indoor video delivery," *in Proc. of the IEEE International Conference on Communications*, pp. 1-6, May 2018.
- [29] T. Akiyama, Y. Teranishi, S. Okamura, S. Shimojo, "A consideration of the precision improvement in WiFi positioning system," *In Proc. of the International Conference on Complex, Intelligent and Software Intensive Systems*, pp. 1112–1117, 2009.
- [30] S. Yamaguchi, V. V. Mai, T. C. Thang, A. T. Pham, "Design and performance evaluation of VLC indoor positioning system using optical orthogonal codes," *In Proc. of the IEEE International Conference on Communications and Electronics* Danang, Vietnam, 2014.
- [31] M. Yasir, S-W. Ho, B. N. Vellambi, "Indoor positioning system using visible light and accelerometer," *J. Lightw. Technol.*, vol. 32, no. 19, pp. 3306–3016, October 2014.
- [32] W. Gu, M. Aminikashani, P. Deng, M. Kavehrad, "Impact of multipath reflections on the performance of indoor visible light positioning systems," *J. Lightw. Technol.*, vol. 34, no. 10, pp. 2578–2587, May 2016.
- [33] B. Zhu, J. Cheng, Y. Wang, J. Yan, J. Wang, "Three-dimensional VLC positioning based on angle difference of arrival with arbitrary tilting angle of receiver," *IEEE J. Sel. Areas Commun.*, vol. 36, no. 1, pp. 8–22, January 2018.
- [34] S. Kitano, S. Haruyama, M. Nakagawa, "LED road illumination communications system," *In Proc. of the 58th IEEE Vehicular Technology Conference*, vol.5, pp. 3346–3350, October 2003.
- [35] N. Kumar, "Smart and intelligent energy efficient public illumination system with ubiquitous communication for smart city," *In Proc. of the IEEE International Conference on Smart Structures and Systems*, pp.152–157, March 2013.

- [36] K. H. Lee, S.W. R. Lee, "Process development for yellow phosphor coating on blue light emitting diodes (LEDs) for white light illumination," *In Proc. of the 2006 8th Electronics Packaging Technology Conference*, Singapore, Singapore, December 2006.
- [37] L. Zeng, D. C. O'Brien, H. L. Minh, G. E. Faulkner, K. Lee, D. Jung, Y. Oh, E. T. Won, "High data rate multiple input multiple output (MIMO) optical wireless communications using white LED lighting," *IEEE J. Sel. Areas Commun.*, vol. 27, no. 9, pp. 1654–1662, December 2009.
- [38] Y. Wang, N. Chi, "Demonstration of high-speed 2x2 non-imaging MIMO nyquist single carrier visible light communication with frequency domain equalization," *J. Lightw. Technol.*, vol. 32, no. 11, pp. 2087–2093, June 2014.
- [39] K. Ying, H. Qian, R. J. Baxley, S. Yao, "Joint optimization of precoder and equalizer in MIMO VLC systems," *IEEE J. Sel. Areas Commun.*, vol. 33, no. 9, pp. 1949–1958, September 2015.
- [40] P. F. Mmbaga, J. Thompson, H. Haas, "Performance analysis of indoor diffuse VLC MIMO channels using angular diversity detectors," *J. Lightw. Technol.*, vol. 34, no. 4, pp. 1254–1266, February 2016.
- [41] H-B. Cai, J. Zhang, Y-J. Zhu, J-K. Zhang, X. Yang, "Optimal constellation design for indoor 2x2 MIMO visible light communications," *IEEE Commun. Lett.*, vol. 20, no. 2, pp. 264–267, February 2016.
- [42] Y. Hong, T. Wu, L-K Chen, "On the performance of adaptive MIMO-OFDM indoor visible light communications," *IEEE Photon. Technol. Lett.*, vol. 28, no. 8, pp. 907–910, April 2016.
- [43] K. Ying, H. Qian, R. J. Baxley, G. T. Zhou, "MIMO transceiver design in dynamic-range-limited VLC systems," *IEEE Photon. Technol. Lett.*, vol. 28, no. 22, pp. 2593–2596, November 2016.
- [44] C-W. Hsu, C-W. Chow, I-C. Lu, Y-L. Liu, C-H. Yeh, Y. Liu, "High speed imaging 3x3 MIMO phosphor white-light LED based visible light communication system," *IEEE Photon. J.*, vol. 8, no. 6, Article Sequence Number: 7907406, December 2016.
- [45] C. Chen, W-D. Zhong, D. Wu, "Non-hermitian symmetry orthogonal frequency division multiplexing for multiple-input multiple-output visible light communications," *IEEE J. Opt. Commun. Netw.*, vol. 9, no. 1, pp. 36–44, January 2017.
- [46] A. Yesilkaya, E. Basar, F. Miramirkhani, E. Panayirci, M. Uysal, H. Haas, "Optical MIMO-OFDM with generalized LED index modulation," *IEEE Trans. Commun.*, vol. 65, no. 8, pp. 3429–3441, August 2017.
- [47] D. Takase, T. Ohtsuki, "Performance analysis of optical wireless MIMO with optical beat interference," *in Proc. of the IEEE International Conference on Communications*, vol. 2, pp. 954–958, May 2005. .

- [48] ——————, “Spatial multiplexing in optical wireless MIMO communications over indoor environment,” *IEICE Trans. Commun.*, vol.E89-B, no. 4, pp. 1364–1371, April 2006.
- [49] R. Mesleh, H. Haas, S. Sinanovic, C. W. Ahn, S. Yun, “Spatial modulation,” *IEEE Trans. Veh. Technol.*, vol. 57, no. 4, pp. 2228–2241, July 2008.
- [50] T. Fath, H. Haas, M. D. Renzo, R. Mesleh, “Spatial modulation applied to optical wireless communications in indoor LOS environments,” in *Proc. of the IEEE Global Telecommunication Conference*, December 2011.
- [51] R. Mesleh, H. Haas, C. W. Ahn, S. Yun, “Spatial modulation-a new low complexity spectral efficiency enhancing technique,” in *Proc. of the IEEE International Conference on Communication and Networking in China*, October 2006.
- [52] A. Younis, M. Di Renzo, R. Mesleh, and H. Haas, “Sphere decoding for spatial modulation,” in *Proc. of the IEEE International Conference on Communications*, June 2011.
- [53] H. Yang, J. Chen, Z. Wang, C. Yu, “Performance of a precoding MIMO system for decentralized multiuser indoor visible light communications,” *IEEE Photon. J.*, vol. 5, no. 4, August. 2013, Art. ID 7800211.
- [54] J. Chen, N. Ma; Y. Hong, C. Yu, “On the performance of MU-MIMO indoor visible light communication system based on THP algorithm,” In *Proc. of the IEEE/CIC Int. Conf. on Communications in China*, pp. 136–140, October 2014.
- [55] T. V. Pham, H. L. Minh, Z. Ghassemlooy, T. Hayashi, and A. T. Pham, “Sum-rate maximization of multi-user MIMO visible light communications,” In *Proc. of the IEEE International Conference on Communications, Workshop on Visible Light Communications and Networking*, London, UK, June 2015.
- [56] Q. H. Spencer, A. L. Swindlehurst, M. Haardt, “Zero-forcing methods for downlink spatial multiplexing in multiuser MIMO channels,” *IEEE Trans. Signal Process.*, vol. 52, no. 2, pp. 461–471, February 2004.
- [57] H. Ma, L. Lampe, S. Hranilovic, “Coordinated broadcasting for multiuser indoor visible light communication systems,” *IEEE Trans. Commun.*, vol. 63, no. 9, pp. 3313–3324, September 2015.
- [58] B. Li, J. Wang, R. Zhang, H. Shen, C. Zhao, L. Hanzo, “Multiuser MISO transceiver design for indoor downlink visible light communication under per-LED optical power constraints,” *IEEE Photon. J.*, vol. 7, no. 4, August 2015, Art. ID 7201415.
- [59] C. E. Shannon, “A mathematical theory of communication,” *Bell Syst. Tech. J.*, vol. 27, no. no. 4, pp. 623–666, October 1948.
- [60] J. G. Smith, “The information capacity of amplitude and variance-constrained scalar Gaussian channels,” *J. Inf. Control*, vol. 18, no. 3, pp. 203–219, April 1971.

- [61] T. V. Pham, H. L. Minh, A.T. Pham, “Multi-user visible light communication broadcast channels with zero-forcing precoding,” *IEEE Trans. on Commun.*, vol 64, no. 6, pp. 2509–2521, June 2017.
- [62] T. V. Pham, A. T. Pham, “Coordination/cooperation strategies and optimal zero-forcing precoding design for multi-user multi-cell VLC networks,” *IEEE Trans. on Commun.*, (major revision, under review), December 2018.
- [63] A. Lapidoth, S. M. Moser, M. A. Wigger, “On the capacity of free-space optical intensity channels,” *IEEE Trans. Inf. Theory*, vol. 55, no. 10, pp. 4449–4461, Oct. 2009.
- [64] T. Cover, J. Thomas, “Elements of information theory,” *Wiley Inter-science*, 2006.
- [65] A. Chaaban, J. M. Morvan, M.-S. Alouini, “Free-space optical communications: capacity bound, approximations, and a new sphere-packing perspective,” *IEEE Trans. Commun.*, vol. 64, no. 3, pp. 1176–1191, March 2016.
- [66] T. Young, M. J. Mohlenkamp, “Introduction to numerical methods and matlab programming for engineers,” *Department of Mathematics*, Ohio University, 2015.
- [67] C. B. Peel, B. M. Hochwald, A. L. Swindlehurst, “A vector-perturbation technique for near-capacity multiantenna multiuser communication-part I: channel inversion and regularization,” *IEEE Trans. Commun.*, vol. 53, no. 1, pp. 195–202, January 2005.
- [68] B. Bandemer, M. Haardt, S. Visuri, “Linear MMSE multi-user MIMO downlink precoding for users with multiple antennas,” *In Proc. of the 2006 IEEE 17th International Symposium on Personal, Indoor and Mobile Radio Communications*, Helsinki, Finland, September 2006.
- [69] V. Stankovic, M. Haardt, “Generalized design of multi-user MIMO precoding matrices,” *IEEE Trans. Wireless Commun.*, vol. 7, no. 3, pp. 953–961, March 2008.
- [70] A. Wiesel, Y. C. Eldar, S. Shamai, “Zero-forcing precoding and generalized inverses,” *IEEE Trans. Signal Process*, vol. 56, no. 9, pp. 4409–4418, September 2008.
- [71] L-N. Tran, M. Juntti, M. Bengtsson, B. Ottersten, “Beamformer designs for MISO broadcast channels with zero-forcing dirty paper coding,” *IEEE Trans. Wireless Commun.*, vol. 12, no. 3, pp. 1173–1185, March 2013.
- [72] D. C. O’Brien, M. Katz, “Optical wireless communications within fourth-generation wireless systems,” *J. Optical Networking*, vol. 4, no. 6, pp. 312–322, 2005.
- [73] T. Parfait, Y. Kuang, and K. Jerry, “Performance analysis and comparison of ZF and MRT based downlink massive MIMO systems, *In Proc. of the 6th International Conference Ubiquitous Future Networks*, pp. 383–388, Shanghai, China, July 2014.

- [74] A. Kammoun, A. Muller, E. Bjornson, and M. Debbah, “Linear precoding based on polynomial expansion: Large-scale multi-cell MIMO systems,” *IEEE J. Sel. Topics Signal Process.*, vol. 8, no. 5, pp. 861–875, October 2014.
- [75] J. Zhu, R. Schober, and V. K. Bhargava, “Secure downlink transmission in massive MIMO system with zero-forcing precoding,” *In Proc. 20th European Wireless Conference*, Barcelona, Spain, May 2014.
- [76] T. V. Pham, A. T. Pham, “Secrecy sum-rate of multi-user MISO visible light communication systems with confidential messages,” *OPTIK-International Journal for Light and Electron Optics*, vol. 151, pp. 65–76, December 2017.
- [77] T. V. Pham, T. Hayashi, A. T. Pham, “Artificial-noise-aided precoding design for multi-user visible light communication channels,” *IEEE Access* (accepted), December 2018.
- [78] A. D. Wyner, “The wire-tap channel,” *Bell Syst. Tech. J.*, vol. 54, pp. 1355–1387, October 1975.
- [79] I. Csiszar, J. Korner, “Broadcast channels with confidential messages,” *IEEE Trans. Inf. Theory*, vol. 24, no. 3, pp. 339–348, May 1978.
- [80] S. Leung-Yan-Cheong, M. Hellman, “The Gaussian wire-tap channel,” *IEEE Trans. Info. Theory*, vol. 24, no. 4, pp. 451–456, July 1978.
- [81] P. Parada and R. Blahut, “Secrecy capacity of SIMO and slow fading channels,” *In Proc. of the IEEE International Symposium on Information Theory*, Adelaide, Australia, September 2005.
- [82] C. Mitrpant, A. J. Vinck, and L. Yuan, “An achievable region for the Gaussian wiretap channel with side information,” *IEEE Trans. Inf. Theory*, vol. 52, no. 5, pp. 2181–2190, May 2006.
- [83] P. Gopala, L. Lai, H. El Gamal, “On the secrecy capacity of fading channels”, *IEEE Trans. Inf. Theory*, vol. 54, no. 10, pp. 4687–4698, October 2008.
- [84] S. Shafiee, N. Liu, and S. Ulukus, “Towards the secrecy capacity of the Gaussian MIMO wire-tap channel: The 2-2-1 channel,” *IEEE Trans. Inf. Theory*, vol. 55, no. 9, pp. 4033–4039, September 2009.
- [85] A. Khisti and G. Wornell, “Secure transmission with multiple antennas I: the MISOME wiretap channel,” *IEEE Trans. Inf. Theory*, vol. 56, no. 7, pp. 3088–3104, July 2010.
- [86] A. Khisti and G. Wornell, “Secure transmission with multiple antennas II: the MIMOME wiretap channel,” *IEEE Trans. Inf. Theory*, vol. 56, no. 11, pp. 5515–5532, November 2010.
- [87] R. Liu, T. Liu, H. V. Poor, and S. Shamai, “New results on multiple-input multiple-output broadcast channels with confidential messages,” *IEEE Trans. Inf. Theory*, vol. 59, no. 3, pp. 1346–1359, March 2013.

- [88] J-Y. Wang, C. Liu, J-B. Wang, Y. Wu, M. Lin, J. Cheng, “Physical-layer security for indoor visible light communications: secrecy capacity analysis,” *IEEE Trans. Commun.*, vol. 66, no. 12, pp. 6423–6436, December 2018.
- [89] X. Zhao, H. Chen, J. Sun, “On physical-layer security in multiuser visible light communication systems with non-orthogonal multiple access,” *IEEE Access*, vol. 6, pp. 34004–34017, June 2018.
- [90] A. Mostafa, L. Lampe, “Pattern synthesis of massive LED arrays for secure visible light communication links,” *In Proc. of the IEEE International Conference Communications (ICC) Workshop - Visible Light Communications and Networking*, pp. 1350–1355, June 2015.
- [91] —————, “Physical-layer security for MISO visible light communication channels,” *IEEE J. Sel. Areas Commun.*, no. 9, vol. 33, pp. 1806–1818, May 2015.
- [92] —————, “Optimal and robust beamforming for secure transmission in MISO visible-light communication links,” *IEEE Trans. Signal Process.*, vol. 64, no. 24, pp. 6501–6516, August 2016.
- [93] —————, “Physical-layer security for indoor visible light communications,” *In Proc. of the IEEE International Conference Communications (ICC)*, pp. 3342–3347, Sydney, NSW, Australia, June 2014.
- [94] —————, “Securing visible light communications via friendly jamming,” *In Proc. of the IEEE Global Communications Conference (GLOBECOM) Workshop-Optical Wireless Communications*, pp. 524–529, Austin, TX, USA, December 2014.
- [95] S. Ma, Z-L. Dong, H. Li, Z. Lu, S. Li, “Optimal and robust secure beamformer for indoor MISO visible light communication,” *J. Lightwave Technol.*, vol. 34, no. 21, pp. 4988–4998, November 2016.
- [96] H. Zaid, Z. Rezki, A. Chaaban, M. S. Alouini, “Improved achievable secrecy rate of visible light communication with cooperative jamming,” *In Proc. of the Symposium on Signal Processing for Optical Wireless Communications*, pp. 1165–1169, Orlando, FL, USA, December 2015.
- [97] M. A. Arfaoui, Z. Rezki, A. Ghrayeb, M. S. Alouini, “On the secrecy capacity of MISO visible light communication channels,” *In Proc. of the IEEE Global Communications Conference (GLOBECOM)*, Washington, DC, USA, December 2016.
- [98] H. Shen, Y. Deng, W. Xu, C. Zhao, “Secrecy-oriented transmitter optimization for visible light communication systems,” *IEEE Photon J.*, vol. 8, no. 5, Oct. 2016, Art. ID 7905914.
- [99] L. Vandenberghe, S. Boyd, S-P. Wu, “Determinant maximization with linear matrix inequality constraints,” *SIAM J. Matrix Anal. Appl.*, vol. 19, no. 2, pp. 499–533, 1998.

- [100] M. Grant, S. Boyd, “CVX: Matlab software for disciplined convex programming version 2.1,” <http://cvxr.com/cvx/>, Jananuary 2015.
- [101] J. Lofberg, “YALMIP: a toolbox for modeling and optimization in MATLAB,” *In Proc. of the IEEE International Symposium on Computer Aided Control Systems Design*, pp. 284–289, Taipei, Taiwan, September 2004.
- [102] D. M. Bradley, R. C. Gupta, “On the distribution of the sum of n non-identically distributed uniform random variables,” *Ann. Inst. Stat. Math.*, vol. 54, no. 3, pp. 689–700, 2002.
- [103] M. S. Lobo, L. Vandenberghe, S. Boyd, H. Lebret, “Applications of second-order cone programming,” *Linear Algebra Appl.*, vol. 284, no. 1-3, pp. 193–228, November 1998.
- [104] H. Sifaou, K. H. Park, A. Kammoun, M. S. Alouini, “Optimal linear precoding for indoor visible light communication system,” *In Proc. of the 2017 IEEE International Conference on Communications (ICC)*, Paris, France, May 2017.
- [105] A. L. Yuille, A. Rangarajan, “The Concave-Convex Procedure (CCCP),” *Neural Comput.*, vol. 15, no. 4, pp. 915–936, April 2003.
- [106] B. K. Sriperumbudur, G. R. G. Lanckriet, “On the Convergence of the Concave-Convex Procedure,” *In Proc. of the Neural Information Processing System*, pp. 1–9, September 2009.
- [107] B. G. Guzman, A. L. Serrano, V. P. G. Jimenez, “Cooperative optical wireless transmission for improving performance in indoor scenarios for visible light communications,” *IEEE Trans. Consum. Electron.*, vol. 61, no. 4, pp. 393–401, Jan. 2016.
- [108] Y. J. Zhu, W. Y. Wang, G. Xin, “Faster-than-Nyquist signal design for multiuser multicell indoor visible light communications,” *IEEE Photon. J.*, vol. 8, no. 1, Feb. 2016, Art. ID 7902012.
- [109] Z. G. Sun, H. Yu, Y. J. Zhu, “Efficient signal design and optimal power allocation for visible light communication attocell systems,” *Appl. Opt.*, vol. 56, no. 32, pp. 8959–8968, November 2017.
- [110] H. Ma, A. Mostafa, L. Lampe, S. Hranilovic, “Coordinated beamforming for downlink visible light communication networks,” *IEEE Trans. Commun.*, DOI:10.1109/TCOMM.2018.2817222, March 2018.
- [111] Z. Yu, R. Baxley, G. T. Zhou, “Multi-user MISO broadcasting for indoor visible light communication,” *In Proc. of the IEEE International Conference on Acoustics, Speech and Signal Processing (ICASSP)*, pp. 4849–4853, May 2013.
- [112] T. Cogalan, H. Haas, E. Panayirci, “Precoded single-cell multi-user MISO visible light communications,” *In Proc. of the European Wireless Conference*, pp. 1–6, May 2015.

- [113] T. V. Pham, A. T. Pham, "Max-min fairness and sum-rate maximization of MU-VLC local networks," *In Proc. of the IEEE Global Communications Conference, Workshop on Optical Wireless Communications*, San Diego, USA, December 2015.
- [114] R. Feng, M. Dai, H. Wang, B. Chen, X. Lin, "Linear precoding for multiuser visible-light communication with field-of-view diversity," *IEEE Photon. J.*, vol. 8, no. 2, April 2016, Art. ID 7902708.
- [115] H. Shen, Y. Deng, W. Xu, C. Zhao, "Rate maximization for downlink multiuser visible light communications," *IEEE Access*, vol. 4, pp. 6567–6573, September 2016.
- [116] R. Wang, Q. Gao, J. You, E. Liu, P. Wang, Z. Xu, Y. Hua, "Linear Transceiver Designs for MIMO Indoor Visible Light Communications Under Lighting Constraints," *IEEE Trans. Commun.*, vol. 65, no. 6, pp. 2494–2508, June 2017.
- [117] H. Marshoud, P. C. Sofotasios, S. Muhaidat, B. S. Sharif, G. K. Karagiannidis, "Optical adaptive precoding for visible light communications," *IEEE Access*, vol. 6, pp. 22121–22130, March 2018.
- [118] H. Sifaou, A. Kammoun, K-H. Park, M-S. Alouini, "Robust precoding design for indoor MU-MISO visible light communication," *In Proc. of the 2018 IEEE Wireless Communications and Networking Conference (WCNC)*, Barcelona, Spain, April 2018.
- [119] S. Chatzinotas, M. A. Imran, C. Tzaras, "Uplink capacity of MIMO cellular systems with multicell processing," in *Proc. of the IEEE International Symposium on Wireless Communication Systems*, October 2008.
- [120] H. Dai and H. Poor, "Asymptotic spectral efficiency of multicell MIMO systems with frequency-flat fading," *IEEE Trans. Signal Processing*, vol. 51, no. 11, pp. 2976–2988, November 2003.
- [121] S. Chatzinotas, M. A. Imran, R. Hoshyar, "On the multicell processing capacity of the cellular MIMO uplink channel in correlated rayleigh fading environment," *IEEE Trans. Wirel. Commun.*, vol. 8, no. 7, July 2009.